

THEORY OF PHASE TRANSITIONS IN
FERROELECTRIC SUPERLATTICES

LIM KOK GENG

FACULTY OF SCIENCE
UNIVERSITY OF MALAYA
KUALA LUMPUR

2015

THEORY OF PHASE TRANSITIONS IN
FERROELECTRIC SUPERLATTICES

LIM KOK GENG

THESIS SUBMITTED IN FULFILMENT OF THE
REQUIREMENTS FOR THE DEGREE OF
DOCTOR OF PHILOSOPHY

DEPARTMENT OF PHYSICS
FACULTY OF SCIENCE
UNIVERSITY OF MALAYA
KUALA LUMPUR

2015

UNIVERSITI MALAYA

ORIGINAL LITERARY WORK DECLARATION

Name of Candidate: **LIM KOK GENG**

I.C./Passport No.: **840214-07-5035**

Registration/Matrix No.: **SHC110008**

Name of Degree: **DOCTOR OF PHILOSOPHY**

Title of Project Paper/Research Report/Dissertation/Thesis (“this Work”):

“THEORY OF PHASE TRANSITIONS IN FERROELECTRIC SUPERLATTICES”

Field of Study: **THEORETICAL PHYSICS**

I do solemnly and sincerely declare that:

- (1) I am the sole author/writer of this Work,
- (2) This work is original,
- (3) Any use of any work in which copyright exists was done by way of fair dealing and for permitted purposes and any excerpt or extract from, or reference to or reproduction of any copyright work has been disclosed expressly and sufficiently and the title of the Work and its authorship have been acknowledged in this Work,
- (4) I do not have any actual knowledge nor do I ought reasonably to know that the making of this work constitutes an infringement of any copyright work,
- (5) I hereby assign all and every rights in the copyright to this Work to the University of Malaya (“UM”), who henceforth shall be owner of the copyright in this Work and that any reproduction or use in any form or by any means whatsoever is prohibited without the written consent of UM having been first had and obtained,
- (6) I am fully aware that if in the course of making this Work I have infringed any copyright whether intentionally or otherwise, I may be subject to legal action or any other action as may be determined by UM.

(Candidate’s Signature)

Date

Subscribed and solemnly declared before,

Witness’s Signature

Date

Name: **ASSOC. PROF. DR. CHEW KHIAN HOOI**

Designation: **ASSOCIATE PROFESSOR**

ABSTRACT

Ferroelectric superlattices comprising two or more different layers are currently a topic of active research because of their potential applications in memories and fundamental scientific interest. A thermodynamic model based on the Landau-Ginzburg theory is proposed to study the phase transitions in ferroelectric superlattices. An interface energy term is introduced in the free energy to describe the formation of intermixed layer with properties different from those of both layers. These intermixed layers are mutually coupled through the local polarization at interfaces.

The effects of electrostatic coupling and interface intermixing on the internal electric field and polarization of superlattices which composed of alternate layers of ferroelectrics and paraelectrics are discussed. As an illustration, the model is applied to a superlattice consisting of a ferroelectric layer as PbTiO_3 (PT) and a paraelectric layer as SrTiO_3 (ST) on a ST substrate. Appropriate electrostatic boundary conditions are considered for the case of superlattice with polarization perpendicular to the surface or interface. The effect of interface intermixing and modulation period on the internal electric field and polarization are studied by changing the volume fraction or thickness ratio of the PT/ST superlattice. In addition, the spatially-varying internal electric field, dielectric susceptibility and polarization of these ferroelectric superlattices are calculated. Effects of modulation period and temperature on the internal electric field, dielectric susceptibility and polarization of these superlattices with inhomogeneous properties are examined. The polarization reversal in PT/ST superlattices with “switchable” polarization in intermixed layers is also studied. The dependence of polarization and internal electric field on an applied electric field is discussed. The polarization and internal electric field profiles at certain applied electric field are examined. Besides that, the effects of alternating interface charges, $\pm\sigma$ of the ferroelectric superlattices are studied by taking into account the intermixing at the

interfaces between layers. The alternating interface charges enhance the polarization of ferroelectric superlattices, and lead to the formation of an effective internal electric field in the superlattices.

Lastly, the thermodynamic model is extended to study the effect of composition and interface intermixing on ferroelectric properties of $\text{BaTiO}_3/\text{Ba}_x\text{Sr}_{1-x}\text{TiO}_3$ (BT/BST) superlattices. Effects of composition and interface intermixing on ferroelectricity of BT/BST superlattices are examined by investigating the modulated profiles of polarization and the mismatch in polarization at the interface.

ABSTRAK

Superkekisi feroelektrik yang terdiri daripada dua atau lebih lapisan yang berbeza merupakan satu topik penyelidikan yang aktif pada masa kini, ini disebabkan aplikasinya yang berpotensi dalam storan ingatan dan kepentingan asas saintifik. Kami telah mencadangkan model termodinamik yang berdasarkan teori Landau-Ginzburg untuk mengkaji peralihan fasa dalam superkekisi feroelektrik. Istilah tenaga antara muka telah diperkenalkan dalam tenaga bebas untuk menggambarkan pembentukan lapisan saling campur yang mempunyai ciri-ciri yang berbeza daripada kedua-dua lapisan. Lapisan-lapisan saling campur ini saling berganding melalui pengkutuban tempatan di antara muka.

Kesan gandingan elektrostatik dan antara muka yang bersaling campur ke atas medan elektrik dalaman dan pengkutuban dalam superkekisi yang terdiri daripada lapisan feroelektrik dan paraelektrik yang berselang-seli telah dibincangkan. Sebagai contoh, kita mengaplikasikan model tersebut ke atas superkekisi yang terdiri daripada PbTiO_3 (PT) sebagai lapisan feroelektrik dan SrTiO_3 (ST) sebagai lapisan paraelektrik di atas substrat ST. Syarat sempadan elektrostatik yang sesuai telah dipertimbangkan untuk kes superkekisi yang pengkutubannya bertegak lurus pada permukaan atau antara muka. Kesan antara muka yang bersaling campur dan tempoh modulasi ke atas medan elektrik dalaman dan pengkutuban telah dikaji dengan menukarkan pecahan isipadu atau nisbah ketebalan superkekisi PT/ST. Di samping itu, perubahan secara ruang terhadap medan elektrik dalaman, kebolehtahanan dielektrik dan pengkutuban untuk superkekisi feroelektrik telah dihitung. Kesan tempoh modulasi dan suhu ke atas medan elektrik dalaman, kebolehtahanan dielektrik dan pengkutuban dalam superkekisi yang bersifat tak homogen juga dikajikan. Kami juga mengkaji perubahan arah pengkutuban dalam superkekisi PT/ST yang mempunyai pengkutuban yang boleh disuisikan dalam lapisan saling campur. Pergantungan pengkutuban dan medan elektrik dalaman ke atas medan

elektrik kenaan juga telah dibincangkan. Profil pengkutuban dan medan elektrik dalaman di bawah pengaruh medan elektrik kenaan yang tertentu telah dikaji. Di samping itu, kesan daripada caj yang bersilih ganti di antara muka, $\pm\sigma$ dalam superkekisi feroelektrik telah dikaji dengan mengambil kira kesan bersaling campur di antara muka. Caj yang bersilih ganti di antara muka ini meningkatkan pengkutuban superkekisi feroelektrik, dan juga membawa kepada pembentukan medan elektrik dalaman efektif dalam superkekisi .

Akhir sekali, kami melanjutkan model termodinamik kami untuk mengkaji kesan komposisi dan antara muka yang bersaling campur ke atas sifat feroelektrik dalam superkekisi $\text{BaTiO}_3/\text{Ba}_x\text{Sr}_{1-x}\text{TiO}_3$ (BT/BST). Kesan komposisi dan antara muka bersaling campur ke atas keferoelektrikan superkekisi BT/BST telah dikaji dengan menyiasat profil modulasi pengkutuban dan perbezaan pengkutuban di antara muka.

ACKNOWLEDGEMENTS

First and foremost, I offer my deepest gratitude to my supervisor, Assoc. Prof. Dr. Chew Khian Hooi for his support, patience and guidance during my graduate studies at University of Malaya.

I am very grateful to Prof. Yoshio Ishibashi for the stimulating scientific discussion during his visit to University of Malaya as an Academic Icon. His valuable discussion and advices are very fruitful for shaping up my ideas and research.

I am indebted to Dr. Danyang Wang for accepting me as a research student under Practicum Exchange Program in School of Materials Science and Engineering, University of New South Wales (UNSW). I would like to thank him for the financial support during my 6 months visit at UNSW.

Many thanks to our collaborators, Assoc. Prof. Ong Lye Hock from Universiti Sains Malaysia and Assoc. Prof. Makoto Iwata from Nagoya Institute of Technology, for their valuable discussions during my research studies.

Besides that, I want to acknowledge the financial support from Bright Spark Unit, University of Malaya for the award of *Skim Bright Sparks Universiti Malaya* (SBSUM) during my Ph.D. study. Besides that, I would also like to thank the Centre for Theoretical and Computational Physics and Department of Physics at University of Malaya.

Last but not least, I want to express my appreciation to my wife, Kanakeswary, for her understanding, love and support. I am also grateful to my family members especially my parents for their greatest support.

TABLE OF CONTENTS

ORIGINAL LITERARY WORK DECLARATION	ii
ABSTRACT	iii
ABSTRAK	v
ACKNOWLEDGEMENTS	vii
TABLE OF CONTENTS	viii
LIST OF FIGURES	xi
LIST OF TABLES	xiv
LIST OF SYMBOLS AND ACRONYMS	xv
LIST OF APPENDICES	xvii
CHAPTER 1: INTRODUCTION	1
1.1 Statement of Present Research	1
1.1.1 Objectives of present Work	2
1.1.2 Organization of the Thesis	2
1.2 Introduction to Ferroelectrics and its Applications	4
1.3 Symmetry in Crystals	6
1.4 Perovskite-oxide Ferroelectrics	8
1.5 Symmetry and Order Parameters	9
1.5.1 Broken Symmetry	9
1.5.2 Order Parameters	12
1.6 Phenomenological Theory of Ferroelectricity	14
1.6.1 Thermodynamic Relations	15
1.6.2 Multiaxial Ferroelectrics (Multicomponent Order Parameters)	16
1.6.3 Uniaxial Ferroelectrics (One-component Order Parameter)	19
1.7 Ferroelectric Hysteresis and Polarization Reversal	24
1.8 Misfit Epitaxial Strain Effect	25
CHAPTER 2: REVIEW OF FERROELECTRIC SUPERLATTICES	31
2.1 Overview	31
2.2 Introduction to Ferroelectric Superlattices	31
2.2.1 Theoretical Methods for the Study of Ferroelectric Superlattices: An Overview	33
2.3 Major Factors Affecting Ferroelectric Superlattices	34
2.3.1 Misfit Strain	35
2.3.2 Electrostatic coupling	37
2.3.3 Volume fraction or thickness ratio	38
2.3.4 Interface effects	39
	viii

2.4	An Overview of Phenomenological Theory for Ferroelectric Superlattices	43
2.5	A Thermodynamic Model for Ferroelectric Superlattices	47
2.5.1	Dipole Lattice Model	47
2.5.2	Continuum Model	50
CHAPTER 3: ELECTROSTATIC COUPLING AND INTERFACE INTERMIXING IN FERROELECTRIC SUPERLATTICES		54
3.1	Introduction	54
3.2	Literature Review	55
3.3	Formalism for Electrostatic Coupling and Interface Intermixing	56
3.3.1	Interface Intermixing	57
3.3.2	Electrostatic Coupling	59
3.4	Calculations For PbTiO ₃ /SrTiO ₃ Superlattices	60
3.5	The effects of electrostatic coupling and interface intermixing	62
3.5.1	Result and Discussion	63
3.6	Modulated Internal Electric Field, Dielectric Susceptibility and Polarization	70
3.6.1	Formalism for Dielectric Susceptibility	71
3.6.2	Result and Discussion	72
3.7	Hysteretic Internal Electric Fields and Polarization Reversal	75
3.7.1	Result and Discussion	75
3.8	Conclusion	79
CHAPTER 4: POLARIZATION DISCONTINUITY AND SCREENING CHARGES IN FERROELECTRIC SUPERLATTICES		81
4.1	Introduction	81
4.2	Literature Review	82
4.3	Formalism	84
4.4	Result and Discussion	87
4.5	Conclusion	94
CHAPTER 5: EFFECT OF COMPOSITION AND INTERFACE INTERMIXING ON FERROELECTRIC SUPERLATTICES		96
5.1	Introduction	96
5.2	Literature Review	97
5.3	In-plane Polarization Case	98
5.3.1	Formalism	99
5.3.2	Result and Discussion	102
5.4	Out-of-plane Polarization Case	108
5.4.1	Formalism	109
5.4.2	Result and Discussion	110
5.5	Conclusion	117
CHAPTER 6: CONCLUSIONS AND FUTURE WORKS		118
6.1	Conclusions	118
6.2	Future Works	121
REFERENCES		123

APPENDICES

133

LIST OF PUBLICATIONS

139

LIST OF FIGURES

Figure 1.1	Relations among piezoelectricity, pyroelectricity and ferroelectricity.	5
Figure 1.2	Classification of crystals according to their structure and properties. Ferroelectric materials have to be pyroelectrics and piezoelectrics.	7
Figure 1.3	Perovskite structure of the ferroelectric oxide PbTiO_3 . (a) high temperature paraelectric phase with cubic structure, (b) low temperature ferroelectric phase with tetragonal structure (Damjanovic, 1998).	9
Figure 1.4	Temperature dependence of the order parameter in case of a second order transition (a), first order close to second order transition (b) and in case of first order transition (c). (Strukov & Levanyuk, 1998)	13
Figure 1.5	Free energy as a function of polarization at various temperature for second order phase transition.	22
Figure 1.6	Free energy as a function of polarization at various temperature in case of a first order phase transition.	23
Figure 1.7	Ferroelectric ($P - E$) hysteresis loop. (a) Ideal single-domain single crystals (b) Polycrystalline materials (Hoffmann-Eifert, Richter, & Kinstry, 2012)	25
Figure 2.1	Schematic illustration of a periodic superlattice composed of a ferroelectric and paraelectric layers with the thicknesses L_1 and L_2 , respectively. $L = L_1 + L_2$ is the periodic thickness of the superlattice. The direction of polarization p , polarization q and applied electric field E are indicated in the figure. (Chew, 2012)	48
Figure 3.1	Schematic illustration of a periodic superlattice composed of a ferroelectric layer and a paraelectric layer. The thicknesses of ferroelectric layer (FE) and paraelectric layer (PE) are d_{FE} and d_{PE} , respectively. Arrow indicates the direction of polarization.	56
Figure 3.2	Spatial dependence of electrical properties at $T = 298K$ (a) with electrostatic coupling and (b) without electrostatic coupling. The values of λ_0 are: 0 (red line), $0.02\xi_0$ (blue line) and ξ_0 (brown line).	64
Figure 3.3	Electrical properties at $T = 293K$ as a function of d_{PT}/d_{ST} (a) with electrostatic coupling and (b) without electrostatic coupling. The values of λ_0 are: 0 (\bullet), $0.02\xi_0$ (\blacksquare) and ξ_0 (\blacktriangle).	65
Figure 3.4	Internal electric field and polarization as a function of period thickness d_{FE}/d_{PE} for PT/ST superlattices with $d_{FE} = d_{PE}$ at $T = 298K$. The values of λ are: 0 (black line), $0.02\xi_0$ (blue line) and ξ_0 (red line).	68
Figure 3.5	(a) Internal electric field and (b) polarization at $T = 298K$, and (c) transition temperature as a function of PT volume fraction ϕ_{FE} of PT/ST superlattices. The values of λ_0 are: 0 (red line), $0.02\xi_0$ (blue line) and ξ_0 (brown line). Solid dots (\bullet) represent the experimental data. The grey line denotes calculated result from Dawber et al. (Dawber et al., 2007).	70

- Figure 3.6 Profiles of polarization, internal electric field and dielectric susceptibility of PT/ST superlattice at $T = 298K$. The three lines represent different period thickness with ratio d_{FE}/d_{PE} (in *u.c.*): 10/15 (blue line), 10/10 (red line) and 10/5 (brown line). 73
- Figure 3.7 Internal electric field, polarization and dielectric susceptibility as a function of temperature for PT/ST superlattice with thickness ratio d_{FE}/d_{PE} (in *u.c.*): 10/15 (blue line), 10/10 (red line) and 10/5 (brown line). Dotted-lines represent the transition temperature. 74
- Figure 3.8 Internal electric field, dielectric susceptibility and polarization as a function of d_{FE}/d_{PE} at $T = 298K$. 75
- Figure 3.9 Polarization-applied electric field ($P - E_{ext}$) hysteresis loop and (b) Internal electric field-applied electric field ($E_{int} - E_{ext}$) hysteresis loop of a PT/ST superlattice with $d_{PT} = 15u.c.$, $d_{ST} = 5u.c.$ at $T = 298K$. 77
- Figure 3.10 The profiles of polarization and internal electric field at applied electric field: (a) $E_{ext} = 0$ (point A), (b) $E_{ext} \sim 0.99E_c$ (point B), (c) $E_{ext} = 1.1745 \times 10^8 \text{V/m} > E_c$ (point C). 78
- Figure 4.1 (a) Schematic illustrations for a PT/ST superlattice on a ST substrate with thicknesses of PT layer and ST layer are L_{PT} and L_{ST} respectively. Black arrows represent the direction of polarizations in the constituent layer. PT/ST superlattices with alternate interface charge of density σ_0 and their boundary conditions for the (b) type I and (c) type II interfaces. Internal electric field in the PT layer $E_{int,PT}$ (green arrows) is against the direction of PT polarization and acts as a depolarization field, $E_{int,PT} < 0$. The electrostatic coupling between ferroelectric PT layers leads to the appearance of internal electric field $E_{int,ST} > 0$ (green arrows) that tends to induce polarization in the ST layers. As the result of the appearance of alternate interface charge density $\pm\sigma_0$, a charge-induced electric field, $E_{\sigma,j}$ ($j : PT$ or ST) (red arrows) builds up in each layer, leading the existence of effective internal field $E_{eff,j}$ (blue arrows) in the constituent layer j . 84
- Figure 4.2 Polarization and internal electric field profiles of PT/ST superlattices with no interface charge. The values of λ_0 are: 0 (red line), $0.02\xi_0$ (blue line) and ξ_0 (brown line). 88
- Figure 4.3 Polarization and internal electric field profiles of PT/ST superlattices with interface of type I (red color) and type II (blue color) for different interface charge density σ_0 . In the figure, σ_0 represents the charge density at interface $z = 0$. Black lines are the profiles for charge-free superlattices σ_0 . The values of λ_0 is set as $0.01\xi_0$. 89
- Figure 4.4 Polarization mismatch Δp_I and internal field mismatch ΔE_I as a function of interface charge density σ_0 at $z = 0$ for three different thickness ratios L_{PT}/L_{ST} (unit cell) of 6/4, 5/5 and 4/6. The values of λ_0 are: $0.005\xi_0$ (red line), $0.01\xi_0$ (blue line), $0.016\xi_0$ (green line), and $0.02\xi_0$ (black line). Blue shaded area denotes the type I interface, whereas with the area shaded with red color corresponds to the type II case. In the figure, the charge-free superlattices are described by $\sigma_0 = 0$, which is located at the border between the two shaded areas. Dotted lines in the upper and lower figures indicate the ‘‘saturated’’ charge density σ_0^* and its corresponding Δp_I^* or ΔE_I^* . 91

- Figure 4.5 (a)Polarization and (b)internal electric field as a function of interface charge density σ_0 at $z = 0$ for three different thickness ratios L_{PT}/L_{ST} (unit cell) of 6/4, 5/5 and 4/6. The values of λ_0 are: $0.005\xi_0$ (red line), $0.01\xi_0$ (blue line), $0.016\xi_0$ (green line), and $0.02\xi_0$ (black line). Blue shaded area denotes the type I interface, whereas with the area shaded with red color corresponds to the type II case. 93
- Figure 4.6 (a) Polarization P and internal electric field E_{eff} as a function of period thickness for PT/ST superlattices with saturated interface charge density σ_0^* . The values of λ_0 are: $0.001\xi_0$ (*), $0.005\xi_0$ (◊) and $0.01\xi_0$ (×) for the superlattice with the type I interface, whereas $\lambda_0 \neq 0$ (△) represents the type II interface. Dash line with symbol (□) indicates a charge-free superlattice with $\lambda_0 = \xi_0$. 94
- Figure 5.1 Schematic illustrations for a BT/BST superlattice on a SmScO₃ substrate with thicknesses of BT layer and BST layer are L_{BT} and L_{BST} , respectively. Arrows represent the direction of polarization. 99
- Figure 5.2 Lattice parameter BST a_{BST} (green) and substrate-induced misfit strain (blue) in BST- x layer $u_{m,BST}$ of BT/BST superlattices grown on SmScO₃ at $T = 298K$ as a function of composition x . 104
- Figure 5.3 Polarization profiles of a BT/BST superlattice with only an in-plane component at $T = 298K$ with composition $x = 0.7, 0.4$ and 0 . The values of λ_0 are: 0 (red line), $0.01\xi_0$ (blue line) and ξ_0 (brown line). 105
- Figure 5.4 Mismatch in polarization at interface $P_{BT}(0) - P_{BST}(0)$ of a BT/BST superlattice at $T = 298K$ as a function of composition x . 106
- Figure 5.5 Polarization P of a BT/BST superlattice with only an in-plane component at $T = 298K$ as a function of composition x . The values of λ_0 are: 0 (red line), $0.001\xi_0$ (blue line) and ξ_0 (brown line). 107
- Figure 5.6 Schematic illustrations for a BT/BST superlattice on a SrTiO₃ substrate with thicknesses of BT layer and BST layer are L_{BT} and L_{BST} , respectively. Arrows represent the direction of polarization. 108
- Figure 5.7 Lattice parameter BST a_{BST} (green) and substrate-induced misfit strain (blue) in BST- x layer $u_{m,BST}$ of BT/BST superlattices grown on SrTiO₃ at $T = 298K$ as a function of composition x . 111
- Figure 5.8 Profiles of polarization $P(C/m^2)$ and internal electric field $E(V/m)$ of BT/BST superlattice with only an out-of-plane component at $T = 298K$ with composition $x = 0.7, 0.4$ and 0 . The values of λ_0 are: 0 (red line), $0.01\xi_0$ (blue line) and ξ_0 (brown line). 114
- Figure 5.9 Mismatch in polarization and internal electric field at interface of a BT/BST superlattice at $T = 298K$ as a function of composition x . 115
- Figure 5.10 Polarization P and internal electric field E of a BT/BST superlattice with only out-of-plane component at $T = 298K$ as a function of composition x . The values of λ_0 are: 0 (red line), $0.001\xi_0$ (blue line), $0.01\xi_0$ (green line) and ξ_0 (brown line). 116

LIST OF TABLES

Table 3.1	List of Helmholtz free energy coefficients used in this study	61
Table 5.1	The Helmholtz free energy coefficients for BT (Shirokov, Yuzyuk, Dkhil, & Lemanov, 2009) and ST (Dawber et al., 2007).	103
Table A1	The Voigt notation with axis 3 perpendicular to the interface.	134

LIST OF SYMBOLS AND ACRONYMS

C	Curie constant.
D	electric displacement.
E	electric field.
E_c	coercive field.
$E_{\sigma,j}$	charge-induced field of layer j .
E_{dj}	depolarization field of layer j .
$E_{eff,j}$	effective internal field of layer j .
E_{ext}	external electric field.
$E_{int,j}$	internal electric field of layer j .
F	Helmholtz free energy.
G	Gibbs free energy.
G_0	high symmetry group.
G_1	low symmetry group.
G_e	elastic Gibbs energy.
P	polarization.
P_r	remanent polarization.
P_s	spontaneous polarization.
P_{sat}	saturation polarization.
Q_{ij}	electrostrictive coefficients.
S	entropy.
T	temperature.
T_0	Curie-Weiss temperature.
T_c	Curie temperature or Curie point.
U	internal energy.
α, β, γ	Landau coefficients.
χ	dielectric susceptibility.
η	order parameter.
κ	gradient coefficient.
λ	interface parameter.
λ_0	temperature-independent interface parameter.
σ	stress.
σ_0	interface charge density.
ϵ_0	dielectric permittivity in vacuum.
ξ_0	characteristic length or correlation length.
a_0	equivalent cubic cell lattice constants of the free standing film.
a_s	lattice parameter of the substrate.
c_{ij}	elastic stiffness.
g_{ij}	electrostrictive constants.
s_{ij}	elastic compliances.
u	strain.
u_m	in-plane misfit strain induced by the substrate due to the lattice mismatch.
AFD	antiferrodistortive.
Ba	barium.
BST	barium strontium titanate, $\text{Ba}_x\text{Sr}_{1-x}\text{TiO}_3$.
BT	barium titanate, BaTiO_3 .
COBRA	coherence Bragg rod analysis.

DFT	density functional theory.
EELS	electron-energy-loss spectra.
FE	ferroelectric.
FeRAM	ferroelectric random access memory.
GMO	gadolinium molybdate.
HAADF	high-angle annular dark field.
KDP	potassium dihydrogen phosphate, KH_2PO_4 .
LG	Landau-Ginzburg.
LGD	Landau-Ginzburg-Devonshire.
MBE	molecular beam epitaxy.
MEMS	microelectro-mechanical system.
PE	paraelectric.
PT	lead titanate, PbTiO_3 .
RF	radio frequency.
Sr	strontium.
ST	strontium titanate, SrTiO_3 .

LIST OF APPENDICES

Appendix A	Voigt Notation	134
Appendix B	Dimensionless Scaling	135
Appendix C	Numerical Methods	138

CHAPTER 1

INTRODUCTION

1.1 Statement of Present Research

Ferroelectric offers a tantalizing potential in many technological applications such as transducers, high-permittivity dielectrics, pyroelectric sensors, piezoelectric devices, tunable ferroelectric capacitor and etc. (Lines & Glass, 1977). The studies of ferroelectric superlattices have attracted immense attention due to its fundamental scientific interest and potential applications (Scott, 2000; Dawber, Rabe, & Scott, 2005). When the ferroelectric system has superlattice or multilayer structures, intermixed layers may form at interfaces between the two layers. These interface intermixed with properties different from those of both layers may affect the properties of superlattices (Pertsev & Tyunina, 2011).

Landau-Ginzburg (LG) is one of the most widely used theoretical models and has long been successfully used to describe the physical properties of ferroelectric materials. Many theoretical studies of ferroelectric superlattices were carried out using the LG theory. The research described in this thesis was aimed to develop a thermodynamic model based on the LG theory to study interface intermixing in ferroelectric superlattices. We introduced an interface energy term in the Landau free energy to describe the formation of intermixed layer with properties different from each constituent layers. These intermixed layers are mutually coupled through the local polarization at interfaces. Furthermore, our model can be extended to take into account the influence of electrostatic coupling, misfit epitaxial strain, interface charge, composition effect and etc., on phase transition and ferroelectric properties in ferroelectric superlattices.

1.1.1 Objectives of present Work

In this research, a thermodynamic model based on the LG theory will be developed to study the polarization and dielectric behaviors in ferroelectric superlattices with nanometric thickness. The effects of interface, substrate-induced strain and electrostatic coupling will be considered in this study.

The specific objectives are:

1. To develop a thermodynamic model based on the Landau-Ginzburg theory for a ferroelectric/paraelectric superlattice with interface intermixed layer to explain the correlation between internal electric field, dielectric susceptibility and polarization.
2. Study the polarization reversal in ferroelectric superlattices with electrostatic coupling and interface intermixing effects.
3. Employ the aforementioned thermodynamic model to study the polarization discontinuity and screening charge in ferroelectric/paraelectric superlattices by considering the existence of screening charge at interface with equal but of opposite sign for alternate interface.
4. To investigate the effect of composition and interface intermixing on ferroelectricity of $\text{BaTiO}_3/\text{Ba}_x\text{Sr}_{1-x}\text{TiO}_3$ (BT/BST) superlattices.

1.1.2 Organization of the Thesis

Overall, this thesis is organized into six chapters. Chapter 1 starts with a brief introduction to what is ferroelectrics and its applications. The basic concepts such as symmetry in crystals, perovskite-oxide ferroelectrics, broken symmetry and order parameters are emphasized first in order to help readers understand the basic background before exploring the Landau phenomenological theory of ferroelectricity. A literature review on the ferroelectric superlattices is given in Chapter 2. A discussion of major factors that affect-

ing ferroelectric superlattices and an overview of phenomenological theory for ferroelectric superlattices are also included. Finally, we will discuss our proposed thermodynamic model based on LG theory to study the ferroelectric phase transitions in superlattices. In Chapter 3, a detailed discussion on electrostatic coupling and interface intermixing in ferroelectric superlattices will be given. The formalism and the detailed calculation for superlattices will be provided. We will discuss the properties of superlattices for instance, polarization, internal electric field, dielectric susceptibility and also the polarization reversal. Chapter 4 gives a detailed discussion of polarization discontinuity and screening charges by taking into account the presence of charges of density at the internal interfaces in superlattices. Chapter 5 is devoted to the study of the effect of composition and interface intermixing on ferroelectric properties of $\text{BaTiO}_3/\text{Ba}_x\text{Sr}_{1-x}\text{TiO}_3$ (BT/BST) superlattices. Conclusions and future works are presented in Chapter 6.

1.2 Introduction to Ferroelectrics and its Applications

The duality symmetry in classical electromagnetic theory was discovered more than a century ago by Heaviside (Heaviside, 1892). He showed that the electric field is the dual of the magnetic field. Similarly, the ferroelectricity is the dual of ferromagnetism because they are in many ways analogous to each other. A ferromagnetic has a spontaneous magnetic moment even in zero applied magnetic field. Analogously, a ferroelectric also exhibits a spontaneous electric dipole moment even in zero applied electric field. These two phenomena have received a sustained study since the early of 20th century.

The term ferroelectric from German “ferroelektrisch” was first coined by Erwin Schrödinger in 1912 (Schrödinger, 1912) before the first discovery of ferroelectricity in Rochelle salt by Valasek in 1920 (Valasek, 1920, 1921). By extending the Debye’s theory of liquid dielectric, he speculated that in solids below a certain temperature, an electric polarization which is analogous to the magnetization, ought to be expected in the absence of an electric field (Joas & Katzir, 2011). Ferroelectricity is a collective phenomena and all ferroelectric materials are both piezoelectric and pyroelectric. To be more precise, they are polar materials that possess at least two equilibrium orientations of the spontaneous polarization vector in the absence of an external electric field. This spontaneous polarization vector can be switched between those orientations by an electric field. Piezoelectric is a class of materials which can be polarized in response to applied mechanical stress, whereas the pyroelectric materials exhibit an electric dipole moment even in the absence of an external electric field. The schematic description of the relations among piezoelectricity, pyroelectricity and ferroelectricity are shown in Fig. 1.1.

Ferroelectric has been found in variety of compounds, for instance, hydrogen-bonded systems such as potassium dihydrogen phosphate (KDP or KH_2PO_4), polymeric systems and the family of ABO_3 compounds. According to traditional view, ferroelectric phase

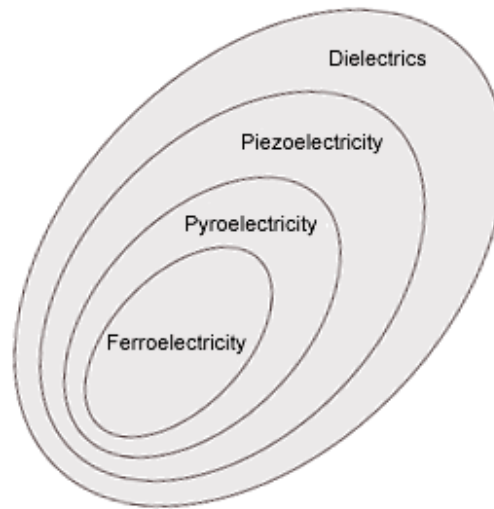


Figure 1.1: Relations among piezoelectricity, pyroelectricity and ferroelectricity.

transitions are commonly classified as either displacive or order-disorder type. The atom in the crystal begins to displace at the phase transition point and the displacement leads to a change in crystal symmetry, such a transition is termed displacive (e.g., BaTiO₃). In case of order-disorder type, a change of symmetry occurs as a result of the redistribution of particles or ions over equiprobable positions at the transition temperature (e.g., hydrogen-bonded system such as KDP). However, the aforementioned classification is not generally applicable in ferroelectrics because a phase transition may demonstrate both displacive and order-disorder features. Recently, the experimental evidence for the coexistence of these two behaviours was found in hydrogen-bonded order-disorder systems like squaric acid, namely H₂SQ and D₂SQ (Dalal, Klymchyov, & Bussmann-Holder, 1998). The detailed description of this intriguing subject is beyond the scope of this thesis. Interested readers are advised to refer the book by Dalal and Bussmann-Holder (Dalal & Bussmann-Holder, 2007) and references therein.

Ferroelectric materials are of technologically important due to its useful properties in wide range of potential applications. Due to the high permittivity of ferroelectrics, it can be used as a non-volatile random access memories or so-called ferroelectric random access memory (FeRAM) for smart cards and portable electronic devices. Its memory

will not lose even after the supply of voltage is switched off. The large dielectric susceptibility of ferroelectrics is used in capacitor applications as they have smaller physical size compared to other dielectric materials. The high piezoelectric effect of these materials is applied in a variety of electromechanical sensors, actuators, transducers, and microelectro-mechanical system (MEMS). Ferroelectric materials are also pyroelectric and they are very useful for pyroelectric detectors or sensors. The electro-optic effect (the change in refractive index with an external applied electric field) of ferroelectrics can be used for the modulation of light or optical waveguides, which are very important for optical communication systems. Ferroelectrics in paraelectric phase have a very high potential in varactor technologies for radio frequency (RF) or microwave tunable devices.

1.3 Symmetry in Crystals

The notion of symmetry is the most powerful and intriguing principle to perceive and describe the inner workings of nature. In short, symmetry is an operation or transformation that doesn't change how thing behaves relative to the outside world. The structure of crystals can be described by symmetry transformations, such as, rotational, inversion, translational symmetries etc. In fact, symmetry can be used to study the invariant aspects of physical properties, physical interactions and physical laws under certain transformations.

The Neumann's principle states that "*The symmetry elements of any physical property of a crystal must include the symmetry elements of the point group of the crystal*" (Nye, 1972). This means that if a physical property is subjected to a symmetry operation of this crystal, the value of this property should remain invariant. As a result, it explains why some properties (such as dielectric permittivity, elastic compliance and electrostriction) are present in all materials and that other properties (such as piezoelectricity and pyroelectricity) can exist only in materials with certain symmetries (Damjanovic, 1998).

The point group of a crystal is the group of macroscopic symmetry elements that its structure possesses. This principle is the basis for the division of crystals into 32 point groups.

The crystalline lattices can be classified into 32 crystallographic point groups. These 32 point groups can be divided into two classes, 11 of them belong to centrosymmetric groups and the remaining 21 are non-centrosymmetric groups. These 11 centrosymmetric groups contain an inversion center and do not have polar properties because any polar vector may be inverted by an existing symmetry transformation. 20 of the non-centrosymmetric groups can exhibit the piezoelectric effect and are called piezoelectric point groups. 10 out of the 20 piezoelectric point groups have a unique polar axis and may exhibit a spontaneous polarization in the absence of an external electric field, and are known as 10 pyroelectric point groups. Among the pyroelectric crystals, those whose direction of spontaneous polarization can be reversed by the external electrical field are called ferroelectrics. Hence, ferroelectric materials have to be pyroelectrics and piezoelectrics, but the reverse is not true. Fig. 1.2 display a schematic description of the classification of crystal according to their structures and properties.

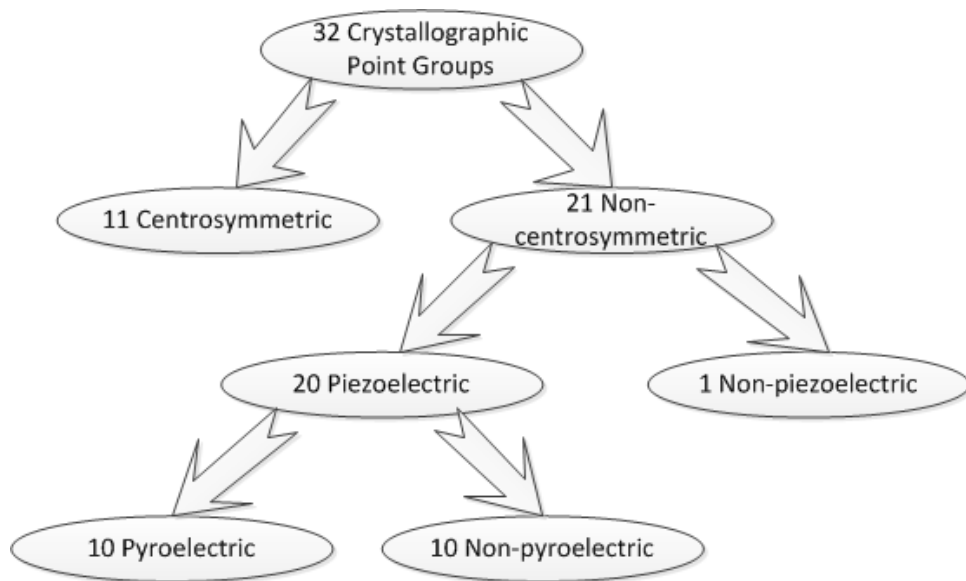


Figure 1.2: Classification of crystals according to their structure and properties. Ferroelectric materials have to be pyroelectrics and piezoelectrics.

1.4 Perovskite-oxide Ferroelectrics

Most of the ferroelectric oxides belong to the family of perovskite oxides. The chemical formula of perovskite structure is represented by ABO_3 , where “A” and “B” are cations and “O” is an anion, oxygen. Generically, the valence of A cations is from +1 to +3 and B cations is from +3 to +6. The typical perovskite structure is shown in Fig. 1.3. It can be seen that the A cation has fractional coordinates given by $(1/2, 1/2, 1/2)$, the B cation is located at the origin, and the coordinates of oxygen atoms are $(1/2, 0, 0)$, $(0, 1/2, 0)$ and $(0, 0, 1/2)$ (Dove, 2003).

The role of symmetry can be illustrated by the ferroelectric tetragonal phase of a perovskite material such as $PbTiO_3$, as shown schematically in Fig. 1.3. At the high temperature paraelectric phase, the ferroelectric oxides exhibit a high symmetry of cubic phase with space group $Pm\bar{3}m$. When the temperature approaches the transition point, these compounds undergo a structural phase transitions leading to ferroelectricity with a low symmetry non-centrosymmetric of tetragonal phase with space group $P4mm$. Most ferroelectrics with perovskite structure undergo a displacive phase transitions. However, order-disorder dynamics are also found in these perovskite systems, such as $BaTiO_3$ and $SrTiO_3$ (Dalal & Bussmann-Holder, 2007). In case of displacive phase transitions, it involves an ionic displacement in such a way that the symmetry of the crystal is changed.

In the case of $PbTiO_3$, it is cubic and paraelectric at high temperature and the crystal transforms to ferroelectric tetragonal phase at 490°C . In the ferroelectric phase of $PbTiO_3$, the direction of spontaneous polarization is along the c_T -axis of the tetragonal unit cell. In fact, the dipole originates from the displacement of O and Ti ions relative to Pb. The crystal is spontaneously strained with $a_T \ll a_C < c_T$ where a_T and a_C are the a -axes of the tetragonal and cubic unit cell (Damjanovic, 1998).

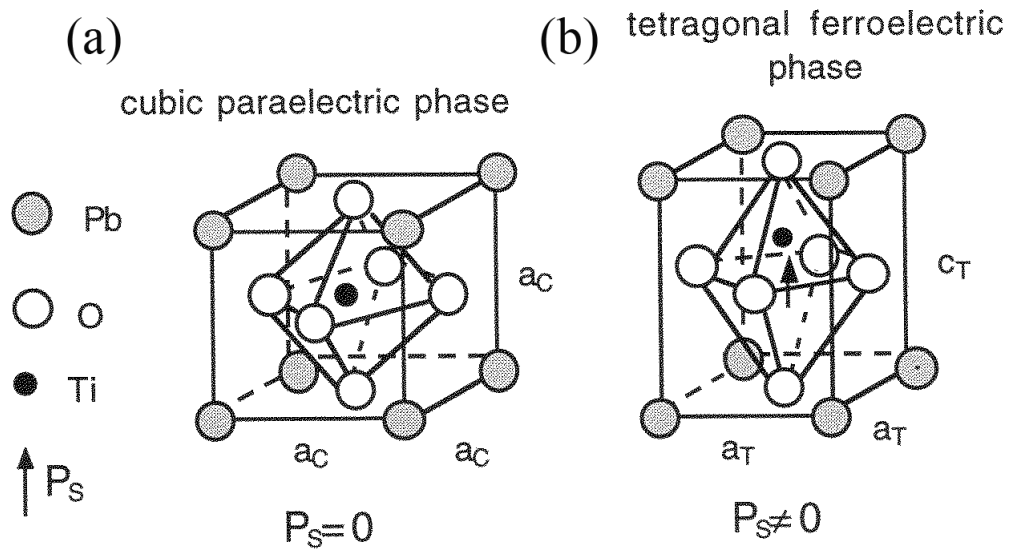


Figure 1.3: Perovskite structure of the ferroelectric oxide PbTiO_3 . (a) high temperature paraelectric phase with cubic structure, (b) low temperature ferroelectric phase with tetragonal structure (Damjanovic, 1998).

1.5 Symmetry and Order Parameters

L. D. Landau is probably the first person to realize the important role of symmetry plays in the phase transitions of equilibrium condensed matter systems. The Landau theory of phase transitions is basically relied on two closely related important concepts: broken symmetry and order parameter (Landau & Lifshitz, 1980). On one hand, the broken symmetry is of prime importance and it can be met in diverse realm of physics, such as particle physics, cosmology and astrophysics, condensed matter physics, etc. On the other hand, the concept of order parameter is the essence of Landau theory, it is zero in the symmetric state and has a non-zero value when the symmetry is broken.

1.5.1 Broken Symmetry

Generally, a phase transition may or may not be associated with a change of symmetry. In fact, a given symmetry element is either present or absent and there is no intermediate state of symmetry. If a symmetry change is involved, a system cannot change continuously between two phases of different symmetry. For instance, the transition from liquid to solid states cannot occur in a continuous manner. However, a continuous path is

only possible if there is no symmetry change involved, such as transition between liquid and gaseous states which is also known as isomorphic transition (Ginzburg, Sobyenin, & Levanyuk, 1983). As P. W. Anderson used to express it as “*Symmetry cannot change continuously: what I have called the first theorem of condensed matter physics*” (Anderson, 2004)

Most ferroelectric materials undergo a structural phase transition from a high temperature paraelectric phase into a low temperature ferroelectric phase. The temperature at the phase transition occurs is called the Curie temperature or Curie point (T_c). In this case, the phase transition is accompanied by a change of symmetry. Under the transformation from the higher to the lower temperature phase, some symmetry elements of the high temperature phase are lost on cooling below T_c . In fact, we might denote G_0 as the high symmetry group of high temperature paraelectric phase and G_1 for the low symmetry group of low temperature ferroelectric phase. It is a fact that the symmetry group G_1 of the new (ferroelectric) phase is always less symmetrical than the old (paraelectric) phase, therefore the symmetry group G_1 is a subgroup of the group G_0 . In brevity, the more symmetrical phase will be termed as the symmetrical one and the less symmetrical phase will be called as non-symmetrical one (Ginzburg et al., 1983).

In reality, the ferroelectric phase transitions are directly related to broken symmetry. The paraelectric phase is a fully disordered phase, it is the broken symmetry that leads it to the ordered phase (ferroelectric) with the value of order parameter (polarization) to be different from zero. This breaking of symmetry at low temperature is also known as spontaneous symmetry breaking. Actually, the ferroelectric phase transitions is associated with broken space inversion symmetry (Feng & Jin, 2005) which is a discrete symmetry group, for example the reflection group $z \rightarrow -z$ is broken (Blinic & Žekš, 1974). This discrete symmetry also known as Ising symmetry and it is invariant under Z_2

group (Chaikin & Lubensky, 1995). In other words, we can say that the system breaks the space inversion invariance “spontaneously”.

Anderson emphasized that the appearance of *generalized rigidity* is actually responsible for the unique properties of the ordered (broken-symmetry) states (Anderson, 1984). The energy is minimized when the symmetry is broken, therefore the system has a strong energetic preference to stay in that broken state. Furthermore, the system tends to resist any attempt from the outside to alter its ordered states. In ferroelectric phase transition, the generalized rigidity phenomenon is literally the ferroelectric hysteresis (Anderson, 1984). A detailed description on ferroelectric hysteresis will be presented in Section 1.7. If a discrete symmetry is broken differently in two adjacent parts of a macroscopic system, the boundary that separates two distinct but energetically equivalent states in system will contain a topological defect (Blundell, 2001). It is known as domain wall in ferroelectric system, these thin boundaries are located at a specific crystal plane and cannot move continuously in space. They must overcome an activation energy to move to the next (Anderson, 1984).

When a symmetry is broken, a phase transition takes place and the system is perfectly ordered. At finite temperature this order is weakened by excitations in the order parameter. In ferroelectric these excitations are called soft modes which emerge upon symmetry breaking (Anderson, 1984; Blundell, 2001). The fundamental concept of the soft mode is that, when a ferroelectric material undergoes a structural phase transition close to the tricritical point, the frequency of one or several normal modes of a crystal lattice tends to zero or greatly decreases (Ginzburg, 2005). A detailed discussion of this soft modes concept can be found in the book by Blinc & Žekš, 1974.

In fact, the concept of broken symmetry can be used to describe the two mechanisms in ferroelectric transitions, namely, displacive and order-disorder types (Blinc, 2011). In the case of displacive ferroelectrics, a discrete symmetry group is broken at T_c and the

phase transition is the result of an instability of the anharmonic crystal lattice against soft polar lattice vibration. On the other hand, in an order–disorder system, a discrete symmetry group is broken due to the ordering of the ions in a rigid lattice potential. However, it should be emphasized that there is no clear boundary line that exists between these two phase transitions. This is because from the perspective of symmetry, there is no difference at all between the two of them (Strukov & Levanyuk, 1998).

1.5.2 Order Parameters

The concept of order parameter is a starting point for Landau theory. It was first introduced by Landau to describe the aspect of the loss of symmetries as the crystal undergoes a transition from a high symmetry phase G_0 to a low symmetry phase G_1 . The order parameter varies in such a way that it vanishes above the Curie temperature, T_c (a high symmetry phase) and has a finite value below the T_c (a low symmetry phase).

In fact, the order parameter is a physical quantity that characterizes the magnitude of the atomic displacement or the degree of their ordering which represents the crystal reconstruction under the phase transition (Ginzburg et al., 1983). It may be a scalar, a vector, a complex number or a more complicated quantity with multicomponents. Moreover, the order parameter can be considered as a field because the state of a system is expressed in terms of a quantity η , which is a function of the position \vec{x} . It can be considered as a mapping from real space into order parameter space (Sethna, 2006; Chaikin & Lubensky, 1995). One can refer the example from the book by Tagantsev, Cross and Fousek (Tagantsev, Cross, & Fousek, 2010) and references therein for the mapping of domain state onto the order parameter space for an improper ferroelectric of gadolinium molybdate (GMO). Hence, we can say that Landau theory is essentially a field theory.

In general, there are two types of phase transitions, first order and second order transition. For the case of first order transition, the order parameter exhibits a discontinuity

change or has a jump at the transition temperature. The two symmetry groups for the high symmetry phase and the low symmetry phase may or may not have any group-subgroup relationship to each other. On the other hand, the order parameter will be a continuous function of temperature in second order transition. The variation of the temperature dependence of order parameter η in the region of structural phase transition are shown in Fig. 1.4. Evidently, the Fig. 1.4(a) shows a second order phase transition and Fig. 1.4(c) corresponds to a first order type. It should be mentioned that there is a case where a first order phase transition close to a second order transition as shown in Fig. 1.4(b).

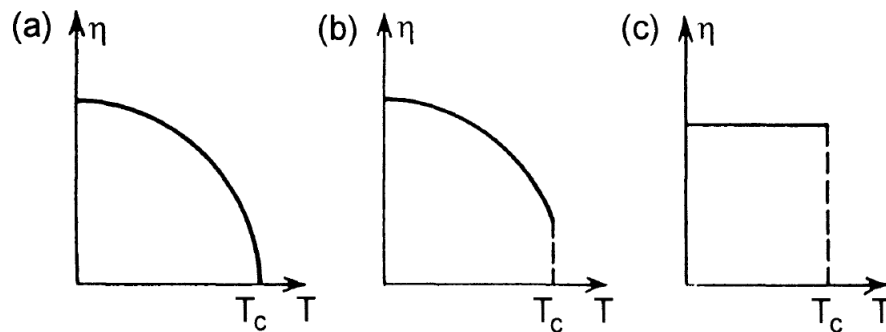


Figure 1.4: Temperature dependence of the order parameter in case of a second order transition (a), first order close to second order transition (b) and in case of first order transition (c). (Strukov & Levanyuk, 1998)

In ferroelectric systems, the order parameter is the polarization vector P whose appearance at the Curie point breaks the symmetry of the paraelectric phase. P is a thermodynamic variable and its magnitude signifies the difference between the non-symmetrical and symmetrical lattice structures. This order parameter also indicates the inner deformation or atomic configuration under phase transition. To illustrate, the order parameter in displacive transitions characterizes the degree of displacement of certain ions or ionic groups (the long range ordering of induced dipoles), whereas the order parameter in order-disorder transitions determines the amount of long range ordering of permanent dipoles (Blinic & Žekš, 1974).

The formula of Landau theory is the expression of thermodynamic potential as a function of order parameter. By minimizing the thermodynamic potential, which is also at the condition of thermal equilibrium, one can find the equilibrium value of P .

1.6 Phenomenological Theory of Ferroelectricity

The phenomenological theory of ferroelectricity was first proposed by V. L. Ginzburg in 1945 (Ginzburg, 1945). Later in 1949, A. F. Devonshire independently developed the same approach (Devonshire, 1949) but omitted some important invariants with P^6 which is admitted by the symmetry and essential in the case of a first-order transition (Ginzburg, 2005). Hence, the phenomenological theory of ferroelectricity is also known as Landau-Ginzburg-Devonshire (LGD) theory.

There are many classical books such as Blinc & Žekš, 1974; Lines & Glass, 1977; Strukov & Levanyuk, 1998, which give a very comprehensive treatise on the formalism of Landau theory in ferroelectrics. Generically, Landau theory is a phenomenological theory which based on symmetry consideration and thermodynamic principles. It is purely a macroscopic theory which equivalent to a mean field theory and cannot describe any microscopic quantities that lead to a phase transition, for example atomic displacement and forces.

The central Ansatz of Landau theory is that the thermodynamic potential can be Taylor expanded in powers of order-parameter in the vicinity of phase transition (Chandra & Littlewood, 2007). In fact, thermodynamic potential also known as free energy, such as Gibbs free energy and Helmholtz free energy. The parameter of this phenomenological theory can, in principle, be determined either by comparison to experiment or from first principle calculation.

1.6.1 Thermodynamic Relations

One can always use different type of thermodynamic potentials to describe the properties of a materials and the choice is simply a matter of convenience. A detail discussion can be found in Lines & Glass, 1977; Defaÿ, 2011. The thermodynamic potential of any system in equilibrium can be defined as a function of three independent variables which can be chosen in eight different ways from the so-called conjugate pairs (Lines & Glass, 1977), namely temperature (T) and entropy (S) for thermal properties, stress (σ) and strain (u) for mechanical properties, and electric field (E) and electric displacement (D) or polarization (P) for dielectric properties. These conjugate pairs can be divided into two variables, i.e. intensive variables (temperature, stress and electric field) and extensive variable (strain, entropy, electric displacement, polarization). An extensive variable has a value that changes depending on the size of the system whereas an intensive variable remains constant (Defaÿ, 2011).

Starting from the first law of thermodynamic, the infinitesimal change of internal energy U is the sum of infinitesimal variation of heat δQ and work δW .

$$dU = \delta Q + \delta W = TdS + \sigma_i du_i + E_i dP_i \quad (1.1)$$

The following two thermodynamic potentials are the most common for the study of ferroelectric (Fatuzzo & Merz, 1967):

$$\text{Helmholtz free energy: } F = U - TS \quad (1.2a)$$

$$\text{Elastic Gibbs energy: } G_e = U - TS - \sigma u \quad (1.2b)$$

Their corresponding differential relations describing infinitesimal changes are:

$$dF = -SdT + \sigma_i du_i + E_i dP_i \quad (1.3a)$$

$$dG_e = -SdT - u_i d\sigma_i + E_i dP_i \quad (1.3b)$$

Henceforth, the function elastic Gibbs energy, G_e will be denoted simply as Gibbs free energy, G .

1.6.2 Multiaxial Ferroelectrics (Multicomponent Order Parameters)

Normally, Gibbs free energy is the most convenient thermodynamic potential. It is expressed as a function of temperature, stress and polarization. G can be expanded as follows (Haun, Furman, Jang, McKinsty, & Cross, 1987):

$$\begin{aligned} G = & \alpha (P_x^2 + P_y^2 + P_z^2) + \beta_{11} (P_x^4 + P_y^4 + P_z^4) + \beta_{12} (P_y^2 P_z^2 + P_z^2 P_x^2 + P_x^2 P_y^2) \\ & + \gamma_{111} (P_x^6 + P_y^6 + P_z^6) + \gamma_{112} [P_x^4 (P_y^2 + P_z^2) + P_y^4 (P_x^2 + P_z^2) + P_z^4 (P_y^2 + P_x^2)] \\ & + \gamma_{123} P_x^2 P_y^2 P_z^2 - \frac{1}{2} s_{11} (\sigma_1^2 + \sigma_2^2 + \sigma_3^2) - s_{12} (\sigma_1 \sigma_2 + \sigma_1 \sigma_3 + \sigma_2 \sigma_3) \\ & - \frac{1}{2} s_{44} (\sigma_4^2 + \sigma_5^2 + \sigma_6^2) - Q_{11} (\sigma_1 P_x^2 + \sigma_2 P_y^2 + \sigma_3 P_z^2) \\ & - Q_{12} [\sigma_1 (P_y^2 + P_z^2) + \sigma_2 (P_x^2 + P_z^2) + \sigma_3 (P_y^2 + P_x^2)] \\ & - 2Q_{44} [\sigma_4 P_y P_z + \sigma_5 P_x P_z + \sigma_6 P_y P_x], \end{aligned} \quad (1.4)$$

where P_i are the polarization and σ_i ($i = 1, 2, \dots, 6$ in the Voigt matrix notation¹) is the stress, α, β, γ are the Landau coefficients and only α is temperature dependence, s_{ij} are the elastic compliances of the material and Q_{ij} are the electrostrictive coefficients at constant polarization.

¹Please refer to Appendix A

The Helmholtz free energy can be expanded in polarization and strain components as below:

$$\begin{aligned}
F = & \alpha (P_x^2 + P_y^2 + P_z^2) + \beta'_{11} (P_x^4 + P_y^4 + P_z^4) + \beta'_{12} (P_y^2 P_z^2 + P_z^2 P_x^2 + P_x^2 P_y^2) \\
& + \gamma_{111} (P_x^6 + P_y^6 + P_z^6) + \gamma_{112} [P_x^4 (P_y^2 + P_z^2) + P_y^4 (P_x^2 + P_z^2) + P_z^4 (P_y^2 + P_x^2)] \\
& + \gamma_{23} P_x^2 P_y^2 P_z^2 + \frac{1}{2} c_{11} (u_1^2 + u_2^2 + u_3^2) + c_{12} (u_1 u_2 + u_1 u_3 + u_2 u_3) \\
& + \frac{1}{2} c_{44} (u_4^2 + u_5^2 + u_6^2) - g_{11} (u_1 P_x^2 + u_2 P_y^2 + u_3 P_z^2) \\
& - g_{12} [u_1 (P_y^2 + P_z^2) + u_2 (P_x^2 + P_z^2) + u_3 (P_y^2 + P_x^2)] \\
& - 2g_{44} [u_4 P_y P_z + u_5 P_x P_z + u_6 P_y P_x], \tag{1.5}
\end{aligned}$$

where α, β', γ are Landau coefficients, u_i ($i = 1, 2, \dots, 6$ in the Voigt matrix notation) are the strain, c_{ij} are the elastic stiffness, g_{ij} are the electrostrictive constants. It should be noted that the Landau coefficient β'_{ij} in Eq.(1.5) are not equal to β_{ij} in Eq.(1.4).

1.6.2.1 Legendre Transformation

It is possible to change the independent variables of the thermodynamic potential from the original set to other by performing a Legendre transformation. The relationship between $F(P_i, u_j)$ and $G(P_i, \sigma_j)$ is given by the Legendre transformation (Sethna, 2006; Iwata, Orihara, & Ishibashi, 2001):

$$G(P_i, \sigma_j) = F(P_i, u_j) - \sum_{k=1}^6 u_k \frac{\partial F(P_i, u_k)}{\partial u_k} \tag{1.6}$$

$$G(P_i, \sigma_j) = F(P_i, u_j) - \sum_{k=1}^6 u_k \sigma_k \tag{1.7}$$

In order to change the set of independent variables of Helmholtz energy (P, u) to Gibbs energy (P, σ), we use $\frac{\partial F(P_i, u_k)}{\partial u_k} = \sigma_k$ and solve the system of equations in order to obtain the strain u_k ($i = 1, 2, \dots, 6$) in term of P and σ . After some lengthy and tedious

mathematical manipulations, we obtain the relationship between the parameters:

$$\beta_{11} = \beta'_{11} - \frac{1}{2} \frac{c_{11}(g_{11}^2 + 2g_{12}^2) + c_{12}(g_{11}^2 - 4g_{11}g_{12})}{(c_{11} - c_{12})(c_{11} + 2c_{12})}, \quad (1.8)$$

$$\beta_{12} = \beta'_{12} - \frac{1}{2} \frac{g_{44}^2}{c_{44}} - \frac{1}{2} \frac{c_{11}(2g_{11}g_{12} + g_{12}^2) - c_{12}(g_{11}^2 + 2g_{12}^2)}{(c_{11} - c_{12})(c_{11} + 2c_{12})}, \quad (1.9)$$

and

$$\begin{aligned} Q_{11} &= \frac{(c_{11} + c_{12})g_{11} - 2c_{12}g_{12}}{(c_{11} - c_{12})(c_{11} + 2c_{12})}, \\ Q_{12} &= \frac{c_{11}g_{12} - c_{12}g_{11}}{(c_{11} - c_{12})(c_{11} + 2c_{12})}, \\ Q_{44} &= \frac{g_{44}}{c_{44}}, \end{aligned} \quad (1.10)$$

and

$$\begin{aligned} s_{11} &= \frac{c_{11} + c_{12}}{(c_{11} - c_{12})(c_{11} + 2c_{12})}, \\ s_{12} &= -\frac{c_{12}}{(c_{11} - c_{12})(c_{11} + 2c_{12})}, \\ s_{44} &= \frac{1}{c_{44}}. \end{aligned} \quad (1.11)$$

Similarly, the conversion of Gibbs free energy coefficients to Helmholtz free energy coefficients are given as:

$$\beta'_{11} = \beta_{11} + \frac{1}{2} \frac{c_{11}(g_{11}^2 + 2g_{12}^2) + c_{12}(g_{11}^2 - 4g_{11}g_{12})}{(c_{11} - c_{12})(c_{11} + 2c_{12})}, \quad (1.12)$$

$$\beta'_{12} = \beta_{12} + \frac{1}{2} \frac{g_{44}^2}{c_{44}} - \frac{1}{2} \frac{c_{11}(2g_{11}g_{12} + g_{12}^2) - c_{12}(g_{11}^2 + 2g_{12}^2)}{(c_{11} - c_{12})(c_{11} + 2c_{12})}. \quad (1.13)$$

Following from Eqs.(1.10), the corresponding electrostrictive constants are given as

$$\begin{aligned}
g_{11} &= 2c_{12}Q_{12} + Q_{11}c_{11}, \\
g_{12} &= c_{11}Q_{12} + c_{12}Q_{11} + c_{12}Q_{12}, \\
g_{44} &= Q_{44}c_{44},
\end{aligned} \tag{1.14}$$

and the elastic stiffnesses from Eqs.(1.11) are

$$\begin{aligned}
c_{11} &= \frac{s_{11} + s_{12}}{(s_{11} - s_{12})(s_{11} + 2s_{12})}, \\
c_{12} &= -\frac{s_{12}}{(s_{11} - s_{12})(s_{11} + 2s_{12})}, \\
c_{44} &= \frac{1}{s_{44}}.
\end{aligned} \tag{1.15}$$

1.6.3 Uniaxial Ferroelectrics (One-component Order Parameter)

Now going back to the more commonly used Gibbs energy, Eq.(1.4) and discuss the simple case when the stress is zero. For simplicity, we assume that the polarization of ferroelectric system lies along a single direction with only one component order parameter (polarization P). The Gibbs energy, Eq.(1.4) also known as Landau free energy is represented as

$$F(P, T) = \int dV \left[\frac{1}{2}\alpha P^2 + \frac{1}{4}\beta P^4 + \frac{1}{6}\gamma P^6 + \frac{\kappa}{2}(\nabla P)^2 + \dots - EP \right], \tag{1.16}$$

where the ellipsis denotes higher order terms. The volume integrals are over the bulk ferroelectric. The introduction of factor 1/2, 1/4 and 1/6 are for the ease of calculation. κ is the gradient coefficient and together with $(\nabla P)^2$ they are known as Ginzburg or gradient term, which is account for the spatial variations and fluctuations of the order parameter, P (Strukov & Levanyuk, 1998). Due to the fact that ferroelectric crystal lattice

has a centre of symmetry and the free energy will be invariant with polarization reversal ($P \rightarrow -P$), the odd terms of the above expansion are vanished.

At present, we consider the case when the order parameter is homogeneous throughout the system so that the Ginzburg term is neglected. The functional of Eq.(1.16) becomes

$$F(P, T) = \frac{1}{2}\alpha P^2 + \frac{1}{4}\beta P^4 + \frac{1}{6}\gamma P^6 + \dots - EP, \quad (1.17)$$

In general, the coefficients β and γ can be assumed to be temperature independent whereas α is not. In particular the coefficient α can be approximated by a Taylor series in powers of $(T - T_0)$ and by keeping only the first order term

$$\alpha = \alpha_0(T - T_0); \quad C = \frac{1}{\alpha_0}, \quad (1.18)$$

where C is the Curie constant and T_0 is the Curie-Weiss temperature which is equal to or lower than the actual transition temperature T_c . Hence, the coefficient α must be negative for the ferroelectric state to be stable.

The equilibrium states are characterized by minima of the free energy

$$\frac{\partial F}{\partial P} = 0 = E - P(\alpha + \beta P^2 + \gamma P^4), \quad (1.19)$$

$$\frac{\partial^2 F}{\partial P^2} = \chi^{-1} = \alpha + 3\beta P^2 + 5\gamma P^4 > 0, \quad (1.20)$$

where χ is the dielectric susceptibility. Eq.(1.19) and Eq.(1.20) are the essential and stability condition for the minima of F .

1.6.3.1 Paraelectric Phase

For the stability of paraelectric phase, Eq.(1.19) is solved by $P = 0$ and the Eq.(1.20) now becomes $\chi^{-1} = \alpha = \alpha_0(T - T_0) > 0$. Evidently, the α must be positive for the

paraelectric phase to be stable at high temperature and T must be larger than T_0 . A comparison of Eq.(1.18) and Eq.(1.20) thus result in a Curie-Weiss law for the dielectric susceptibility of the paraelectric phase:

$$\chi = \frac{C}{T - T_0}. \quad (1.21)$$

1.6.3.2 Ferroelectric Phase - Second Order Transition

If $\beta > 0$, a second order transition occurs at $T = T_0$ to the ferroelectric state. The sixth and higher order terms in Eq.(1.17) are often ignored. For zero applied electric field fro Eq.(1.19), we have

$$\frac{\partial F}{\partial P} = P(\alpha_0(T - T_0) + \beta P^2) \quad (1.22)$$

with the solution either $P = 0$ or $P^2 = -\alpha_0(T - T_0)/\beta$. For $T < T_0$, a spontaneous polarization P_s exists and the result is:

$$P_s = \left[\frac{\alpha_0}{\beta}(T_0 - T) \right]^{1/2}. \quad (1.23)$$

The spontaneous polarization P_s will increase while the temperature start to decrease from the point $T = T_0$. Therefore, the phase transition occurs when the Curie temperature T_c is equal to the Curie-Weiss temperature T_0 . It will evolve continuously as a function of temperature.

The corresponding dielectric susceptibility is obtained by inserting Eq.(1.23) into Eq.(1.20) with $\gamma = 0$

$$\chi = \frac{C}{2(T - T_0)} \quad (T < T_0). \quad (1.24)$$

It should be noticed that the dielectric susceptibility becomes infinite at the transition temperature.

Fig. 1.5 schematically shows the free energy as a function of polarization at various temperature for the second order phase transition. For $T > T_c$ a minimum is found at $P = 0$. When T is below T_c , the minimum of the free energy gradually shifts to a finite value of P_s .

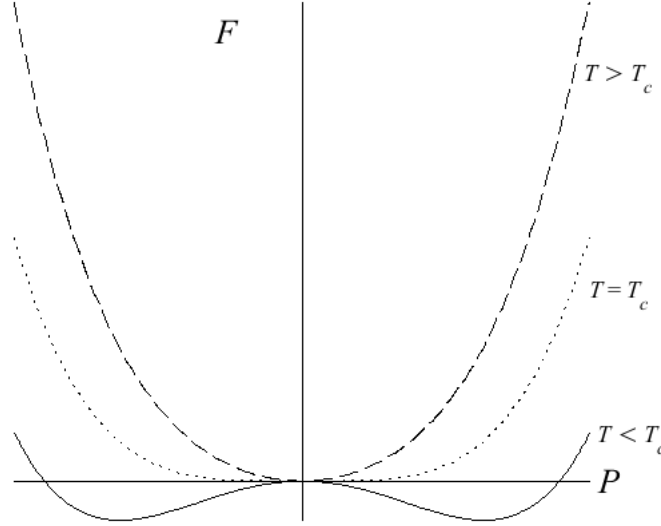


Figure 1.5: Free energy as a function of polarization at various temperature for second order phase transition.

1.6.3.3 Ferroelectric Phase - First Order Transition

For first order transition, β is chosen as negative and $\gamma > 0$. The equilibrium condition for $E = 0$ will be defined by Eq.(1.19) with solution $P = 0$ or

$$P_s^2 = \left\{ |\beta| + \sqrt{\beta^2 - 4\alpha_0\gamma(T - T_0)} \right\} / 2\gamma. \quad (1.25)$$

In order to fulfil the condition $\partial^2 F / \partial P^2 > 0$, the positive sign in the bracket is required to obtain a stable state. We can obtain the transition temperature T_c based on the condition that the free energy of paraelectric and ferroelectric are equal, $F(0, T) = F(P_s, T)$. At this temperature $T = T_c$:

$$T_c = T_0 + \frac{3}{16} \frac{\beta^2}{\alpha_0\gamma}. \quad (1.26)$$

On substituting Eq.(1.25) into free energy Eq.(1.20), the dielectric susceptibility of the first order transition is obtained as:

$$\chi^{-1} = \frac{\beta^2}{\gamma} \sqrt{\left(1 - \frac{4\alpha_0\gamma}{\beta^2}(T - T_0)\right)} \left\{ \sqrt{\left(1 - \frac{4\alpha_0\gamma}{\beta^2}(T - T_0)\right)} + 1 \right\}. \quad (1.27)$$

Fig. 1.6 shows the first order phase transition from the paraelectric state to ferroelectric state. When $T \gg T_c$, the free energy shows a parabolic shape with a minimum correspond to a stable paraelectric phase. During cooling and temperature still higher than T_c , the depth of central minima is lower than the two side minima. During this time, the ferroelectric phase is metastable whereas the paraelectric phase is stable. Upon further decreasing the temperature, the central minimum has the same depth as the two other minima at $T = T_c$. The temperature at this point is given by Eq.(1.26) and the free energies of the paraelectric and ferroelectric are equal. When $T_0 < T < T_c$, there is a co-existence of the paraelectric phase and the ferroelectric phase with the paraelectric phase being metastable. For T below T_0 , the free energy has two minima which correspond to $P = \pm P_s$.

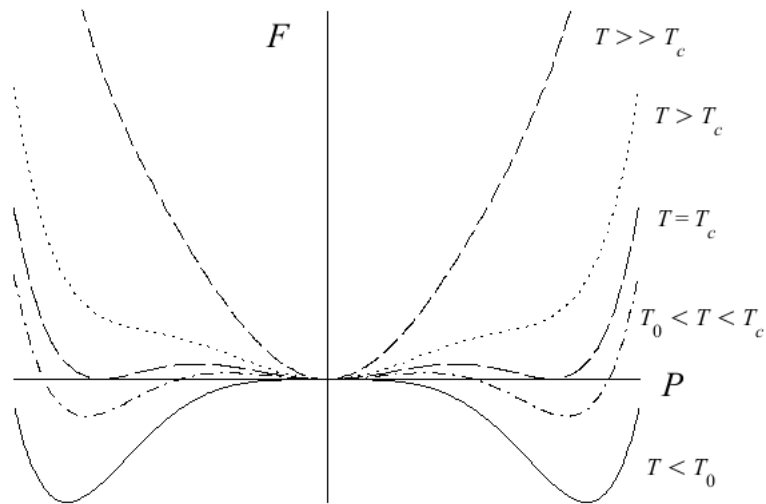


Figure 1.6: Free energy as a function of polarization at various temperature in case of a first order phase transition.

1.7 Ferroelectric Hysteresis and Polarization Reversal

The most important feature that distinguishes the ferroelectrics from other pyroelectrics is the polarization reversal (or switching) by an applied electric field. By plotting the change of polarization against applied electric field, it displays a hysteresis loop which resembling the magnetic hysteresis loop. It shows that the polarization of ferroelectric materials is not only depend on the applied electric field but also on their previous history. The Sawyer-Tower circuit is customarily used in experiment for the ferroelectric switching measurements (Sawyer & Tower, 1930).

Fig. 1.7 shows a typical ideal hysteresis loop and an experimental observed hysteresis loop when driven by a continuous applied electric field. Before discussion, we first define the notations. The coercive field, E_c is the required applied electric field to bring the polarization to zero. The value of polarization at zero field (point E) is called the remanent polarization, P_r and the spontaneous polarization is P_s .

In case of an ideal single-domain single crystals, the ideal hysteresis loop is shown in Fig. 1.7(a). The value of P_s is equal to the P_r . All the dipoles have to be switched together to reverse the direction of polarization. An applied electric field with amplitude $E > E_c$ is required to switch the polarization.

The hysteresis loop in a polycrystalline material is shown in Fig. 1.7(b). Especially in the case of polydomain ferroelectric ceramics, there is a statistical distribution of domains before the material is polarized for the first time (Hoffmann-Eifert et al., 2012). As shown in Fig. 1.7(b) in segment AB, P start to increase from zero when applied electric field is increase at the same time. At a low applied electric field, polarization increases linearly with the field and the ferroelectric behaves like an ordinary dielectric. Eventually, the polarization reaches saturation at point B. The saturation polarization P_{sat} is determined by extrapolating the CB segment until it intersect the vertical axis at $E = 0$.

After saturation if one starts to decrease the applied electric field until $E = 0$, a remanent polarization P_r is found. In order to further reduce the P to zero, a negative electric field which corresponds to the coercive field E_c has to be applied. Further increase the negative field, the hysteresis loop is traced in the reverse manner.

There are many factors that may affect the coercive field, spontaneous and remanent polarization and shape of the hysteresis loop. For instance: mechanical stresses, the thickness of the film, the presence of charged defects such as oxygen vacancies, preparation conditions and thermal treatment (Damjanovic, 1998).

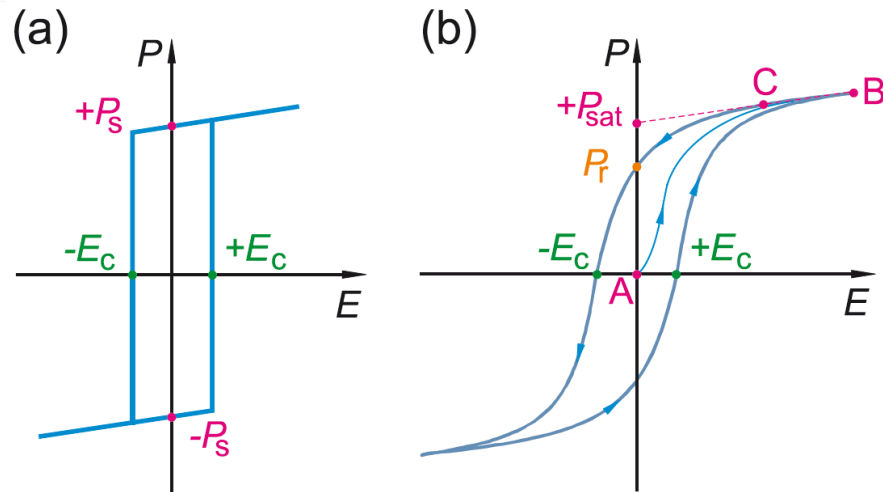


Figure 1.7: Ferroelectric ($P - E$) hysteresis loop. (a) Ideal single-domain single crystals (b) Polycrystalline materials (Hoffmann-Eifert et al., 2012)

1.8 Misfit Epitaxial Strain Effect

The strong coupling between polarization and strain has a dramatic effects on ferroelectric properties especially ferroelectric film which is particularly sensitive to mechanical boundary conditions. Epitaxial strain can have a substantial impact on the structure, ferroelectric transition temperatures, and other properties such as the dielectric and piezoelectric responses. The epitaxial growth of the ferroelectric thin film on a substrate with a difference lattice parameter can achieve a homogeneous epitaxial strain.

A phenomenological approach is developed to study the ferroelectric thin films which epitaxially grown on a substrate. First of all, the mechanical boundary conditions for a thin film epitaxially grown on a substrate is identified. On the one hand, an in-plane strains is induced due to the lattice mismatch between the film and the thick substrate. On the other hand, the out-of-plane strain vanishes because there are no traction acting on the top of film surface. Hence, the epitaxial ferroelectric thin films is subject to mixed mechanical boundary conditions, namely in-plane strain and out-of-plane strain. Under these mechanical boundary conditions imposed by substrate, the epitaxial thin film tends to minimize the elastic energy by either elongation or compression of the lattice vector perpendicular to the film surface (Ghosez & Junquera, 2006).

In fact, the above mixed mechanical conditions can be simplified and written in a succinct mathematical expression (Defaÿ, 2011). First, the top of thin film surface is mechanically free, so no stress is applied on it:

$$\sigma_3 = \sigma_4 = \sigma_5 = 0. \quad (1.28)$$

Second, the in-plane strains of the surface (u_1, u_2 and u_6) are actually imposed by the substrate. Therefore the strains along the directions 1 and 2 are equal ($u_1 = u_2$) and that shear stress between these two directions is zero ($u_6 = 0$) since the directions 1 and 2 are perpendicular. If the film/substrate interface is commensurate, then

$$u_1 = u_2 = u_m = \frac{a_s - a_0}{a_s}, \quad (1.29)$$

where u_m is the in-plane misfit strain induced by the substrate due to the lattice mismatch. a_0 is the equivalent cubic cell lattice constants of the free standing film and a_s is the lattice parameter of the substrate.

Due to the above mixed mechanical conditions, the thermodynamic potential of a strained ferroelectric thin film is essentially different from the bulk ferroelectrics. The new modified thermodynamic potential must reach the minimum at thermodynamic equilibrium where the strain components u_1, u_2, u_6 and the stress components $\sigma_3, \sigma_4, \sigma_5$ are fixed (Tagantsev et al., 2010). The differential form of Gibbs energy G , Eq.(1.3b) and Helmholtz energy F , Eq.(1.3a) with the aforementioned conditions can be expressed mathematically as:

$$dG = -SdT - u_1d\sigma_1 - u_2d\sigma_2 - u_6d\sigma_6 + \sum_{i=1}^3 E_idP_i, \quad (1.30)$$

$$dF = -SdT + \sigma_3du_3 + \sigma_4du_4 + \sigma_5du_5 + \sum_{i=1}^3 E_idP_i. \quad (1.31)$$

Therefore, a new form of thermodynamic potential with function of polarization, misfit strain must be used to find equilibrium thermodynamic states of an epitaxial thin films.

Starting from the Gibbs energy G , the modified thermodynamic potential \tilde{G} for a 2D-clamping case can be derived via the Legendre transformation (Pertsev, Zembilgotov, & Tagantsev, 1998)

$$\tilde{G} = G(P_i, \sigma_j) - \sum_{k=1}^6 \sigma_k \frac{\partial G(P_i, \sigma_k)}{\partial \sigma_k} = G + u_1\sigma_1 + u_2\sigma_2 + u_6\sigma_6, \quad (1.32)$$

by using Eq.(1.30) and $\partial G/\partial \sigma = -u$. This modified thermodynamic potential is necessarily to study the case of a (001) thin ferroelectric film grown on a cubic thick substrate.

We consider the system of an uniaxial ferroelectric where the polarization is perpendicular to the substrate (in the z direction) and the in-plane polarizations P_1 and P_2 will be zero. For simplicity, $P_3 = P$ and the Gibbs free energy with mechanical conditions (1.28)

can be rewritten as:

$$G = \alpha P^2 + \beta_{11} P^4 + \gamma_{111} P^6 - \frac{1}{2} s_{11} (\sigma_1^2 + \sigma_2^2) - Q_{12} [(\sigma_1 + \sigma_2) P^2] - s_{12} \sigma_1 \sigma_2 - \frac{1}{2} s_{44} \sigma_6^2, \quad (1.33)$$

where s_{ij} and Q_{ij} is the elastic compliances and the electrostrictive coefficients. Based on the aforementioned mechanical conditions in the film, $\partial G / \partial \sigma_1 = \partial G / \partial \sigma_2 = -u_m$, $\partial G / \partial \sigma_6 = 0$ and we solve for the case $\sigma_1 = \sigma_2 = \sigma_m$ with $\sigma_6 = 0$. After some algebraic manipulation, the modified thermodynamic potential (1.32) become:

$$\tilde{G} = \alpha^* P^2 + \beta_{11}^* P^4 + \gamma_{111} P^6 + \frac{u_m^2}{s_{11} + s_{12}}, \quad (1.34)$$

where

$$\alpha^* = \alpha - \frac{2Q_{12}}{s_{11} + s_{12}} u_m \quad (1.35)$$

and

$$\beta_{11}^* = \beta_{11} + \frac{Q_{12}^2}{s_{11} + s_{12}}. \quad (1.36)$$

Hence, the coefficients of both the quadratic and the quartic polarization terms in the thermodynamics potential are renormalized. By setting $\alpha^* = 0$, we find that

$$T^* = T_0 + \frac{2Q_{12}}{\alpha_0(s_{11} + s_{12})} u_m. \quad (1.37)$$

As a consequence of the in-plane misfit strain of the film by the substrate, the transition temperature shifts from the bulk value T_0 to T^* . Furthermore, the sign of shifting in transition temperature depends on the relative sign and magnitude of Q_{12} , s_{11} and s_{12} . It is noticeable that according to Eq.(1.36), the misfit epitaxial strain can change the transition from first order to second order $\beta_{11} < 0$ but $\beta_{11}^* > 0$

In addition, the above thermodynamic formulation for describing the mechanical substrate effect can actually be developed from the Helmholtz energy Eq.(1.5), F (Pertsev, Tagantsev, & Setter, 2000). Similarly, the appropriate thermodynamic function can be obtained via the following Legendre transformation of F :

$$\tilde{F} = F(P_i, u_j) - \sum_{k=1}^6 u_k \frac{\partial F(P_i, u_k)}{\partial u_k} = F - u_3 \sigma_3 - u_4 \sigma_4 - u_5 \sigma_5, \quad (1.38)$$

by using Eq.(1.31) and $\partial F / \partial u = \sigma$. In the case of ferroelectric thin film with a mechanically free upper surface, Eq.(1.28) $\sigma_3 = \sigma_4 = \sigma_5 = 0$, the thermodynamic function \tilde{F} reduces to the Helmholtz free energy F , Eq.(1.5). Likewise, only the case of uniaxial ferroelectric is consider, $P_1 = P_2 = 0$, $P_3 = P$, the Helmholtz free energy is simplified with mechanical conditions (1.28):

$$F = \alpha P^2 + \beta'_{11} P^4 + \gamma_{111} P^6 + \frac{1}{2} c_{11} (u_1^2 + u_2^2 + u_3^2) + c_{12} [(u_1 u_2 + u_1 u_3 + u_2 u_3)] - g_{11} u_3 P^2 + \frac{1}{2} c_{44} (u_4^2 + u_5^2) - g_{12} (u_1 + u_2) P^2. \quad (1.39)$$

The mixed mechanical conditions state that $u_1 = u_2 = u_m$ and the shear strain $u_6 = 0$. The conditions $\sigma_3 = \sigma_4 = \sigma_5 = 0$ imply that we can find the u_3, u_4 and u_5 from the relations $\partial F / \partial u_3 = \partial F / \partial u_4 = \partial F / \partial u_5 = 0$. After some calculation, we obtain the following expression:

$$F = \alpha'^* P^2 + \beta'_{11}{}^* P^4 + \gamma P^6 + \frac{c_{11}^2 + c_{11} c_{12} - 2c_{12}^2}{c_{11}} u_m^2, \quad (1.40)$$

where the coefficients denoted by * are renormalized by strain constraint. They are given by

$$\alpha'^* = \alpha + 2 \left(\frac{c_{12}}{c_{11}} g_{11} - g_{12} \right) u_m, \quad (1.41)$$

$$\beta'_{11}^* = \beta'_{11} - \frac{g_{11}^2}{2c_{11}}. \quad (1.42)$$

Similarly by letting $\alpha'^* = 0$ and since $\alpha = \alpha_0(T - T_0)$, we obtain the shift of transition temperature due to misfit strain as

$$T^* = T_0 - \frac{2}{\alpha_0} \left(\frac{c_{12}}{c_{11}} g_{11} - g_{12} \right) u_m. \quad (1.43)$$

CHAPTER 2

REVIEW OF FERROELECTRIC SUPERLATTICES

2.1 Overview

In this chapter we will begin with an introduction to ferroelectric superlattice and briefly describe different types of ferroelectric superlattices. Theoretical methods that are mainly used to study ferroelectric superlattices will be briefly elucidated as well. Next, the key factors that affect the properties of ferroelectric superlattices will be discussed. Since this thesis is a theoretical work using Landau theory, an overview on the theoretical works of ferroelectric superlattices based on the phenomenological approach will be presented. At the end, we will discuss in detailed the thermodynamic model based on Landau-Ginzburg theory that we used in the present study of phase transitions in ferroelectric superlattices.

2.2 Introduction to Ferroelectric Superlattices

Artificially layered ferroelectric superlattices comprising of two or more different layers are currently a topic of active research (Dawber, Rabe, & Scott, 2005; Scott, 2013) because of their potential applications (Scott, 2000; Murali, 2000; Scott, 2007) and fundamental scientific interest (Ríos et al., 2003; Dawber, Lichtensteiger, et al., 2005). Typically, the thickness of each constituent layer in ferroelectric superlattices is several nanometers or a few unit cells. In fact, superlattices are an alternative approach to investigate and exploit the properties of ferroelectric thin films (Rijnders & Blank, 2005) because its specific properties can be designed by tailoring their composition at the atomic level. Basically, there are three main motivations to fabricate these artificial materials (Dawber & Bousquet, 2013): (i) superlattice structures offers a promising way to tune or

tailor the ferroelectric properties for specific applications. (ii) ferroelectric superlattices can exhibit enhanced physical properties and functionalities unachievable in bulk or its parent compounds and (iii) superlattice produce an artificial layer single crystal with new physical phenomena that are completely absent in the parent compounds and improve its properties.

There are several important growth techniques that can fabricate epitaxial ferroelectric superlattices, such as molecular beam epitaxy (MBE) (Tsurumi, Ichikawa, Harigai, Kakemoto, & Wada, 2002a; N. Wang et al., 1999; J. C. Jiang, Pan, Tian, Theis, & Schlom, 1999), radio-frequency (RF) magnetron sputtering deposition (Dawber, Lichtensteiger, et al., 2005; Tsai, Liang, & Lee, 2005; Chiu, Liu, Lee, Yu, & Huang, 2011), pulse laser deposition (PLD) (Tabata, Tanaka, & Kawai, 1994; Kim et al., 2002; B. D. Qu, Evstigneev, Johnson, & Prince, 1998), metalorganic chemical vapor deposition (Z. Wang & Oda, 2000), and chemical solution deposition (Q. Wang & Shen, 2005). Molecular-beam epitaxy (MBE) and sputter deposition can produce high quality of superlattices, but the latter requires a proper control of processing parameters (Bao, 2008).

In the field of ferroelectric (FE) perovskite, recently there are many experimental works focused on “bicolor” superlattices, for example: FE/dielectric, FE/FE, FE/relaxor, and etc. The term “color” refers to a distinct parent constituent layer within the superlattice. Those “bicolor” system for FE/dielectric including $\text{BaTiO}_3/\text{SrTiO}_3$ (Tabata et al., 1994; Zhao et al., 1999; Shimuta et al., 2002; Tsurumi, Ichikawa, Harigai, Kakemoto, & Wada, 2002b; A. Q. Jiang, Scott, Lu, & Chen, 2003; Ríos et al., 2003; Tenne et al., 2006), $\text{PbTiO}_3/\text{SrTiO}_3$ (J. C. Jiang et al., 1999; Dawber, Lichtensteiger, et al., 2005; Dawber et al., 2007; Zubko, Stucki, Lichtensteiger, & Triscone, 2010; Jo et al., 2011), $\text{KNbO}_3/\text{KTaO}_3$ (H. Christen et al., 1996; H.-M. Christen, Specht, Norton, Chisholm, & Boatner, 1998; Specht, Christen, Norton, & Boatner, 1998; Sigman, Norton, Christen, Fleming, & Boatner, 2002) and etc. FE/FE superlattice combining two distinct ferro-

electric materials together, such as PbTiO_3 and BaTiO_3 (Le Marrec et al., 2000). A recent experimental work showed that a different type of FE/dielectric superlattices like $\text{PbTiO}_3/\text{SrRuO}_3$ can be fabricated by combining ferroelectric materials with metallic magnetic perovskite oxides (Callori et al., 2012). On the other hand, ferroelectric materials can also be combined with relaxor such as $\text{PbTiO}_3 / \text{PbMg}_{1/3}\text{Nb}_{2/3}\text{O}_3$ superlattice (Ranjith, Nikhil, & Krupanidhi, 2006). Some other studies including tricolor superlattices which alternating between three different materials, for example, $\text{SrTiO}_3/\text{BaTiO}_3/\text{CaTiO}_3$ (Warusawithana, Colla, Eckstein, & Weissman, 2003; H. N. Lee, Christen, Chisholm, Rouleau, & Lowndes, 2005) with broken inversion symmetry.

2.2.1 Theoretical Methods for the Study of Ferroelectric Superlattices: An Overview

In this section, an overview of theoretical methods that are mainly used in studying ferroelectric superlattices will be briefly discussed. Generally, the theoretical study of ferroelectric superlattices are mainly pursued by two approaches, i.e. macroscopic theory and microscopic theory. The macroscopic theory also known as phenomenological approach based on the Landau-type theory (Chandra & Littlewood, 2007) or phase-field method using time-dependent Ginzburg-Landau equations (Chen, 2008). On the microscopic level, one usually start with a microscopic many-body Hamiltonian and applying the quantum statistical techniques to consider the interaction between particles in a crystal. For instance, the lattice dynamic models is used for the displacive type ferroelectrics whereas the Ising model in a transverse field is used for the order-disorder type ferroelectrics (Blic & Žekš, 1974). Especially in the case of ferroelectric superlattices, there are a series of papers that used transverse Ising Model (TIM) to study the properties of ferroelectric superlattices (B. D. Qu, Zhong, & Zhang, 1994; B. Qu, Zhong, & Zhang, 1995; Xin, Wang, Zhong, & Zhang, 1999). Another method involves atomistic modeling of ferroelectric materials is known as first-principles or *ab initio* techniques. These

methods are free of empirically adjustable parameters and solely based on the fundamental laws of quantum mechanics. Among all the first-principles approaches, density functional theory (DFT) has emerged as one of the best methodological tools to study ferroelectrics (Ghosez & Junquera, 2006). In order to extend the first-principles modeling to provide access to finite-temperature thermodynamic properties, a “second principles” methods has been developed to explore the physical phenomena with a few parameters that can be extracted directly from DFT calculations (Lichtensteiger et al., 2012). Among them, the most common methods are the effective Hamiltonian (W. Zhong, Vanderbilt, & Rabe, 1994, 1995) and shell models (Sepiarsky, Asthagiri, Phillpot, Stachiotti, & Migoni, 2005). There are several good reviews on the first-principles studies of ferroelectric superlattices, such as Dawber, Rabe, & Scott, 2005; Rabe, 2005; Ghosez & Junquera, 2006; Rabe & Ghosez, 2007. Each theory has its own merits, however, this study will only focus particularly on Landau phenomenological theory on ferroelectric superlattices. The other aforementioned microscopic methods and atomic modelings are lie beyond the scope of this thesis, it will not be discussed in detail.

2.3 Major Factors Affecting Ferroelectric Superlattices

Ferroelectric superlattices that will be discussed in this study are mainly focus on ferroelectric oxide with perovskite structure. Due to the complexity of the physics of ferroelectric superlattices, their properties can be influenced by numerous factors, such as finite size effects, electrostatic effect, mechanical effect and etc. On top of that, recent studies shown that a new intriguing physics of phenomena arise in complex oxides heterostructures due to interface effect (Zubko, Gariglio, Gabay, Ghosez, & Triscone, 2011). In the following discussions, the key factors that affect the properties of ferroelectric superlattices will be discussed in detailed.

2.3.1 Misfit Strain

Superlattices are customarily produced by fabricating alternate layers of epitaxially ferroelectric perovskites with different properties and lattice parameters. Hence, the substrate is very important in obtaining a single-crystalline epitaxial film in order to grow a high-quality superlattice. Similar to grow an epitaxial oxide thin film, one usually start from an atomically flat substrate surface otherwise it would be difficult to assure correct atomic-scale layer ordering during film growth. If a thin film grows on a rough starting surface, it can leads to a variety of structural defects (Posadas et al., 2007). As a consequence, it could affect the properties of the film such as dielectric, ferroelectric and others. Besides that, the surface flatness over multiple layers is very crucial when fabricating a superlattices. Any roughness on the substrate surface can cause an unintentional electrical short in thin barrier layers (Posadas et al., 2007).

Besides that, it is possible to induce considerable epitaxial strains in the ferroelectric superlattices by growing epitaxial thin films on lattice mismatched substrates. This epitaxial thin films are considerably different from those of their bulk parent material (Dawber, Rabe, & Scott, 2005; Schlom et al., 2007). Hence, epitaxial strain is one of the major factors determining the structures and properties of epitaxial superlattices. The ionic positions in thin films and its lattice vibration, particularly the ferroelectric soft mode is very sensitive to the strain effect (Ortega et al., 2011). It has been experimentally observed and theoretically proved that epitaxial strain have a substantial impact on the structure and properties of ferroelectric thin films and superlattices (Dawber, Rabe, & Scott, 2005; Schlom et al., 2007; Dawber & Bousquet, 2013).

An important consideration is the limitation on the thickness of the superlattice that can be achieved while retaining the coherent growth required to maintain the epitaxial strain condition imposed by substrate (Posadas et al., 2007). The strain constraint of a suf-

ficiently thick superlattice can be either partially or fully relaxed through the formation of misfit dislocations, thereby allowing more complicated strain interactions between different constituent layers. More often than not, superlattice structure tends to inhibit the formation of misfit dislocations and can be grown coherently with layers sufficiently thicker than single material films. This behaviour can be seen in the case of BaTiO₃/SrTiO₃ superlattice on a SrTiO₃ substrate where the epitaxial strain from the substrate can be maintained throughout the sample to a thickness greater than single BaTiO₃ films (Posadas et al., 2007). Firstly, this is due to the fact that the overall lattice misfit of BaTiO₃/SrTiO₃ superlattice relative to the substrate is less than single BaTiO₃ films. Secondly, by reducing the thickness of the individual layers that are under strain, the multilayer structure itself may tend to impede the formation of misfit dislocation.

Furthermore, the influence of epitaxial strain on superlattice can cause other interesting and striking behaviours from a practical point of view. Another example is the PbTiO₃/SrTiO₃ superlattices, a very thin and high-quality layers of SrTiO₃ can be grown within PbTiO₃ layers at much lower temperatures than the growth of single thick SrTiO₃ films (Dawber, Lichtensteiger, et al., 2005; Posadas et al., 2007). On the other hand, the results of experimental works (A. Q. Jiang et al., 2003; Ríos et al., 2003) and first-principles calculation (Johnston, Huang, Neaton, & Rabe, 2005) on BaTiO₃/SrTiO₃ superlattices showed that the SrTiO₃ layers can achieve an in-plane polarization but not the BaTiO₃ layers.

Recently, Ortega et al. (Ortega et al., 2011, 2013) have demonstrated that the strain among the inter- and intra-layer of BaTiO₃/(Ba, Sr)TiO₃ superlattices can be manipulated by changing the composition of the constituent layer. Their results show that the dielectric and ferroelectric properties of the superlattices can be tuned by varying the Ba/Sr ratio of the constituent layer without changing the periodicity and the total thickness of the superlattices.

Hence, strain engineering in artificial superlattices allowed us to fine tune their ferroelectric properties and acquire new functionalities that are unachievable in bulk.

2.3.2 Electrostatic coupling

Electrostatic coupling between individual layers of superlattice exists when the polarization is perpendicular to the interface or along the modulation direction. Similar to ferroelectric thin films, the electrostatics coupling between layers of superlattices also plays a major role in determining the properties of ferroelectricity (Dawber, Rabe, & Scott, 2005; Ghosez & Junquera, 2006; Dawber & Bousquet, 2013).

In the absence of free charges at interfaces, there is a uniform electric displacement through out the superlattice. The continuity of the displacement field across the interfaces resulting in a polarization mismatch between the individual layers (Posadas et al., 2007). Thereby it gives rise to the presence of non-vanishing electric field in each different layers. This electrostatic coupling effect has been proven by first-principles calculation in BaTiO₃/SrTiO₃ (Neaton & Rabe, 2003) and by both experiment and theory in PbTiO₃/SrTiO₃ (Dawber, Lichtensteiger, et al., 2005; Aguado-Puente, García-Fernández, & Junquera, 2011; Zubko et al., 2012). In their studies, they have shown that the internal fields in a polarizable materials has a significant influence on polarization and structural properties of the system. To illustrate, the field within BaTiO₃ layers is oppose its polarization whereas the field (with opposite sign) in SrTiO₃ layers is tend to polarize this paraelectric layers (Neaton & Rabe, 2003). Due to the tendency of the system to minimize electrostatic energy, it force the structure to adopt a nearly uniform polarization throughout the system (Neaton & Rabe, 2003; Dawber, Lichtensteiger, et al., 2005; Aguado-Puente et al., 2011).

It has been demonstrated from both experiment and Landau theory in KTaO₃/KNbO₃ system (Specht et al., 1998; Sepliarsky, Phillpot, Wolf, Stachiotti, & Migoni, 2001;

Stephanovich, Luk'yanchuk, & Karkut, 2005) that there is a progressive transition from a strong electrostatic interlayer coupling in the thin layer limit (which applies to thickness below a few unit cells) to a weak electrostatic coupling regime in the thick layer limit. The same phenomenon is also observed by experiment and first-principles calculation in $\text{PbTiO}_3/\text{SrTiO}_3$ superlattices (Zubko et al., 2012; Aguado-Puente et al., 2011; Aguado-Puente & Junquera, 2012).

Besides that, a series of papers based on Landau theory explicitly considering electrostatic interaction between ferroelectric-paraelectric bilayers and multilayers (Roytburd, Zhong, & Alpay, 2005; S. Zhong, Alpay, & Mantese, 2006; S. Zhong, Alpay, Roytburd, & Mantese, 2006). Their thermodynamic model showed that the electrostatic coupling can lead to a large enhancement of dielectric properties in multilayers.

2.3.3 Volume fraction or thickness ratio

In general, superlattices consist of two or more layers with thickness and order that are repeated many times. It is found that the volume fraction or thickness ratio is one of the key factors that controls the properties in superlattice. For example in the case of $\text{PbTiO}_3/\text{SrTiO}_3$ superlattices, it has been demonstrated by both experiment and theory (Dawber et al., 2007; Zubko et al., 2010) that the polarization, dielectric susceptibility and phase transition temperature depend on the volume fraction of PbTiO_3 .

On the other hand, the enhancement of ferroelectricity in two-component superlattices has been reported in $\text{BaTiO}_3/\text{SrTiO}_3$ grow on SrTiO_3 substrate (Shimuta et al., 2002; Neaton & Rabe, 2003; Tian et al., 2006; Tenne et al., 2006). By increasing the volume fraction of BaTiO_3 , the polarization of the superlattices can be enhanced and it exceeds that of bulk BaTiO_3 . This enhanced polarization is attributed to the high concentration of the ferroelectric components BaTiO_3 and compressive strain imposed by SrTiO_3 substrate.

2.3.4 Interface effects

Recent progress in deposition techniques have made it possible to fabricate high-quality nanoscale artificial oxide heterostructures such as perovskite ferroelectric superlattices. Thus, it leads to the discovery of new intriguing physics of phenomena that arise at the interfaces between these multifunctional materials (Zubko et al., 2011). According to first-principles calculations, the interface atomic relaxations between alternating layers influences the chemical bonding and the short range interatomic force near the interface. The Born effective charges at interface is differ from the bulk values due to the modification of long range dipole-dipole interaction (Ghosez & Junquera, 2006). The rearrangement of atoms at the surface or interface in layered ferroelectrics leads to a different crystal symmetry and unexpected new behaviours compare to bulk.

2.3.4.1 *Inhomogeneous Polarization and Polar Discontinuity at Interfaces*

The spatial inhomogeneity of polarization is very important when dealing with ferroelectric domains. A more detailed description of ferroelectric domains can be found in the book by Tagantsev et al., 2010. Phenomenological theories predicted that the inhomogeneous and changes of polarization are expected near the surface of ferroelectrics (Kretschmer & Binder, 1979; D. Tilley & Žekš, 1984) and the interface of superlattices (B. D. Qu, Zhong, & Prince, 1997).

It has been predicted theoretically (Y. L. Li et al., 2007; D. Lee et al., 2009) and inferred by indirect experimental methods (A. Q. Jiang et al., 2003; Tenne et al., 2006; Bruchhausen et al., 2008) that the superlattices composed of ferroelectric and paraelectric layers are expected to give rise to an inhomogeneous polarization profile. By make use of electron-energy-loss spectra (EELS) and high-angle annular dark field (HAADF), Torres-Pardo et al. and Zubko et al. (Torres-Pardo et al., 2011; Zubko et al., 2012) were able to observe the local structural distortions in $\text{PbTiO}_3/\text{SrTiO}_3$ superlattices. They have

identified local structural distortion at the single unit-cell scale across the interface, and revealed the existence of inhomogeneous polarization profile within the ferroelectric and paraelectric layers. While the length scale of inhomogeneity extends over 5-6 unit cells was attributed to ferroelectric domains, the effect of intermixing confines to 1 unit cell from interface may also be present and should not be ruled out. Their interesting works implied that any theoretical study based on homogeneous polarization model (Pertsev & Tyunina, 2011; Chew, Ong, Osman, & Tilley, 2000; Roytburd et al., 2005; Dawber et al., 2007; Neaton & Rabe, 2003) is most likely inapplicable in superlattices.

Recently, a first-principles studies demonstrated that a superlattice consisting alternate layers of ferroelectrics and paraelectrics may form a polar discontinuity at interface (Das, Spaldin, Waghmare, & Saha-Dasgupta, 2010). Their results show that the coupling at the interface between the switchable induced-polarization of paraelectric layer and the electrically switchable spontaneous polarization of ferroelectric layer leads to polarization continuities or discontinuities at interface.

2.3.4.2 *Interface coupling*

In superlattices composed of thin layers of ferroelectric and paraelectric compound, there is an additional coupling originates from the interaction at the interface which may affect the ferroelectric properties of the structure. Indeed, the coupling at the interface between the two constituent layers has been demonstrated in experiments (Sigman et al., 2002; Bousquet et al., 2008) to play an important role in governing their properties.

The experimental works on $\text{KTaO}_3/\text{KNbO}_3$ superlattices showed that there is a significant long-range ferroelectric coupling across the KTaO_3 layers (H.-M. Christen et al., 1998; Specht et al., 1998). Moreover, this system is further investigated by Stephanovich et al. using Landau-Ginzburg theory (Stephanovich et al., 2005). It has been shown that the coupling between ferroelectric layers in this superlattice is caused by the de-

polarization field which emerge from the domain structure of the ferroelectric layers. Besides that, a transition from ferroelectric to antiferroelectric orderings is observed in $\text{KTaO}_3/\text{KNbO}_3$ superlattices experimentally (Sigman et al., 2002) further indicating the existence of strong coupling across the interface between the two layers.

In the limit of ultra-short periods, a $\text{PbTiO}_3/\text{SrTiO}_3$ superlattice shows an unusual recovery of ferroelectricity that cannot be explained by a simple electrostatic model alone (Dawber, Lichtensteiger, et al., 2005). First-principles study suggests that this is essentially an interface effect which involves an unusual coupling between FE and antiferrodistortive (AFD) instabilities (Bousquet et al., 2008). Another first-principles results by Junquera group show that there is an existence of a strong coupling between FE and AFD modes with strain in monodomain $\text{PbTiO}_3/\text{SrTiO}_3$ superlattices (Aguado-Puente et al., 2011). Both the magnitude and the relevant directions of the FE polarization and the rotation axis of oxygen octahedra can be tuned by controlling the epitaxial strain. Thus, the coupling of structural instabilities at interface introduces a unique approach for designing new functional materials which is not restricted to the superlattice system itself (Zubko et al., 2011).

There have been a number of theoretical studies for the coupling between layers at interface in superlattices within the framework of Landau theory. Several varieties of terms have been proposed to account for the coupling between layers, for instance the works by D. R. Tilley, 1988; B. D. Qu et al., 1997; Ma, Shen, & Xu, 2000; Chew, Ishibashi, G. Shin, & L. W. Chan, 2003. The detailed discussion of this topic will be presented in Section 2.4.

2.3.4.3 Intermixing at interfaces

In multilayer structures such as superlattices, intermixed layers may form at interfaces between dissimilar layers. The formation of intermixed layers at interfaces with

properties different from those of both constituents, may affect the properties of multi-layer structures (Chew, 2012). These intermixed layers can be formed due to the short-range interactions between contacting dissimilar materials, surface or interface reconstruction, cation intermixing, or composition deviations at the interfaces in superlattices of ferroelectric solid solutions (Pertsev & Tyunina, 2011).

Recently there was an experiment demonstrated that BaTiO₃/SrTiO₃ superlattices can be fabricated without interface intermixing by using chemical solution deposition method (Hosokura et al., 2011). However, the intermixing at heterointerfaces is usually difficult to control experimentally at high temperature using high-energy lasers, where the stoichiometry of the deposited films changes in a complicated manner under the prescribed deposition conditions (Mizoguchi, Ohta, Lee, Takahashi, & Ikuhara, 2011; Ohnishi, Koinuma, & Lippmaa, 2006). On the other hand, Mizoguchi and co-workers (Mizoguchi et al., 2011) have found an experiment method to control the atomic-scale intermixing at interfaces and improve the properties of SrTiO₃ based superlattice by constructing an abrupt heterointerface.

The interface structure of PbTiO₃ thin films grown on SrTiO₃ substrates were studied experimentally by Fong et al. (Fong et al., 2005) using a high resolution coherence Bragg rod analysis (COBRA) to reveal details of the film structure. Their work suggests that cation intermixing may exist at the interfaces of PbTiO₃/SrTiO₃ superlattices. A detail evaluation of interface diffusion or intermixing in BaTiO₃/SrTiO₃ superlattices grown by molecular beam epitaxy was performed by Ishibashi, Ohashi and Tsurumi (Ishibashi, Ohashi, & Tsurumi, 2000). Besides that, Hung et al. also identified the presence of compositional intermixing at interfaces in PbZrO₃/BaZrO₃ (Hung, Chueh, Wu, & Chou, 2005). A recent study on the structural evolution of surfaces during the layer-by-layer growth of BaTiO₃ films on SrRuO₃ indicates that the surface reconstruction of SrRuO₃ increases the oxygen concentration, and leads to both intermixing and structural change

in BaTiO₃ at the interface (Shin et al., 2010). Their finding further reveals the possible existence of intermixed layer at oxide interface.

On the theoretical side, the first-principles study of interface intermixing effect in short-period PbTiO₃/SrTiO₃ was done by Cooper, Johnston and Rabe (Cooper, Johnston, & Rabe, 2007), they have shown that the interfacial intermixing can significantly enhance the polarization in superlattices. On the other hand, Pertsev and Tyunina (Pertsev & Tyunina, 2011) based on phenomenological theory demonstrated that the short-range interactions and intermixing between dissimilar constituents in contact can give rise to the formation of an interface layer with physical properties different from those of both layers.

2.4 An Overview of Phenomenological Theory for Ferroelectric Superlattices

A number of papers using phenomenological approach have appeared to study the phase transition of ferroelectric superlattices. In fact, the theoretical studies of these works started even earlier than the first fabrication of superlattices in experiment (Levanyuk & Misirlioglu, 2011). In this section, an overview on the theoretical works of ferroelectric superlattices which based on phenomenological theory or Landau theory is reviewed.

In fact, many theoretical works that based on Landau theory have adopted the idea of extrapolation length which borrowed from the literature on surface superconductivity (Kretschmer & Binder, 1979; D. Tilley & Žekš, 1984). By using extrapolation length, Li et al. (S. Li, Eastman, Vetrone, Newnham, & Cross, 1997) used Landau formulation to studied the ferroelectricity of superlattices by assuming that the polarization is continuous at the interface. Based on the same assumption that the polarization is continuous at the interface, Schwenk et al. (Schwenk, Fishman, & Schwabl, 1990) considered the surface interactions by introduced the surface Ginzburg-Landau functional to study soft modes in ferroelectric superlattices. On the other hand, D. R. Tilley (D. R. Tilley, 1988)

proposed a Landau formulation for coupled ferroelectric superlattices by introduced an interface coupling energy term. Later on, Qu and co-workers (B. D. Qu et al., 1997) presented the thermodynamic model to study interfacial coupling ferroelectric superlattices based on Landau-like formulation by taking the continuum mean-field expressions of the transverse Ising model. Their model use two surface parameters or extrapolation lengths to describe the inhomogeneity of polarization near surfaces and an interface coupling parameter gives the strength of the interface polarization coupling. Nonetheless, their work did not explicitly address how the interface polarization coupling affects the local polarization across the interface. Later, Ma and co-workers (Shen & Ma, 2000; Ma et al., 2000; Shen & Ma, 2001) reconsidered the Qu model by including the long-range coupling effect, but the spatial distribution of polarizations was not reported and discussed. The recent works by Chew et al. and Ong et al. (Chew, Ong, & Iwata, 2011c; Ong, Lee, & Chew, 2012) on the study of switching dynamics in ferroelectric superlattices show that the Qu's model (B. D. Qu et al., 1997) using extrapolation length can only describe polarization discontinuities at the interface. Misirlioglu and co-workers (Misirlioglu, Akcay, Zhong, & Alpay, 2007) applied the idea of extrapolation length in their nonlinear thermodynamic model to investigate the effect of interface on polarization of BaTiO₃/SrTiO₃ bilayer by considering the depolarization effect. Although the extrapolation length has been extensively studied in ferroelectric thin films and superlattices, to our knowledge, there is no direct experimental confirmation of this enigmatic idea.

Most of the earlier theoretical works of Landau theory in ferroelectric superlattice only considered the simple case of polarization parallel to the surfaces or interfaces such as D. R. Tilley, 1988; B. D. Qu et al., 1997; Shen & Ma, 2000; Ma et al., 2000; Shen & Ma, 2001. Hence, there is no depolarization field in this configuration and the electrostatic coupling effect can be neglected. In fact, this configuration of in-plane polarization in superlattices can be measured using interdigital electrodes (Harigai, Tanaka,

Kakemoto, Wada, & Tsurumi, 2003). In the case of polarization is perpendicular to the interface, the depolarization field due to electrostatic coupling between layer is crucial to the ferroelectric properties of superlattices. Roytburd and co-worker have developed a thermodynamic model by explicitly take into account electrostatic interactions between layers of superlattices and the depolarization field effect (Roytburd et al., 2005; S. Zhong, Alpay, & Mantese, 2006; S. Zhong, Alpay, Roytburd, & Mantese, 2006). Recently, Kesim et al. (Kesim, Cole, Zhang, Misirlioglu, & Alpay, 2014) employed the Roytburd's model (Roytburd et al., 2005) to examine the dielectric properties of ferroelectric-dielectric multilayers by taking into account the thermal stresses that develop during cooling from the growth temperature. However, the Roytburd's model did not consider the effect of surface or interface, the polarization coupling at interface is ignored, the polarization is homogeneous within the superlattices according to their results. On the other hand, Stephanovich et al. (Stephanovich et al., 2005) employed the Ginzburg-Landau equations coupled with electrostatic equations which was first proposed by Chenskii and Tarasenko (Chenskii & Tarasenko, 1982) to discuss the phase transition of ferroelectric superlattices. Subsequently, Levanyuk and Misirlioglu (Levanyuk & Misirlioglu, 2011) adapted the same approach as Stephanovich et al. (Stephanovich et al., 2005) to show that the periodicity assumption along the out-of-plane direction is not justified. By using the Landau-Ginzburg-Devonshire theory coupled with electrostatic equation, Misirlioglu et al. (Misirlioglu, Kesim, & Alpay, 2014) demonstrated that the electrostatic boundary conditions have a significant effect on the dielectric response of $\text{PbZr}_{0.3}\text{Ti}_{0.7}\text{O}_3/\text{SrTiO}_3$ superlattices. This is due to the existence of internal electric fields at the interfaces resulting from the polarization mismatch between the layers.

In addition, there are several other Landau phenomenological models proposed by different authors for studying ferroelectric superlattices. Based on the Landau-Ginzburg theory, Cui et al. (Cui, Lü, Xu, & Zhou, 2009) applied the idea of surface transition layer

(Lü & Cao, 2002) in each constituent layer and interface coupling between two constituent layers. In their model, however, the surface transition layers or inhomogeneity of polarization across interface are represented by a distribution function that are based on mathematics argument and its underlying physical meaning is difficult to justified. On the other hand, Pertsev and Tyunina (Pertsev & Tyunina, 2011) introduced an interface nanolayer with properties different from those of both constituents to investigate the permittivity of superlattice. However, they assumed the polarization is homogeneous, the effect of surface or interface is neglected and the local polarization coupling at interfaces is not considered.

Recently, there are number of papers study the space charges effect in ferroelectric multilayer or superlattices within the framework of Landau theory. Misirlioglu and co-workers (Misirlioglu, Alexe, Pintlilie, & Hesse, 2007) investigate the effect of interfacial space charge in ferroelectric superlattices using the Roytburd's model (Roytburd et al., 2005) and follow the approach for space charge distribution by Bratkovsky and Levanyuk (Bratkovsky & Levanyuk, 2000). Their results show that the polarization and its switching characteristics of ferroelectric superlattices can be affected by the presence of an interface charge. By treating the ferroelectric perovskites as wide band-gap semiconductors instead of insulators, Liu and Li (Y. Y. Liu & Li, 2010) studied the effect of space charges on the ferroelectric superlattices based on a continuum model. They found that a large electric field near the superlattice interface is due to the accumulation of space charge at interface. As a result, it gives rise to the enhancement of polarization and asymmetric in the hysteresis loop. Okatan et al. (Okatan, Misirlioglu, & Alpay, 2010) developed a thermodynamic model to study the contribution of localized charges to the polarization and dielectric properties of $\text{PbTiO}_3/\text{SrTiO}_3$ superlattices. Their study shows that there exists a critical volume fraction of PT below which the superlattice is in the paraelectric

phase. Furthermore, there is a recovery of in ferroelectric polarization near to the vicinity of ferroelectric-paraelectric phase transition.

2.5 A Thermodynamic Model for Ferroelectric Superlattices

From what have been discussed in the preceding session, undoubtedly the interface effects have a dominant influence on the properties of ferroelectric superlattices. In order to develop a thermodynamic model based on Landau-Ginzburg theory for ferroelectric superlattices, the interface effects such as interface coupling, intermixing have to be taken into account. The presence of interface effect can give rise to the changes of polarization at interface of superlattices, hence the Ginzburg term or gradient term must be considered in the free energy functional.

Recently, Chew and co-worker have proposed a thermodynamic model to study the ferroelectric properties of superlattices consisting of alternate ferroelectric and paraelectric layers (Ishibashi & Iwata, 2007; Chew, Iwata, Shin, & Ishibashi, 2008; Chew, Iwata, & Shin, 2009; Chew et al., 2011c; Chew, Ishibashi, & G. Shin, 2006; Chew, Ong, & Iwata, 2011a). Their model can be constructed using the concept of interaction of dipole lattices, which are characterized by polarizations with double potential wells (Chew, 2012; Chew et al., 2011a). In the model, an interface energy term is introduced in the free energy to describe the local polarization coupling at interface between the two contacting ferroelectrics, and the formation of an intermixed layer (Chew et al., 2003). Despite its simplification, the approach has captured the essential physics which associate with polarization continuities or discontinuities, polarization inhomogeneities, intermixing and local polarization coupling at interfaces (Chew, 2012).

2.5.1 Dipole Lattice Model

On the basis of Landau-Ginzburg theory, a thermodynamic model is proposed to study the periodic superlattice $-ABABAB-$ consist of two different ferroelectric/paraelectric

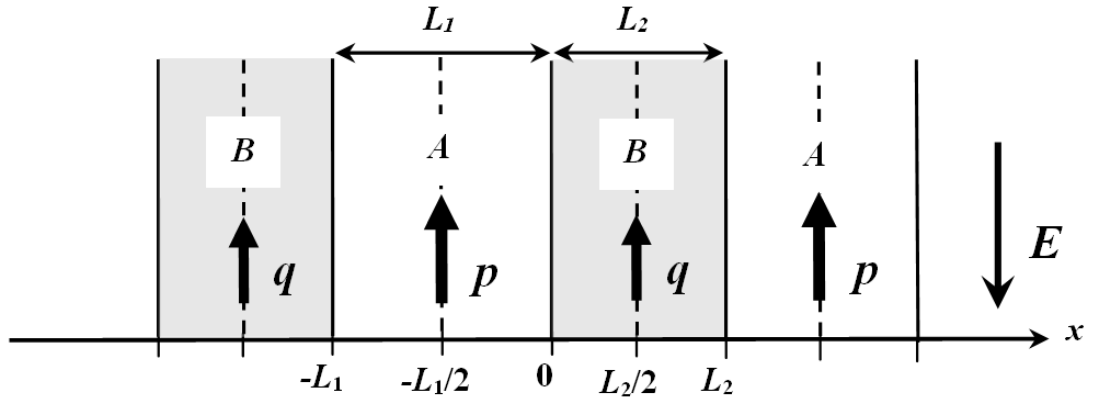


Figure 2.1: Schematic illustration of a periodic superlattice composed of a ferroelectric and paraelectric layers with the thicknesses L_1 and L_2 , respectively. $L = L_1 + L_2$ is the periodic thickness of the superlattice. The direction of polarization p , polarization q and applied electric field E are indicated in the figure. (Chew, 2012)

layers as shown in Fig.2.1. In general, layer A is ferroelectric material whereas layers B can be either ferroelectric or paraelectric. The two constituent layers interact with each other via the polarizations located at the interfaces. For simplicity, we consider the case when the polarization is parallel to surfaces or interfaces, so there is no depolarization field in the system. At the beginning, we construct the model using a dipole lattice model as proposed by Ishibashi (Ishibashi, 1990; Omura, Adachi, & Ishibashi, 1991; Ishibashi, 1992; Omura, Adachi, & Ishibashi, 1992; Omura, Mihara, & Ishibashi, 1993). In fact, this dipole lattices model has been used to study the polarization reversal in ferroelectric thin films (Ricinschi, Lerescu, & Okuyama, 2000; Ricinschi, Ishibashi, Iwata, & Okuyama, 2001; Baudry & Tournier, 2001).

The dipole lattice model assumes that each layer is an ensemble of dipole lattices characterized by polarization which has double potential wells. To illustrate, we consider a simple case of one-dimensional ferroelectric superlattices composed of alternating layer A and layer B with total number of M and N lattices, respectively. The p_m and q_m represent the dipole lattices located at the m -th sites of layer A and n -th of layer B. Each dipole

interacts with its nearest-neighboring dipole. κ_1 and κ_2 are the corresponding interaction parameter between the nearest-neighboring dipoles within layer A and layer B .

The free energy for the layer A with total dipole lattices M , is (Chew et al., 2006, 2011a)

$$F_1 = \sum_{m=1}^M \left[\frac{\alpha_1}{2} p_m^2 + \frac{\beta_1}{4} p_m^4 - E p_m \right] + \sum_{m=2}^M \left[\frac{\kappa_1}{2} (p_m - p_{m-1})^2 \right] \quad (2.1)$$

and the free energy for the layer B with total lattices N is

$$F_2 = \sum_{n=1}^N \left[\frac{\alpha_2}{2} q_n^2 + \frac{\beta_2}{4} q_n^4 - E q_n \right] + \sum_{n=2}^N \left[\frac{\kappa_2}{2} (q_n - q_{n-1})^2 \right] \quad (2.2)$$

where the higher order q terms are truncated. E is the applied electric field. In the ferroelectric phase, $\alpha_i < 0$ and $\beta_i > 0$, whereas $\alpha_i > 0$ for the paraelectric layer.

The dipoles at the interface of layer A and layer B are given by $p_1 = p_M$ and $q_1 = q_N$, respectively. It is easily seen that the interaction energy between the dipoles at the interface of the two constituent layers is given by (Chew et al., 2006)

$$F_i = \frac{\lambda}{2} \left[(p_M - q_1)^2 + (p_1 - q_N)^2 \right] \quad (2.3)$$

where λ denote the interaction parameter between the interface dipole lattices. By assuming that the variation of the order parameter within each layer is sufficiently smooth and each layer consists of a large number of dipoles, then the interaction energy of layer A (second term in Eq.(2.1)) can be written approximated as (Chew et al., 2011a)

$$\sum_{m=2}^M \left[\frac{\kappa_1}{2} (p_m - p_{m-1})^2 \right] \approx \int_0^{L_1} \frac{\kappa_1}{2} \left(\frac{dp}{dx} \right)^2 dx \quad (2.4)$$

where $L_1 = M a_1$ and a_1 are the thickness and the lattice constant of layer A , respectively. Similarly, the interaction energy of layer B with thickness $L_2 = N a_2$ and its lattice constant

a_2 (second term in Eq.(2.2)) is given by (Chew et al., 2011a)

$$\sum_{n=2}^N \left[\frac{\kappa_2}{2} (q_n - q_{n-1})^2 \right] \approx \int_0^{L_2} \frac{\kappa_2}{2} \left(\frac{dq}{dx} \right)^2 dx \quad (2.5)$$

where the periodic thickness is $L = L_1 + L_2$. Periodic boundary conditions are considered for describing the infinite ferroelectric superlattice. The periodic boundary condition indicates that we only have to consider a one-period superlattice structure.

Since there are only two dipoles at each interface contribute to the interface coupling energy, the interface energy (2.3) remains unchanged. Thus, it is clear that the interface energy has the same form as the interaction energy term of the dipole lattice model or the gradient term of the continuum model or the Landau-Ginzburg theory, which describes the inhomogeneity of polarization within the constituent layer.

2.5.2 Continuum Model

Now we rewrite the free energies Eqs. (2.1), (2.2) and (2.3) into a continuum Landau-Ginzburg theory. Hence, the final form of the total free energy per unit area of the superlattices with periodic thickness, $L = L_1 + L_2$ is

$$F = F_1 + F_2 + F_i, \quad (2.6)$$

where the total free energy densities of layer A and B are (Chew et al., 2011a)

$$F_1 = \int_{-L_1}^0 \left[\frac{\alpha_1}{2} p^2 + \frac{\beta_1}{4} p^4 + \frac{\kappa_1}{2} \left(\frac{dp}{dx} \right)^2 - Ep \right] dx, \quad (2.7)$$

$$F_2 = \int_0^{L_2} \left[\frac{\alpha_2}{2} q^2 + \frac{\beta_2}{4} q^4 + \frac{\kappa_2}{2} \left(\frac{dq}{dx} \right)^2 - Eq \right] dx, \quad (2.8)$$

respectively. In Eq. (2.7) and (2.8), the α_j ($j : A$ or B) is temperature dependent as $\alpha_j = \alpha_{0,j}(T - T_0)$. β_j is the coefficients and κ_j is the gradient coefficient determining the energy cost due to the inhomogeneity of polarization.

The interface energy can be written as (Chew et al., 2003; Ho Tsang, Chew, Ishibashi, & G. Shin, 2004; Chew, Ishibashi, & G. Shin, 2005; Chew et al., 2008, 2009; Ishibashi & Iwata, 2007; Chew et al., 2011c, 2011a)

$$F_i = \frac{\lambda}{2} (p_i - q_i)^2 = \frac{\lambda}{2} (p_i^2 + q_i^2) - \lambda p_i q_i. \quad (2.9)$$

where p_i and q_i are the polarizations at interface with the periodic boundary condition gives $p_m = p_1 = p_i$ and $q_n = q_1 = q_i$. In Eq. (2.9), the interface parameter λ can be conveniently related to the dielectric permittivity in vacuum ϵ_0 as (Chew, Ong, & Iwata, 2011b; Lim, Chew, Ong, & Iwata, 2012)

$$\lambda = \frac{\lambda_0}{\epsilon_0} \quad (2.10)$$

where λ_0 denote the temperature-independent interface parameter.

Basically, the interface energy term (2.9) is characterized by the interface-related parameter λ . It is important to note that the right-hand side of interface energy term (2.9) can be divided into two parts: (i) non-ferroelectric part (“ $\lambda p_i^2/2$ ” and “ $\lambda q_i^2/2$ ”) and (ii) polarizations coupling part (“ $\lambda p_i q_i$ ”) (Chew et al., 2011a; Chew, 2012; Lim et al., 2012). On the basis of Landau theory, Bratkovsky and Levanyuk have illustrated that the strong smearing of phase transition in ferroelectric thin films by considering the surface as a defect coupled to the order parameter (Bratkovsky & Levanyuk, 2005, 2009). In their model (Bratkovsky & Levanyuk, 2005), the surface energy term consists of a “dead layer” and its field component. It is noteworthy that in our model, the non-ferroelectric terms

(“ $\lambda p_i^2/2$ ” and “ $\lambda q_i^2/2$ ”) are also corresponding to the formation of “dead layers” at the interface region. Besides that, it has been proven by first-principles calculations (Stengel & Spaldin, 2006; Stengel, Vanderbilt, & Spaldin, 2009) and experimentally (Chang, Alexe, Scott, & Gregg, 2009) that the dead layer is an intrinsic effect and unavoidable phenomena at metal-ferroelectric interface. The bonding at the metal-ferroelectric interfaces of ultrathin ferroelectric capacitors can significantly affects the properties at interface. As a result, it gives rise to the formation of intrinsic dipole moments at interface or so-called dead layer. In fact, these dead layers are actually linear dielectrics, and their dielectric stiffnesses are determined by the interface parameter $\lambda > 0$. On the other hand, the polarization coupling part “ $\lambda p_i q_i$ ” describes the mutual interaction between the local polarization at interfaces due to the modification of bonding at the interfaces which has the same form as the coupling term (the linear term) in the Qu model (B. D. Qu et al., 1997).

In our model, λ describes the effect of interface intermixing in the superlattices and it governs the inhomogeneity of polarization near the interface. Therefore, the continuity or discontinuity of polarizations across the interface depends upon the nature of the intermixed layer formed at interfaces. If $\lambda \neq 0$, an intermixed layer which is analogous to a dead layer with properties different from those of both constituents is expected to form at the interface region (Chew et al., 2003; Ho Tsang et al., 2004). If layer B is ferroelectric, the formation of intermixed layer gives rise to an inhomogeneity of polarization near interfaces. However, if layer B is paraelectric, the polarization may induce at interface of this layer which depends on its dielectric stiffness. On the contrary, if $\lambda = 0$, no intermixed layer forms at the interface region. As a consequence, the polarization in the B layer is homogeneous if it is ferroelectric layer, while no induced-polarization in the B layer if it is paraelectric layer.

In equilibrium, the stable states of the ferroelectric superlattice correspond to the minima of F with respect to the polarization. These are given by solving the Euler-

Lagrange equations $\frac{\partial F}{\partial p} - \frac{\partial F}{\partial x} \left(\frac{\partial F}{\partial p'} \right) = 0$ with $p' = \frac{dp}{dx}$:

$$\left. \begin{aligned} \kappa_1 \frac{d^2 p}{dx^2} &= \alpha_1 p + \beta_1 p^3 - E \\ \kappa_2 \frac{d^2 q}{dx^2} &= \alpha_2 q + \beta_2 q^3 - E \end{aligned} \right\}. \quad (2.11)$$

with the boundary conditions for the polarizations at the interfaces as

$$\left. \begin{aligned} \frac{dp}{dx} &= -\frac{\lambda}{\kappa_1} (p_i - q_i) \\ \frac{dq}{dx} &= \frac{\lambda}{\kappa_2} (p_i - q_i) \end{aligned} \right\}. \quad (2.12)$$

There have been a number of papers reported the analytical solutions of this continuum Landau-Ginzburg model in study ferroelectric superlattice consist of ferroelectrics and paraelectrics layers. The earliest works of this continuum Landau-Ginzburg model were published by Chew and co-workers (Chew et al., 2003) focus on interface structure in double-layer ferroelectrics. Later on, Ishibashi and Iwata (Ishibashi & Iwata, 2007) applied this continuum Landau-Ginzburg model based on the lattice model (Chew et al., 2006) to discuss the phase transitions of a ferroelectric superlattice. They considered the coupling between ferroelectric and paraelectric layers through the interface interaction. The analytical solutions of the polarization modulation profile via interface coupling in a superlattice was later reported by Chew et al. (Chew et al., 2009). Their works shown that the polarization modulation profile of a ferroelectric superlattice is determined by the interface-induced polarizations in the paraelectric layer which can be strongly induced via the interface coupling. Later on, they further investigate and obtained the exact expressions for the polarization profiles induced by an external electric field and the dielectric susceptibilities in the paraelectric phase (Chew et al., 2008). The complete reviews of this Landau-Ginzburg model of ferroelectric superlattices are given by Chew et al., 2011b and Chew, 2012.

CHAPTER 3

ELECTROSTATIC COUPLING AND INTERFACE INTERMIXING IN FERROELECTRIC SUPERLATTICES

3.1 Introduction

Ferroelectric superlattices present an opportunity for developing artificial structures with fascinating properties for device applications. Superlattices combining a ferroelectric and a paraelectric have been studied extensively both by experiment and theory. Many superlattices have been fabricated and studied, such as BaTiO₃/SrTiO₃ (Tabata et al., 1994; Tsurumi et al., 2002b), PbTiO₃/SrTiO₃ (Dawber, Lichtensteiger, et al., 2005; Dawber et al., 2007), KTaO₃/KNbO₃ (H.-M. Christen et al., 1998; Specht et al., 1998), BiFeO₃/SrTiO₃ (Ranjith, Kundys, & Prellier, 2007), BaTiO₃/(Ba, Sr)TiO₃, etc. While many thermodynamic models have been put forward to study ferroelectric superlattices (B. D. Qu et al., 1997; Chew et al., 2000; Roytburd et al., 2005; Stephanovich et al., 2005; Dawber et al., 2007; Pertsev, Janolin, Kiat, & Uesu, 2010), they all generally do not take into account of intermixing at interfaces. In layered structures, intermixed layers may form at interfaces between two layers and affect the properties of superlattices (Pertsev & Tyunina, 2011).

In this chapter, a thermodynamic model is developed to study electrostatic coupling and interface intermixing in superlattices comprising alternate layers of ferroelectrics and paraelectrics. The superlattice is modelled by considering them as layers of strained ferroelectric or paraelectric with appropriate electrostatic boundary conditions (Stephanovich et al., 2005; Lim et al., 2012). Interface intermixing leads to inhomogeneous internal electric field and polarization in superlattices. On the basis of our thermodynamic model, we will discuss the effect of electrostatic coupling and interface intermixing in superlattice

which comprising alternate layers of ferroelectric and dielectric in Section 3.5. The relationship between these ferroelectric properties including internal electric field, dielectric susceptibility and polarization will be examined and discussed in Section 3.6. Finally, the polarization reversal in ferroelectric superlattices with “switchable” polarization in intermixed layers is examined in Section 3.7.

3.2 Literature Review

In the preceding chapter in Section 2.3, we have discussed some key factors that affect ferroelectric superlattices. To sum up, Torres-Pardo et al., 2011 and Zubko et al., 2012 have recently demonstrated the local structural distortion across the interface which indicating the presence of inhomogeneous ferroelectric properties in superlattices. Induced changes in polarization due to electrostatic coupling can have significant effects on the superlattice properties (Roytburd et al., 2005). Epitaxial strains are well known to have a strong impact on the properties of these superlattices (Dawber, Rabe, & Scott, 2005). The properties of these superlattices can be manipulated by changing the ferroelectric volume fraction (Dawber et al., 2007). Interface coupling (B. D. Qu et al., 1997; Bousquet et al., 2008) and intermixing (Pertsev & Tyunina, 2011; Cooper et al., 2007) effects have also been shown to be important in these superlattices.

Chew and co-worker have proposed a thermodynamic model to study interface intermixing in ferroelectric superlattices (Chew et al., 2006; Ishibashi & Iwata, 2007; Chew et al., 2008, 2009, 2011c, 2011a; Chew, 2012). An interface energy term is introduced to describe the local polarization coupling at interfaces. The existence of interface polarization coupling leads to the formation of intermixed layer at interfaces (Chew et al., 2003) and a periodic modulation in polarization. In the works, however, it is assumed that the polarization aligns parallel to surface of superlattices, and thus the depolarization effect is ignored. We have recently extended the model by taking into account the effect of elec-

trostatic coupling and epitaxial strain on phase transition, polarization, internal electric field and dielectric susceptibility in ferroelectric superlattices (Lim et al., 2012; Chew, Lim, Ong, & Iwata, 2013; Lim, Chew, Ong, & Iwata, 2013).

3.3 Formalism for Electrostatic Coupling and Interface Intermixing

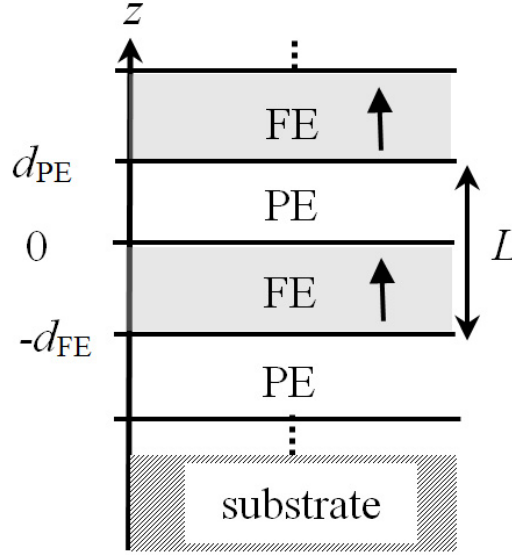


Figure 3.1: Schematic illustration of a periodic superlattice composed of a ferroelectric layer and a paraelectric layer. The thicknesses of ferroelectric layer (FE) and paraelectric layer (PE) are d_{FE} and d_{PE} , respectively. Arrow indicates the direction of polarization.

We consider a superlattice composed of two constituents: a ferroelectric layer and a paraelectric layer (hereafter, we denote the superlattice as a ferroelectric/paraelectric superlattice), which grows on a substrate, as schematically shown in Fig. 3.1.

By assuming that all spatial variation of polarization takes place along the z -direction, the Helmholtz free energy per unit area for one period of the superlattice can be expressed as following:

$$F = F_{FE} + F_{PE} + F_I. \quad (3.1)$$

The free energy per unit area of ferroelectric layer with thickness d_{FE} is $F_{FE} = \int_{-d_{FE}}^0 f_{FE} dz$, and the free energy per unit area of paraelectric layer with thickness d_{PE} is $F_{PE} = \int_0^{d_{PE}} f_{PE} dz$.

f_{FE} and f_{PE} are the free energy densities, given as (Pertsev et al., 2000)

$$f_j = \alpha_j^* p_j^2 + \beta_j^* p_j^4 + \gamma_j p_j^6 + \frac{\kappa_j}{2} \left(\frac{dp_j}{dz} \right)^2 - \frac{1}{2} E_{d,j} p_j + \left(\frac{c_{11,j}^2 + c_{11,j} c_{12,j} - 2c_{12,j}^2}{c_{11,j}} \right) u_{m,j}^2 - E_{ext} p_j \quad (3.2)$$

In Eq. (3.2), p_j corresponds to the polarization of layer j (j : FE or PE). $\alpha_j^* = \alpha_j + 2(c_{12,j} g_{11,j} / c_{11,j} - g_{12,j}) u_{m,j}$ and $\beta_j^* = \beta_j - g_{11,j}^2 / 2c_{11,j}$ where α_j (temperature dependent), β_j and γ_j are the Landau coefficients. $c_{11,j}$ and $c_{12,j}$ are the elastic stiffness coefficients, whereas $g_{11,j}$ and $g_{12,j}$ denote the electrostrictive constants. $u_{m,j} = (a_s - a_j) / a_s$ denotes the in-plane misfit strain induced by the substrate due to the lattice mismatch. a_j is the unconstrained equivalent cubic cell lattice constant of layer j and a_s is the lattice parameter of the substrate. κ_j denotes the gradient coefficient that determines the energy cost due to the inhomogeneity of polarization p_j . $E_{d,j}$ acts as the depolarization field of layer j , if its direction is opposite to the direction of ferroelectric polarization. If $E_{d,j}$ inclines in the same direction of polarization, it cannot be regarded as the depolarization field; thus, we denote $E_{d,j}$ as “the internal electric field”. The E_{ext} is the external electric field.

3.3.1 Interface Intermixing

The interface energy is given by (Chew, 2012; Ishibashi & Iwata, 2007; Chew et al., 2008, 2009, 2011c)

$$F_I = \frac{\lambda_0}{2\epsilon_0} \left[(p_{FE}(0) - p_{PE}(0))^2 + (p_{FE}(-d_{FE}) - p_{PE}(d_{PE}))^2 \right], \quad (3.3)$$

where λ_0 is the temperature-independent interface parameter and ϵ_0 is the dielectric permittivity in vacuum. $p_{FE}(0)$ and $p_{FE}(-d_{FE})$ represent the polarization at the interface of ferroelectric layer, whereas interface polarizations of paraelectric layer are represented by

$p_{PE}(0)$ and $p_{PE}(d_{PE})$. It is important to mention that the interface energy (3.3) possesses a similar form as the gradient terms in Eq. (3.2) (Chew, 2012; Chew et al., 2011a).

The physical origin of the interface energy (3.3) can be interpreted as follows (Chew, 2012; Chew et al., 2011a). By symmetry, we have $p_{FE}(0) = p_{FE}(-d_{FE}) = p_i$ and $p_{PE} = p_{PE}(d_{PE}) = q_i$ and thus, equation (3.3) can be written as $F_i = \frac{\lambda_0}{\epsilon_0} (p_i - q_i)^2 = \frac{\lambda_0}{\epsilon_0} (p_i^2 + q_i^2) - 2\frac{\lambda_0}{\epsilon_0} p_i q_i$. In other words, the interface energy expression can be clearly interpreted by separating it (3.3) into two parts: (i) non-ferroelectric part and (ii) polarizations coupling part. It is well-known that dead layers are intrinsic and appear inevitably at the metal-ferroelectric interface (Stengel et al., 2009; Chang et al., 2009). The bonding at the metal-ferroelectric interfaces of ultrathin ferroelectric capacitors, which constituted the dead layers, strongly affects the properties at interface through the formation of intrinsic dipole moments at interface. In the present model, the former term is analogous to the formation of “dead” layers (Stengel et al., 2009; Chang et al., 2009) at interfaces, i.e. the surfaces of layer FE (“ $\lambda_0 p_i^2 / \epsilon_0$ ”) layer and layer PE (“ $\lambda_0 q_i^2 / \epsilon_0$ ”) layer. The dead layers are linear dielectrics, and their dielectric stiffnesses are determined by the interface parameter $\lambda_0 > 0$. The polarization coupling part “ $\lambda_0 p_i q_i / \epsilon_0$ ” describes the mutual interactions between the local polarization at interfaces due to the modification of bonding at the interfaces.

In the present study of superlattices, the interface parameter λ_0 describes the effect of interface intermixing in the superlattice as a whole. The explicit expression derived from interface structure for the simple case without electrostatic boundary conditions indicates that the intermixed layer is governed by the physical properties of the two constituent layers (Chew et al., 2003; Ho Tsang et al., 2004). The interface intermixing effects are governed by the inhomogeneity of polarization near the interface which may arise from the formation of intrinsic dipole moments and effect of coupling between the local polarization at the interface. The continuity or discontinuity of polarizations across the

interface depends upon the nature of the intermixed layer formed at interfaces. If $\lambda_0 \neq 0$, an intermixed layer (Chew et al., 2003; Ho Tsang et al., 2004) (analogous to a dead layer (Stengel et al., 2009; Chang et al., 2009)) with properties different from those of both constituent layers is expected to form at the interface region. Polarization may be induced at interface of the paraelectric layer, depending on its dielectric stiffness. If $\lambda_0 = 0$, no intermixed layer is formed at the interface region. Therefore, the polarization in the ferroelectric layer is homogeneous and no induced-polarization can be found in the paraelectric layer.

At the interface, the boundary conditions for the polarization are

$$\left\{ \begin{array}{l} -\kappa_{FE} \frac{dp_{FE}}{dz} \Big|_{z=-d_{FE}} + \frac{\lambda_0}{\epsilon_0} [p_{FE}(-d_{FE}) - p_{PE}(d_{PE})] = 0 \\ \kappa_{PE} \frac{dp_{PE}}{dz} \Big|_{z=0} + \frac{\lambda_0}{\epsilon_0} [p_{FE}(0) - p_{PE}(0)] = 0 \\ \kappa_{FE} \frac{dp_{FE}}{dz} \Big|_{z=0} + \frac{\lambda_0}{\epsilon_0} [p_{FE}(0) - p_{PE}(0)] = 0 \\ -\kappa_{PE} \frac{dp_{PE}}{dz} \Big|_{z=d_{PE}} + \frac{\lambda_0}{\epsilon_0} [p_{FE}(-d_{FE}) - p_{PE}(d_{PE})] = 0. \end{array} \right. \quad (3.4)$$

3.3.2 Electrostatic Coupling

The internal electric field E_{dj} within the constituent layer may be found using the Maxwell's equation that are, in the present case with no free charges (Stephanovich et al., 2005; Landau, Pitaevskii, & Lifshits, 1998),

$$\nabla \cdot (\epsilon_0 \mathbf{E} + \mathbf{P}) = 0, \quad (3.5a)$$

$$\nabla \times \mathbf{E} = 0 \quad (3.5b)$$

where \mathbf{E} is the electric field and \mathbf{P} is the polarization. Equation (3.5b) indicates that we may define a scalar function ϕ_j , i.e. the electrostatic potential, which satisfies $E_{d,j} = -\nabla \phi_j$. Using $E_{d,j} = -\nabla \phi_j$ ($j : FE$ or PE), the Euler-Lagrange equations follow from

the equations (3.2) can be expressed in term of the electrostatic potential φ_j as

$$\kappa_j \frac{d^2 p_j}{dz^2} = 2\alpha_j^* p_j + 4\beta_j^* p_j^3 + 6\gamma_j p_j^5 + \frac{1}{2} \frac{d\varphi_j}{dz} - E_{ext} \quad (3.6)$$

where the electrostatic potentials are (Stephanovich et al., 2005; Landau et al., 1998)

$$-\epsilon_0 \frac{d^2 \varphi_j}{dz^2} + \frac{dp_j}{dz} = 0 \quad (3.7)$$

and can be found using the Maxwell's equation (3.5a).

For the electrostatic boundary conditions, the continuity of electric displacement at the interface gives

$$\begin{cases} -\epsilon_0 \frac{d\varphi_{FE}}{dz} \Big|_{z=0} + \epsilon_0 \frac{d\varphi_{PE}}{dz} \Big|_{z=0} = -(p_{FE}(0) - p_{PE}(0)), \\ -\epsilon_0 \frac{d\varphi_{FE}}{dz} \Big|_{z=-d_{FE}} + \epsilon_0 \frac{d\varphi_{PE}}{dz} \Big|_{z=d_{PE}} = -(p_{FE}(-d_{FE}) - p_{PE}(d_{PE})), \end{cases} \quad (3.8)$$

and the continuity of tangential component of electric field gives the following conditions on the electric potentials

$$\begin{cases} \varphi_{FE}(0) = \varphi_{PE}(0), \\ \varphi_{FE}(-d_{FE}) = \varphi_{PE}(d_{PE}). \end{cases} \quad (3.9)$$

3.4 Calculations For PbTiO₃/SrTiO₃ Superlattices

For illustration, we apply the model to perform a numerical calculation on a superlattice consisting of ferroelectric layer as PbTiO₃ (PT) and paraelectric layer as SrTiO₃ (ST) on a ST substrate, as a representative system.

For the convenient of discussion, our free energy is based on an expansion of the Helmholtz free energy in terms of polarization and strain. As shown in Table 3.1, we

adopt the Helmholtz free energy coefficients of the chosen materials from Dawber et al., 2007. The free energy coefficients of PT are taken from Pertsev et al., 1998 in Gibbs free energy form, whereas the free energy coefficients of ST are from Pertsev et al., 2000 in Helmholtz free energy form. The coefficients of Gibbs free energy are converted into the coefficients of Helmholtz free energy by using Legendre transformation which has been discussed in the preceding Section 1.6.2.1.

In the calculations, we take 1 *unit cell*(*u.c.*) $\approx 0.4\text{nm}$ (Fong et al., 2004) and the characteristic length or correlation length ξ_0 is defined as

$$\xi_0 = \sqrt{\kappa_{FE}/(\alpha_{0FE}T_{0FE})} \sim 0.6\text{nm}, \quad (3.10)$$

corresponds to the estimated length of domain wall half width (Stephanovich et al., 2005; Fong et al., 2004). The lattice constants in the cubic phase are $a_{FE} = 3.969\text{\AA}$ and $a_{PE} = 3.905\text{\AA}$ for PT and ST, respectively (Dawber et al., 2007). Based on the lattice constants, the lattice misfit strains in the PT and ST layers are obtained as $u_{m,FE} = -0.0164$ and $u_{m,PE} = 0$, respectively.

Table 3.1: List of Helmholtz free energy coefficients used in this study

	PT	ST	Units
α	$3.8(T - T_{0PT})$	$7.45(T - T_{0ST})$	$\times 10^5 \text{JmC}^{-2}$
β	4.229	20.2	$\times 10^8 \text{Jm}^5 \text{C}^{-4}$
γ	2.6	-	$\times 10^8 \text{Jm}^9 \text{C}^{-6}$
T_0	752	51.64	K
g_{11}	1.14	1.25	$\times 10^{10} \text{JmC}^{-2}$
g_{12}	4.63	-10.8	$\times 10^8 \text{JmC}^{-2}$
c_{11}	1.746	3.36	$\times 10^{11} \text{Jm}^{-3}$
c_{12}	0.794	1.07	$\times 10^{11} \text{Jm}^{-3}$
κ	1.029	1.029	$\times 10^{-10} \text{Jm}^3 \text{C}^{-2}$

It is convenient to rescale all the variables into their dimensionless forms, please refer to Appendix B for details. In the calculations, the Euler-Lagrange equations (3.6) and electrostatic equations (3.7) were transformed into a system of nonlinear equations by

using the finite-difference method. Solving the nonlinear equations numerically with the interface boundary conditions, Eq. (3.4) and electrostatic boundary conditions, Eq.(3.8) & (3.9), we obtain the spatial dependence of internal electric field (or electrostatic potential) and polarization for the superlattices. Please refer to Appendix C for the description of our numerical methods.

The average polarization is defined as

$$P = \frac{1}{L} \left(\int_{-d_{FE}}^0 p_{FE} dz + \int_0^{d_{PE}} p_{PE} dz \right) \quad (3.11)$$

with the periodic thickness $L = d_{FE} + d_{PE}$. Similarly, the average internal electric fields is defined as

$$E_d = \frac{1}{L} \left(\int_{-d_{FE}}^0 e_{d_{FE}}(z) dz + \int_0^{d_{PE}} e_{d_{PE}}(z) dz \right). \quad (3.12)$$

3.5 The effects of electrostatic coupling and interface intermixing

In this section, we study the effects of electrostatic coupling and interface intermixing on the internal electric field and polarization of superlattices, composed of alternate layers of ferroelectrics (PbTiO₃) and paraelectrics (SrTiO₃), which can be grown on a substrate, as schematically shown in Fig. 3.1 (Lim et al., 2012). It is the objective of this study to investigate the case of polarization perpendicular to the surface or interface of a superlattice with the appropriate electrostatic boundary conditions. The correlation between the internal electric field and ferroelectric properties of the superlattice is examined by looking at the modulation profiles. Furthermore, the effect of interface intermixing and modulation period on the internal electric field and polarization are studied by changing the volume fraction or thickness ratio of the superlattice.

3.5.1 Result and Discussion

We will discuss both the cases of superlattices with electrostatic boundary conditions (Fig. 3.2(a) and 3.3(a)) and superlattices with non-electrostatic boundary conditions (Fig. 3.2(b) and 3.3(b)) at the ferroelectric/paraelectric interfaces. The case for non-electrostatic boundary condition can be assumed when the polarization in superlattices aligns parallel to interfaces, the effect of electrostatic coupling between ferroelectric layers, represented by $\frac{1}{2}E_{d,j}p_j$, can be ignored. This configuration of in-plane polarization is discussed with the objective of differentiating the effects of interface intermixing and electrostatic coupling.

We first look at the spatial dependence of polarization and internal electric field of the PT/ST superlattices with electrostatic boundary conditions. Fig. 3.2(a) shows the spatial profiles of polarization and internal electric field of PT/ST superlattices with $\phi_{FE} = 0.5$ (i.e. both the thickness of PT and ST layers are $3u.c.$) for different values of λ_0 . Cases for $\lambda_0 \neq 0$ indicate the formation of intermixed layers or “dead layers” at $z = 0$ (Chew et al., 2003; Ho Tsang et al., 2004). The thickness of intermixed layer is $1u.c.$ The existence of intermixed layer leads to an inhomogeneity of polarization near the interfaces, forming the interface region. The spatial dependence of polarization extends into the bulk over a distance governed by its correlation length. It is seen that the continuity or discontinuity of polarization and internal electric field across the interface depends sensitively on the nature of intermixed layer. The polarization and internal electric field vary spatially in a periodic manner, indicating a periodic interface-induced modulation. As λ_0 increases, both the magnitudes and the gaps of polarization and internal electric field at the interfaces are reduced. Another important features is that the modulated profiles of internal electric field and polarization are correlated. An interesting change of sign in the local internal electric field at the interface region is predicted in a superlattice with $\lambda_0 = \xi_0$ (brown

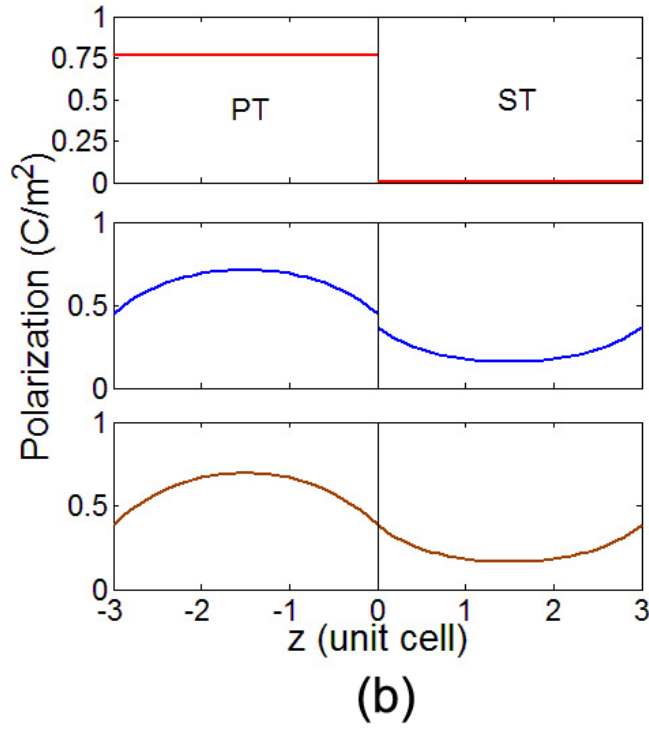
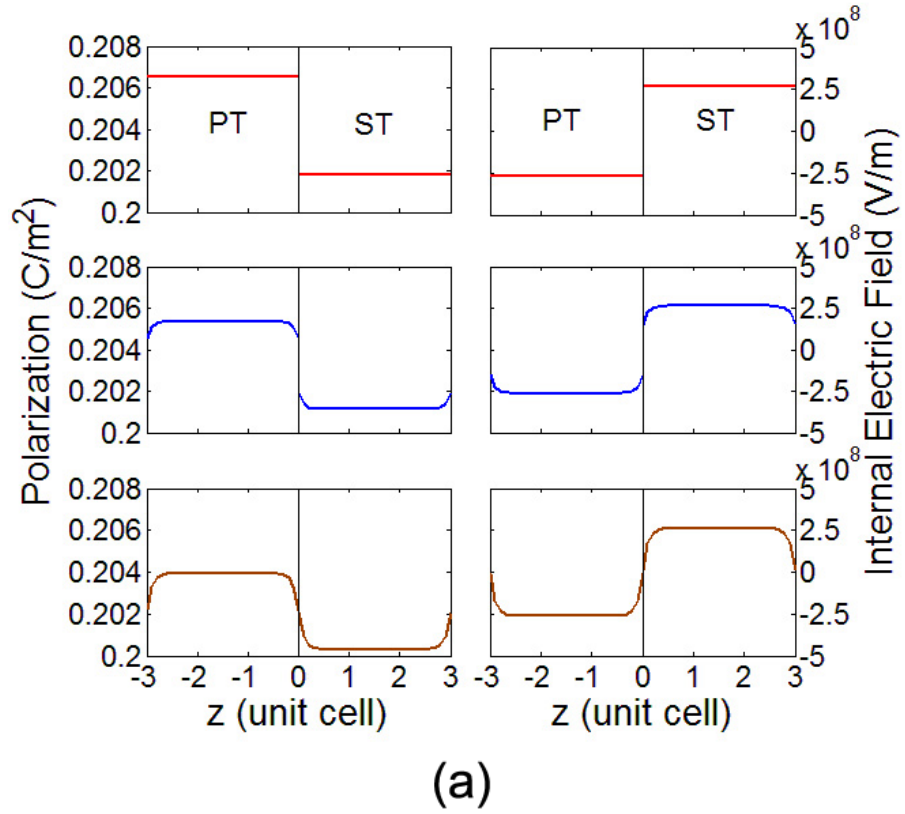


Figure 3.2: Spatial dependence of electrical properties at $T = 298K$ (a) with electrostatic coupling and (b) without electrostatic coupling. The values of λ_0 are: 0 (red line), $0.02\xi_0$ (blue line) and ξ_0 (brown line).

line). The internal field in PT layer acts as the depolarization field $E_{d,PT}(z) < 0$, whereas $E_{d,ST}(z) > 0$ tends to enhance the polarization in ST layer. The internal electric field in

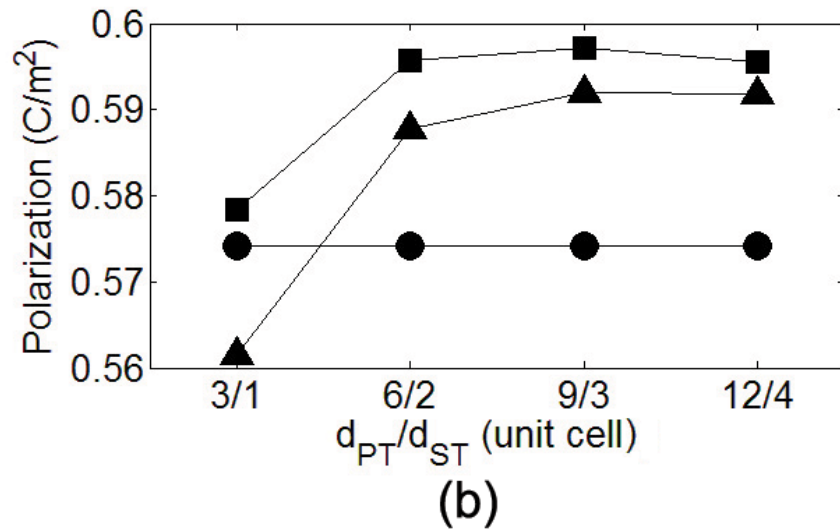
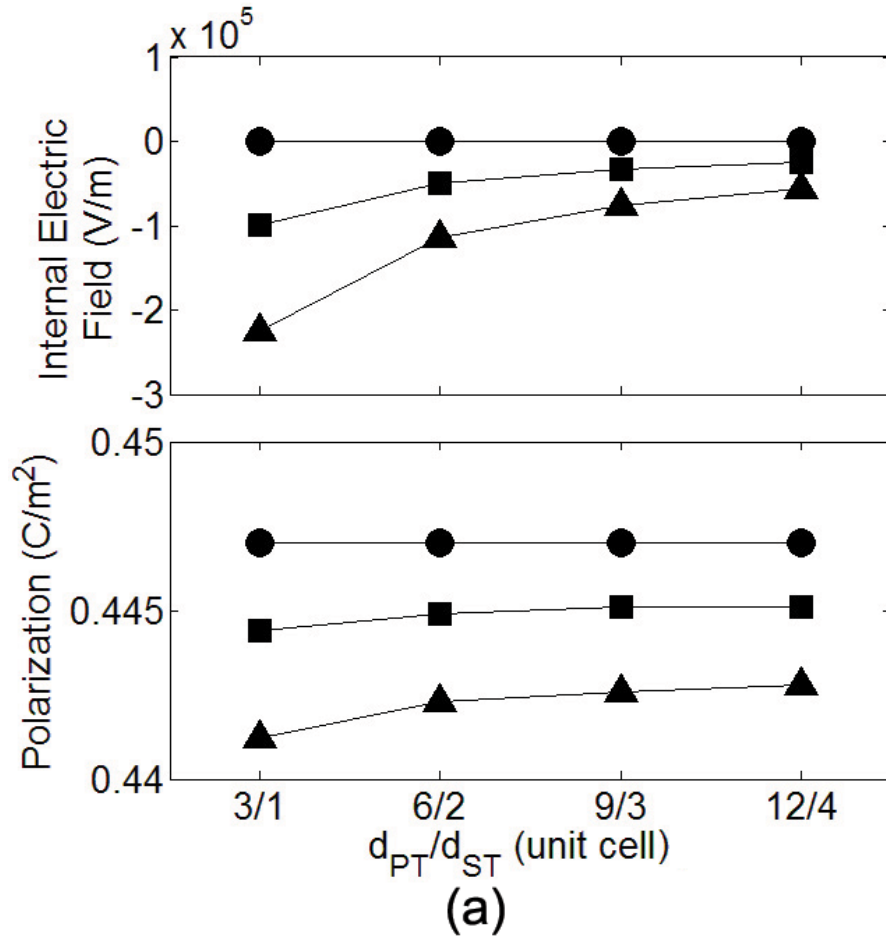


Figure 3.3: Electrical properties at $T = 293K$ as a function of d_{PT}/d_{ST} (a) with electrostatic coupling and (b) without electrostatic coupling. The values of λ_0 are: 0 (●), $0.02\xi_0$ (■) and ξ_0 (▲).

ST layer originates from the electrostatic interaction between polarizations in different PT layers across the ST layer (Roytburd et al., 2005). Hereafter, we denote it as “polarization-induced internal electric field”. The magnitude of the depolarization in PT layer for the

superlattice with $\lambda_0 = 0$ is $|E_{d,PT}| \sim 250\text{MV/m} \sim 0.4E_{C,PT}$ from our calculation, where the bulk coercive field of PT $E_{C,PT}$ is estimated as $E_{C,PT} = 4\alpha_{PT}^*(-\alpha_{PT}^*/6\beta_{PT}^*)^{1/2}/3 \sim 640\text{MV/m}$. Note also that Fig. 3.2(a) shows the internal field-induced polarization in the ST layer is almost the same as the spontaneous polarization of the PT layer.

In order to clarify the effect of intermixing at ferroelectric/paraelectric interfaces, we compare the configuration when the polarization of superlattice aligns along the surfaces or interfaces where the electrostatic coupling between ferroelectric layers can be neglected (Lim & Chew, 2014). We show the modulation profiles of polarization for PT/ST superlattices without considering the electrostatic boundary conditions, as illustrated in Fig. 3.2(b). This configuration with in-plane polarization is analogous to superlattices with interdigital electrodes (Harigai et al., 2003). In this case, there is no depolarization field in PT layer and internal electric field in ST layer does not exist. If no intermixing occurred, i.e. $\lambda_0 = 0$, the polarization in PT layer is equivalent to its bulk of $P \sim 0.75\text{C/m}^2$, whereas $P = 0$ for ST layer at $T = 298\text{K}$, as expected. From Figs. 3.2(a) and 3.2(b), it is clearly seen that electrostatic coupling between ferroelectric layers plays a dominant role in enhancing the polarization of superlattices with polarizations align perpendicular to interfaces. Even if no intermixing occurred, the polarizations of both the PT and ST layers are almost similar, as shown in Fig. 3.2(a).

We now investigate the average polarizations P and internal electric field E_d of PT/ST superlattices as a function of unit period with thickness ratio fixed at $d_{FE}/d_{PE} = 3$. Let us first examine the superlattice with electrostatic coupling, as shown in Fig. 3.3(a). With decreasing periodic thickness from long-period (PT/ST = 12/4) to short-period (PT/ST = 3/1) structures, both the values of P and E_d of a superlattice with $\lambda_0 = 0$ (●) remain almost constant. The internal electric field of the superlattice with $\lambda_0 = 0$ (●) is equal to $E_d \sim 0\text{V/m}$, implying that the depolarization field in PT layer and internal field in ST layer compensate each other. For the case of superlattices with $0.02\xi_0$ (■) and ξ_0 (▲),

P decreases with decreasing the periodic thickness, whereas the strength of depolarization field E_d increases with decreasing the periodic thickness. $E_d \neq 0$ of superlattices with $\lambda_0 \neq 0$ is clearly due to the inhomogeneous properties at interfaces as a result of the formation of intermixed layer at $z = 0$, as discussed in Fig. 3.2(a). Fig. 3.3(b) shows P and E_d of PT/ST superlattices without electrostatic coupling as a function of unit period. In this case, changes in P and E_d are purely due to intermixing at interface. Without intermixing $\lambda_0 = 0$, $P \sim 0.575C/m^2$ is unaffected by varying layer thicknesses, as expected from Fig. 3.3(a). For the case with intermixing $\lambda_0 \neq 0$, it is seen that P can be tuned by changing the layer thickness. Compared to superlattices with electrostatic coupling (as shown Fig. 3.3(a)), the change in P is more marked. From Figs. 3.3(a) and 3.3(b), it is seen that electrostatic coupling plays an important role in governing the properties of superlattices with polarizations align perpendicular to interfaces.

In Fig. 3.4, we show the internal electric field and polarization as a function of period thickness for a PT/ST superlattice with ferroelectric volume fraction $\phi = d_{FE}/(d_{FE} + d_{PE}) = 0.5$ (or thickness ratio of ferroelectric to dielectric $d_{FE}/d_{PE} = 0.5$). Without intermixing (black), both internal field and polarization are essentially independent from changing the layer thickness $d_{FE} = d_{PE}$. The depolarization field in PT layer and polarization-induced internal electric field in ST layer completely compensate each other, resulting in a zero net internal field in the superlattice. While the formation of intermixed layer gives rise to the existence of depolarization field, it has little influence on the polarization behaviour of the PT/ST superlattices (blue and red). The enhancement of depolarization field is clearly due to the inhomogeneous polarization at the interface region.

Finally, we compare the calculated polarization and transition temperature using our model with electrostatic couplings to those obtained in experiments (Dawber et al., 2007). In this discussion, the thickness of ST layer is maintained at $d_{PE} \approx 3u.c.$. Fig. 3.5 illustrates the average polarization P and internal electric field E_d of a PT/ST superlattice as

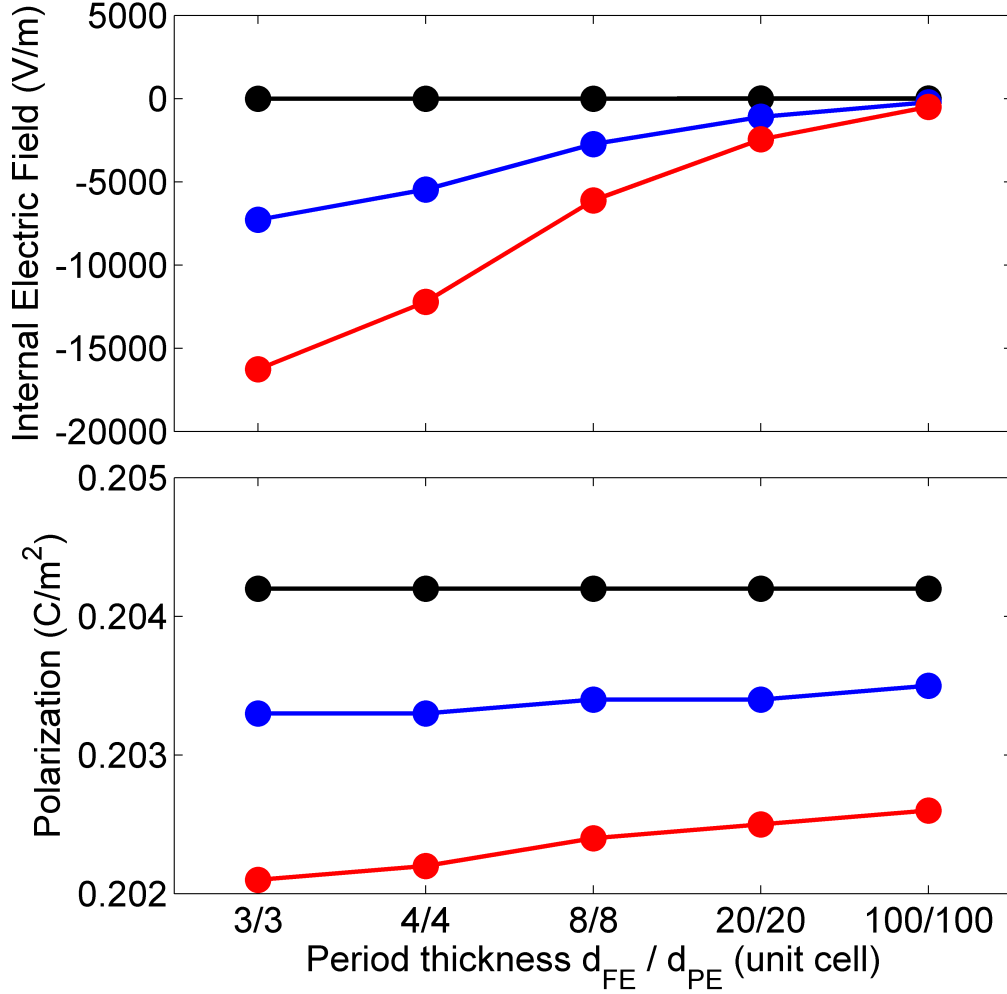


Figure 3.4: Internal electric field and polarization as a function of period thickness d_{FE}/d_{PE} for PT/ST superlattices with $d_{FE} = d_{PE}$ at $T = 298K$. The values of λ are: 0 (black line), $0.02\xi_0$ (blue line) and ξ_0 (red line).

a function of PT volume fraction, $\phi_{FE} = d_{FE}/(d_{FE} + d_{PE})$ for different λ_0 . Generally, P increases with increasing the PT volume fraction ϕ_{FE} . For the superlattice with $\lambda_0 = 0$ (red line), $E_d = 0V/m$ for all PT volume fraction ϕ_{FE} , as expected. For the case with $\lambda_0 \neq 0$, $E_d < 0$ implies an internal electric field, acts as a depolarization field, exists in the superlattices. It is seen that E_d increases with increasing ϕ_{FE} until it reaches its maximum value at $\phi_{FE} \sim 0.87$ before dying out (i.e. $E_d \sim 0$) at $\phi_{FE} \sim 1$. This is expected because PT approaches its bulk at $\phi_{FE} \sim 1$ with the bulk polarization $P \sim 0.75C/m^2$ and intermixing at interface no longer has a strong effect on the internal electric field. Formation of intermixed layer at interface $z = 0$ enhances the depolarization field E_d (see

Fig. 3.5(a)). Polarization P and transition temperature T_C (see inset of Fig. 3.5(b) and Fig. 3.5(c)) of the superlattices are almost unaffected by intermixing at interface, as expected. For comparison, the experimental measurements (solid dots) of polarization and transition temperature are also shown in Fig. 3.5(b) and 3.5(c), respectively. It is seen that there is a reasonable agreement between the calculated and measured polarizations for all values of λ_0 , indicating that intermixing at interfaces does not have a significant effect on the ferroelectric properties of superlattices (as discussed in Fig. 3.2(a) and 3.3(a)). We also compare the results with the predictions from the model proposed by Dawber et al. (Dawber et al., 2007). In the limit of very-short periods, the interface effect in PT/ST superlattices is induced by the coupling between antiferrodistortive and ferroelectric instabilities (Bousquet et al., 2008). Since the coupling of structural instabilities at interfaces is not considered, it is reasonable that the model cannot quantitatively capture the experimental data at low volume fraction $\phi_{FE} \lesssim 0.3$.

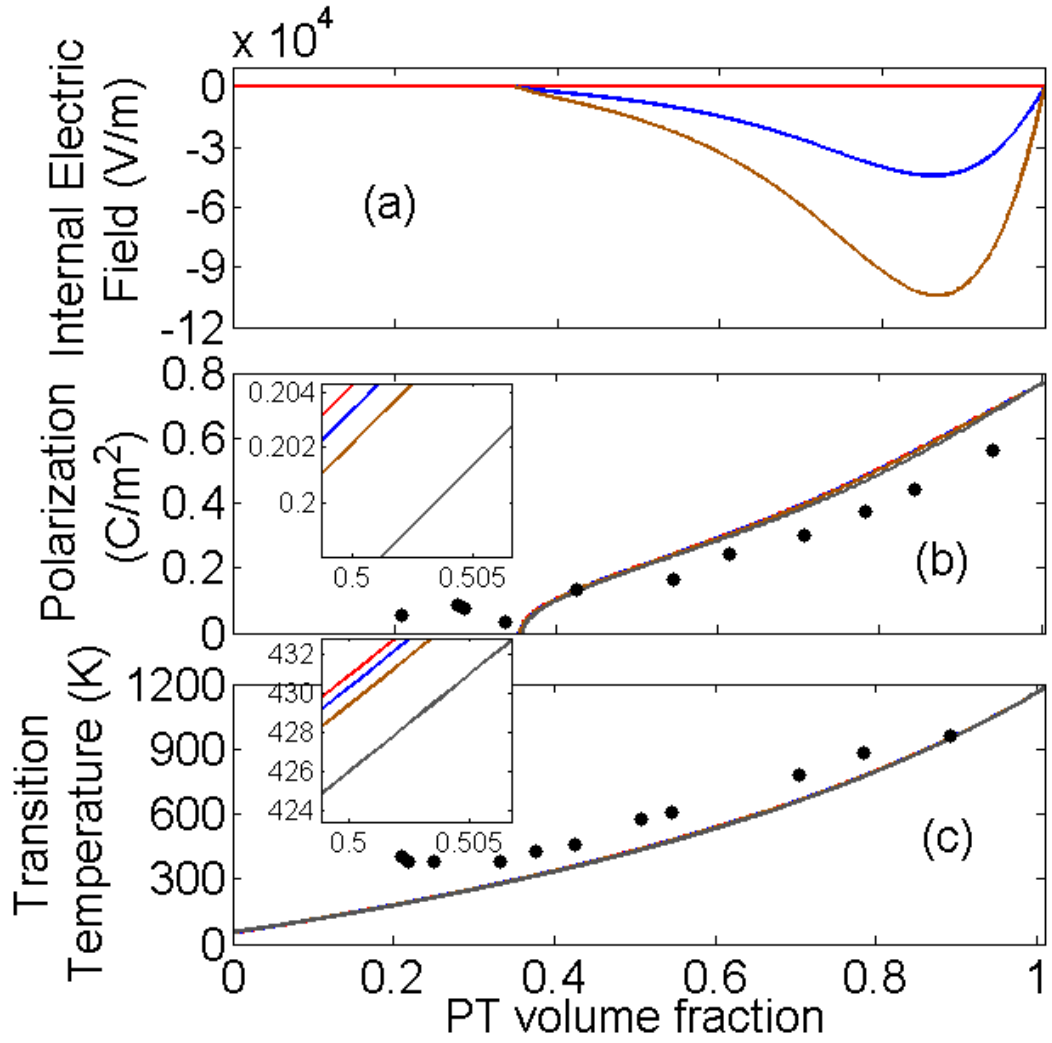


Figure 3.5: (a) Internal electric field and (b) polarization at $T = 298K$, and (c) transition temperature as a function of PT volume fraction ϕ_{FE} of PT/ST superlattices. The values of λ_0 are: 0 (red line), $0.02\xi_0$ (blue line) and ξ_0 (brown line). Solid dots (\bullet) represent the experimental data. The grey line denotes calculated result from Dawber et al. (Dawber et al., 2007).

3.6 Modulated Internal Electric Field, Dielectric Susceptibility and Polarization

In this section, our thermodynamic model will be used to calculate the spatially-varying internal electric field, dielectric susceptibility and polarization of these superlattices (Lim, Chew, Ong, & Iwata, 2013). Effects of modulation period and temperature on the internal electric field, dielectric susceptibility and polarization of these superlattices with inhomogeneous properties are examined. Correlation between these ferroelectric properties is established and discussed.

3.6.1 Formalism for Dielectric Susceptibility

The dielectric susceptibility of the superlattice under a weak electric field can be found by taking the differentiation of Eq. (3.6)

$$\kappa_j \frac{d^2 \chi_j}{dz^2} = (2\alpha_j^* + 12\beta_j^* p_j^2 + 30\gamma_j p_j^4) \chi_j - \frac{1}{2\epsilon_0} \frac{\partial E_{d,j}}{\partial E_{ext}} - \frac{1}{\epsilon_0}, \quad (3.13)$$

using $\chi = 1/\epsilon_0(\partial p_j/\partial E_{ext})$ and $j : FE$ or PE . In order to calculate the derivative of depolarization field with respect to external electric field in each layer, we expand the electric displacement as below:

$$\begin{aligned} \epsilon_0 E + p_j(z) &= D \\ \epsilon_0 (E_{d,j} + E_{ext}) + p_j(z) &= D \\ E_{d,j} &= \frac{1}{\epsilon_0} (D - p_j(z)) - E_{ext} \\ \frac{\partial E_{d,j}}{\partial E_{ext}} &= \frac{1}{\epsilon_0} \left(\frac{\partial D}{\partial E_{ext}} - \frac{\partial p_j(z)}{\partial E_{ext}} \right) - 1 \\ \frac{\partial E_{d,j}}{\partial E_{ext}} &= \frac{1}{\epsilon_0} \frac{\partial D}{\partial E_{ext}} - \chi_j(z) - 1 \\ \frac{\partial E_{d,j}}{\partial E_{ext}} &= \frac{1}{\epsilon_0} (\epsilon_0 + \epsilon_0 \bar{\chi}) - \chi_j(z) - 1 \\ &= \bar{\chi} - \chi_j(z) \end{aligned}$$

Here we have make use of the dielectric permittivity compliance (Lines & Glass, 1977; Grindlay, 1970), which is given as

$$\frac{\partial D_i}{\partial E_j} = \epsilon_{ij} = \epsilon_0 (\delta_{ij} + \chi_{ij}), \quad (3.14)$$

where $\epsilon_{ij} = \epsilon_0(\delta_{ij} + \chi_{ij})$ is the dielectric permittivity of the material, δ_{ij} is Kronecker's symbol and χ_{ij} is the dielectric susceptibility. Since our system is a superlattice model and $i = j$, we will consider the mean dielectric susceptibility and write it as $\bar{\chi}$. Hence, the

Eq. (3.13) can be rewrite by using the permittivity compliance, $\partial D/\partial E_{ext} = \epsilon_0(1 + \bar{\chi})$ as

$$\kappa_j \frac{d^2 \chi_j}{dz^2} = (2\alpha_j^* + 12\beta_j^* p_j^2 + 30\gamma_j p_j^4) \chi_j - \frac{1}{2\epsilon_0} (\bar{\chi} - \chi_j) - \frac{1}{\epsilon_0}. \quad (3.15)$$

Differentiation of polarization boundary conditions Eq. (3.4) with respect to E_{ext} yields the boundary conditions for the dielectric susceptibility at interface as

$$\left\{ \begin{array}{l} -\kappa_{FE} \frac{d\chi_{FE}}{dz} \Big|_{z=-d_{FE}} + \frac{\lambda_0}{\epsilon_0} [\chi_{FE}(-d_{FE}) - \chi_{PE}(d_{PE})] = 0 \\ \kappa_{PE} \frac{d\chi_{PE}}{dz} \Big|_{z=0} + \frac{\lambda_0}{\epsilon_0} [\chi_{FE}(0) - \chi_{PE}(0)] = 0 \\ \kappa_{FE} \frac{d\chi_{FE}}{dz} \Big|_{z=0} + \frac{\lambda_0}{\epsilon_0} [\chi_{FE}(0) - \chi_{PE}(0)] = 0 \\ -\kappa_{PE} \frac{d\chi_{PE}}{dz} \Big|_{z=d_{PE}} + \frac{\lambda_0}{\epsilon_0} [\chi_{FE}(-d_{FE}) - \chi_{PE}(d_{PE})] = 0. \end{array} \right. \quad (3.16)$$

Finally, the mean dielectric susceptibility, $\bar{\chi}$ of the superlattice is determined by the following formula

$$\frac{1}{1 + \bar{\chi}} = \frac{1}{L} \int_{-d_{FE}}^{d_{PE}} \frac{1}{1 + \chi_j(z)} dz. \quad (3.17)$$

In this work, Eqs.(3.6) and Eqs.(3.7) are solved numerically subject to the boundary conditions of Eq.(3.4), Eq. (3.8) and Eq.(3.9). After that, by inserting the result of polarization and electrostatic potential into Eqs.(3.15), the configuration of dielectric susceptibility can be calculated numerically subjected to the boundary conditions Eq.(3.16).

3.6.2 Result and Discussion

In this section, we use our model in Section 3.3 to apply to a superlattice consisting of PbTiO₃ (PT) as FE and SrTiO₃ (ST) as PE on ST substrate. The formalism and calculation are explained in Section 3.3 and Section 3.4. For ease of calculation, we first rescale all the variables into their dimensionless forms as described in Appendix B. In this work, the

interface intermixing parameter is set as $\lambda_0 = \xi_0$, implying that an intermixed layer with inhomogeneous properties are formed at interface region (Lim et al., 2012).

Fig. 3.6 shows the profiles of polarization, internal electric field and dielectric susceptibility in PT/ST superlattices for different thickness ratio. It is seen that intermixed layers with properties difference than that of both layers are formed at interfaces $z = 0$ (Lim et al., 2012). The formation of intermixed layer leads to inhomogeneity in polarization, internal field and dielectric susceptibility near the interfaces. The internal field in PT layer acts as the depolarization field $E_{d,FE} < 0$, whereas $E_{d,PE} > 0$ tends to induce the polarization in ST layer (Roytburd et al., 2005; Torres-Pardo et al., 2011). The internal field in ST layer originates from the electrostatic coupling between different PT layers (across the ST layer), and plays an important role in determining the ferroelectricity of these superlattice. The spatial profiles of polarization, internal electric field and dielectric susceptibility depend sensitively on the layer thickness of superlattice.

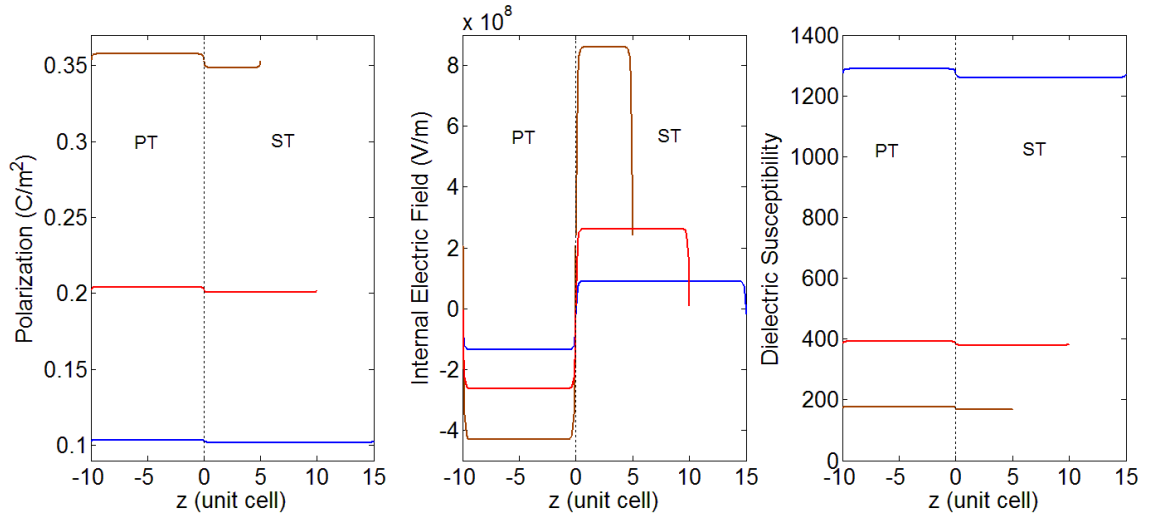


Figure 3.6: Profiles of polarization, internal electric field and dielectric susceptibility of PT/ST superlattice at $T = 298K$. The three lines represent different period thickness with ratio d_{FE}/d_{PE} (in u.c.): 10/15 (blue line), 10/10 (red line) and 10/5 (brown line).

The dependence of average internal electric field, polarization and dielectric susceptibility of superlattice on temperature for different thickness ratio is shown in Fig. 3.7. Internal electric field and polarization disappear at the transition temperature, whereas

the dielectric susceptibility diverges. It can be seen that the phase transition temperature of superlattices increases with increasing the thickness ratio d_{FE}/d_{PE} .

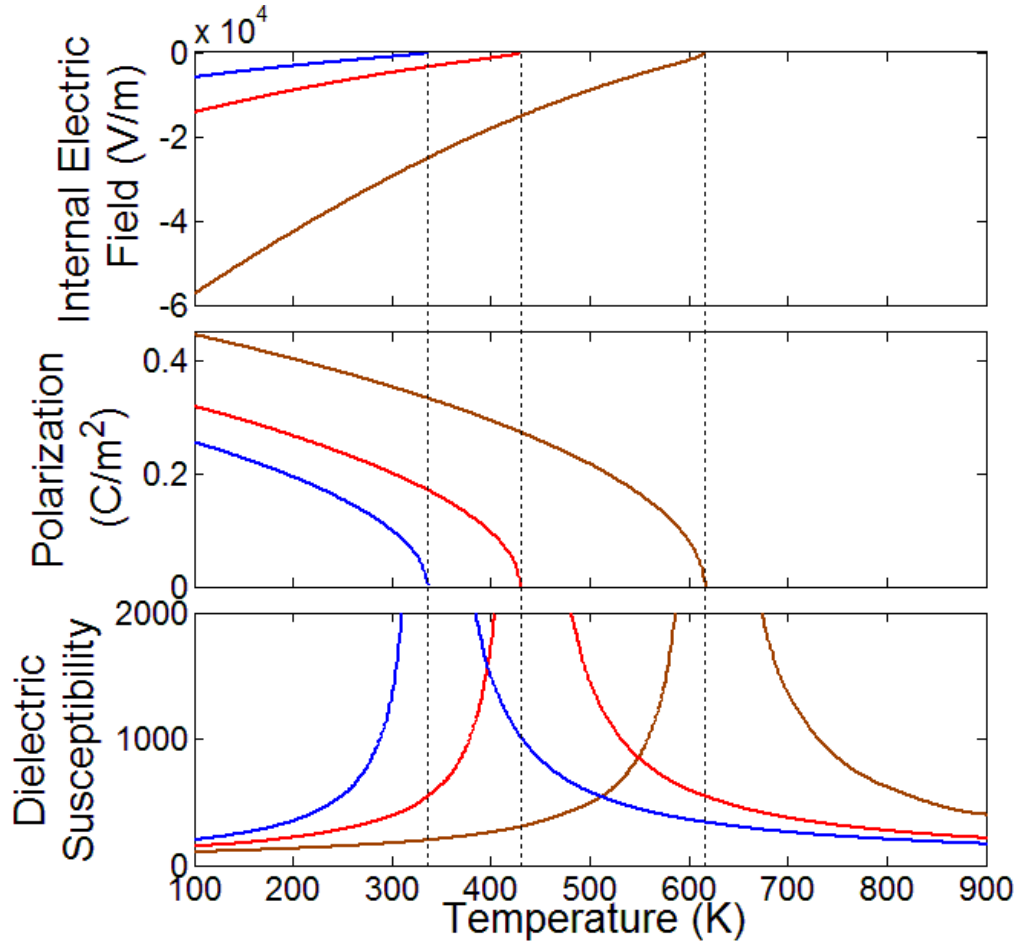


Figure 3.7: Internal electric field, polarization and dielectric susceptibility as a function of temperature for PT/ST superlattice with thickness ratio d_{FE}/d_{PE} (in *u.c.*): 10/15 (blue line), 10/10 (red line) and 10/5 (brown line). Dotted-lines represent the transition temperature.

In Fig. 3.8, we show the internal electric field, dielectric susceptibility and polarization as a function of d_{FE}/d_{PE} . As the thickness ratio increases from 10/15 to 20/10, the polarization and depolarization field of superlattice increases. On the other hand, the dielectric susceptibility decreases from ~ 1200 to ~ 200 . From Figs. 3.7 and 3.8, it is seen that the control of thickness ratio or volume fraction allows the tuning of ferroelectric properties in these superlattices (Dawber et al., 2007).

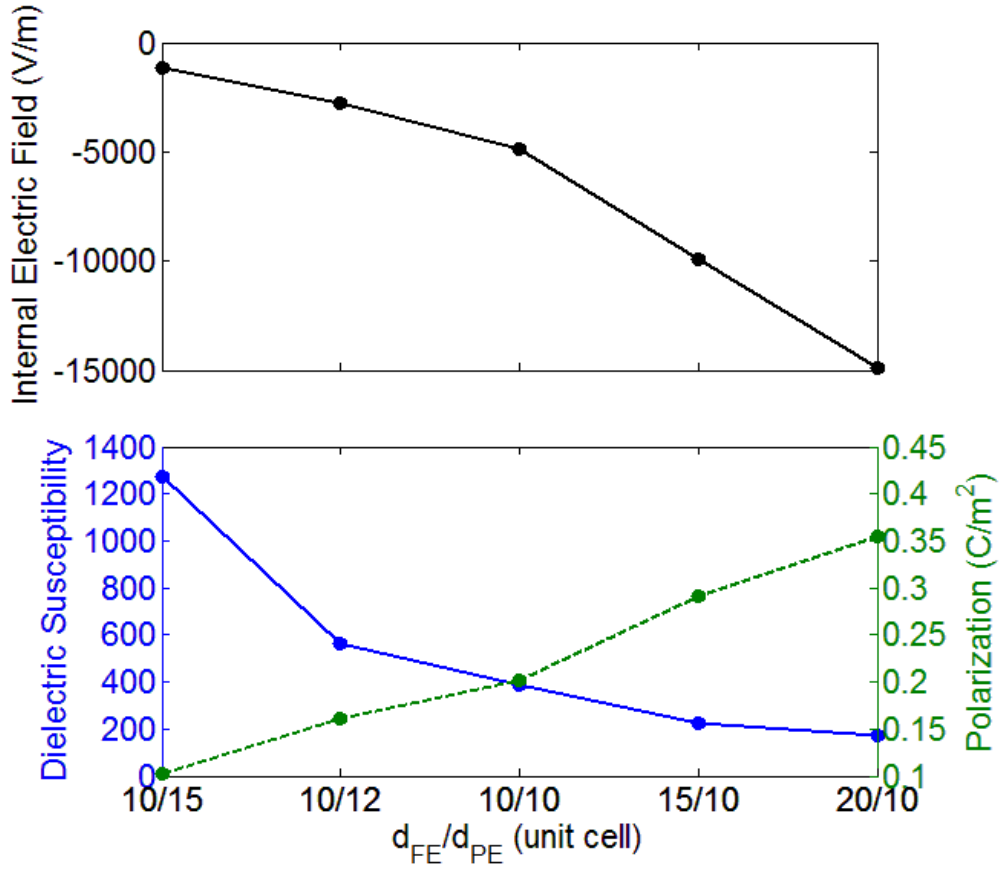


Figure 3.8: Internal electric field, dielectric susceptibility and polarization as a function of d_{FE}/d_{PE} at $T = 298K$.

3.7 Hysteretic Internal Electric Fields and Polarization Reversal

In this section, we will use our model to study the polarization reversal in ferroelectric superlattices with “switchable” polarization in intermixed layers (Lim, Chew, & Ong, 2013). The dependence of polarization and internal electric field on an applied electric field is discussed. Our results reveal that polarization hysteresis in ferroelectric superlattices is accompanied by hysteresis in internal electric fields. The underlying physical mechanisms that induce the internal electric field dependence of applied electric field are discussed by looking at the polarization and internal field profiles.

3.7.1 Result and Discussion

As an illustration, a superlattice comprising $PbTiO_3$ (PT) as ferroelectric layer and $SrTiO_3$ (ST) as paraelectric layer on ST substrate is used as a model system. Their ther-

modynamic coefficients and elastic constants are listed in Table 3.1. In this work, the interface intermixing parameter is set as $\lambda_0 = \xi_0$, implying that an intermixed layer with inhomogeneous properties are formed at interface region (Lim et al., 2012). For simplicity, we assume that the induced-polarization of intermixed layers is “switchable”. The thickness of PT and ST is set as $d_{PT} = 15u.c.$ and $d_{ST} = 5u.c.$, respectively. Unless stated otherwise, the parameter values have been retained at $T = 298K$ for all of the results presented below.

Fig. 3.9 shows the dependence of polarization and internal electric field on the applied electric field of the PT/ST superlattices. In general, the shape of the $P - E$ hysteresis loop is a square. Internal electric field E_{int} of the superlattice also exhibits an interesting square hysteresis loop as a function of E . At $E = 0$, the polarization $P \sim 0.4429C/m^2$ (e.g. at the positive state) and the corresponding internal electric field is $E_{int} = -4.5549 \times 10^4 V/m$. $E_{int} < 0$ implies that the average internal field of the superlattice acts as a depolarization field. Polarization reversal occurs at the coercive field of $E_c \sim 70.58MV/m$ and the switching of polarization in superlattice is accompanied by a change of sign in E_{int} . Going from low to high positive applied electric field, the position A ($E = 0$) corresponds to a negative polarization state of $P \sim -0.4429C/m^2$ (Fig. 3.9(a)) with an internal field of $E_{int} = 4.5549 \times 10^4 V/m$. As the applied field increases (e.g. at $E_{ext} = 70.47MV/m \sim 0.99E_c$ (point B)), the magnitude of P and internal field decreases. Upon further increasing $E_{ext} = 1.1745 \times 10^8 V/m > E_c$ (point C), polarization switches from the negative to positive state. The reversal of polarization is accompanied by a change of sign in the internal electric field of superlattice.

In order to gain insight on the physical mechanism that causes the polarization and internal electric field dependence of applied electric field, we examine the spatial dependence of polarization and internal electric field of the superlattices at a particular E_{ext} . Fig. 3.10 depicts the profile of polarization and internal electric field at $E_{ext} = 0$,

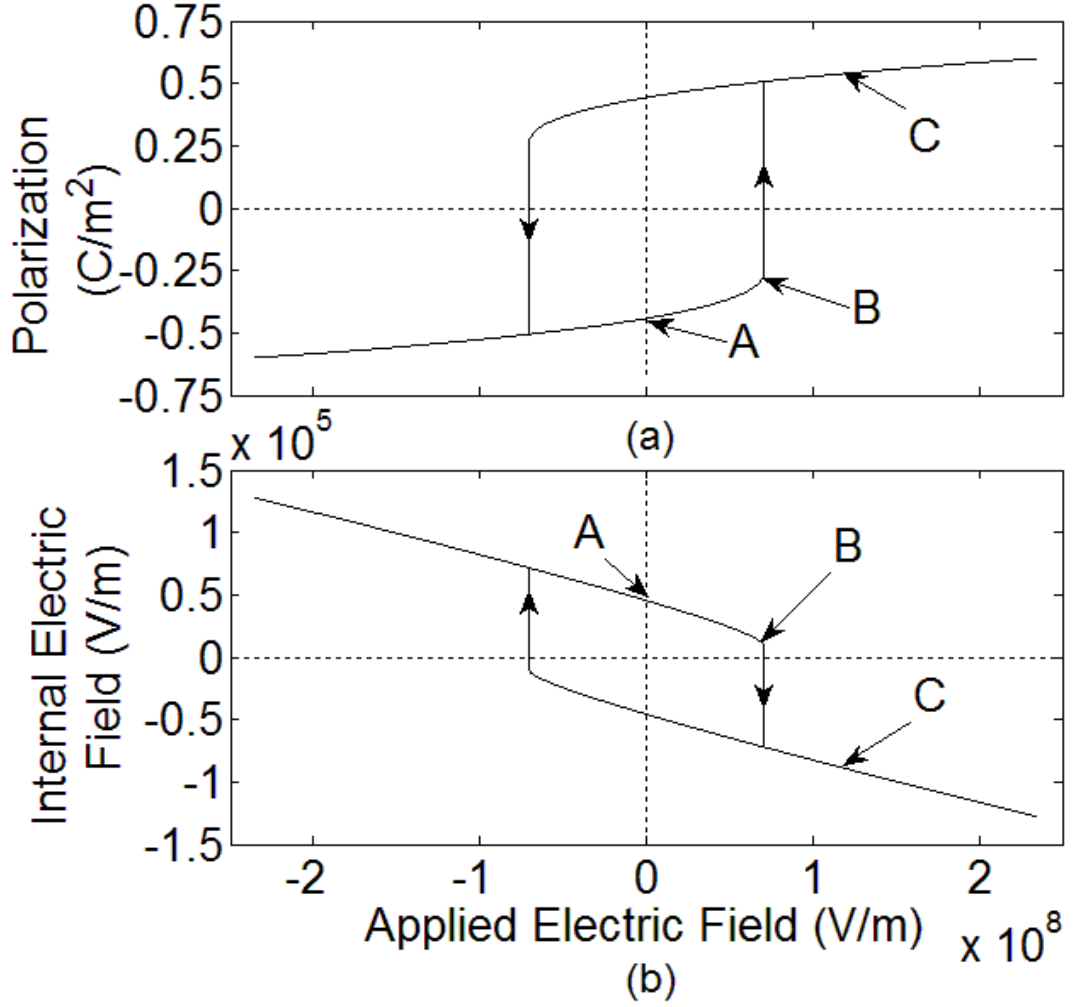


Figure 3.9: Polarization-applied electric field ($P - E_{ext}$) hysteresis loop and (b) Internal electric field-applied electric field ($E_{int} - E_{ext}$) hysteresis loop of a PT/ST superlattice with $d_{PT} = 15u.c.$, $d_{ST} = 5u.c.$ at $T = 298K$.

$E_{ext} \sim 0.99E_c$, $E_{ext} = 1.1745 \times 10^8 \text{V/m} > E_c$, which corresponds to the point A, B and C in Fig. 3.9. At $E_{ext} = 0$, it is seen that intermixed layer formed at the interface. Formation of intermixed layer leads to inhomogeneity in the polarization and the internal field. The internal field in PT behaves as the depolarization field $E_{int} < 0$, whereas $E_{int} > 0$ tends to induce the polarization in the ST layer. Note here that the electrostatic coupling between different PT layers strongly induces the polarization in the ST layer. The polarization of PT and ST layers are almost uniform throughout the superlattice. When $E_{ext} \sim 0.99E_c$ (point B), the polarization and induced-polarization in PT layer and ST layer remain in negative states. The magnitude of polarization in PT and ST layers decrease due to the

applied electric field E_{ext} . The reduction of polarization leads to a decrease in the magnitude of internal electric field in PT and ST layers. Upon further increases the applied electric field $E_{ext} > E_c$ (point C), polarization reversal from negative to positive states occurs. The switching of polarization in the superlattices is accompanied by a sign change of internal electric field in the PT and ST layers.

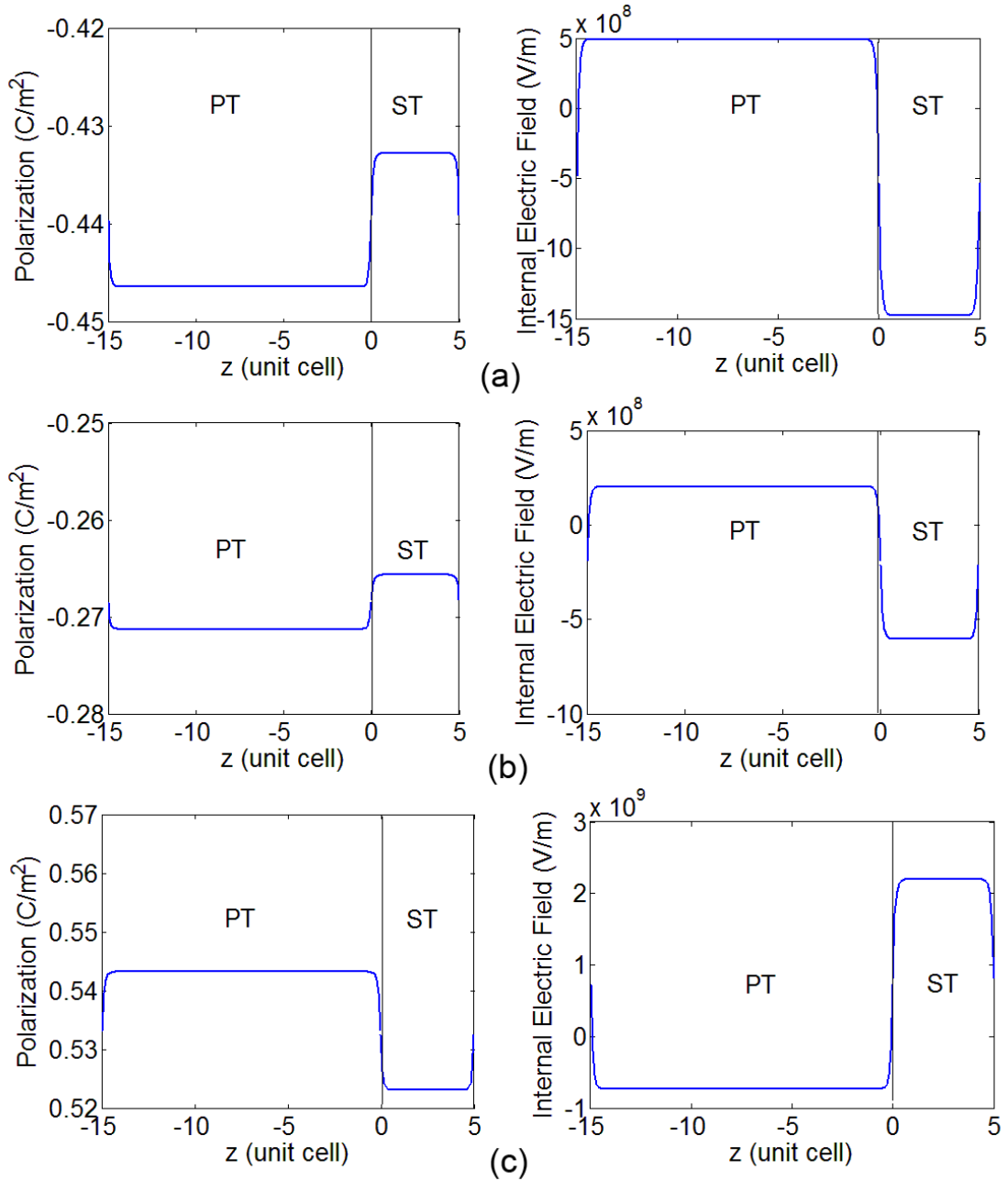


Figure 3.10: The profiles of polarization and internal electric field at applied electric field: (a) $E_{ext} = 0$ (point A), (b) $E_{ext} \sim 0.99E_c$ (point B), (c) $E_{ext} = 1.1745 \times 10^8$ $V/m > E_c$ (point C).

3.8 Conclusion

In conclusion, we have proposed a thermodynamic model to study electrostatic coupling and interface intermixing in superlattice consisting of alternate layers of ferroelectrics and paraelectrics. We have calculated the internal electric field, polarization and transition temperature, and explained the recently observed polarization and transition temperature in PT/ST superlattices. Our study indicates that intermixing at interfaces forms intermixed layers with properties different from its constituent layers. Formation of intermixed layer gives rise to inhomogeneous ferroelectric properties in superlattices. Spatial dependence of polarization extends into the constituent layer over a distance governed by its correlation length. We have shown that periodic modulations of internal electric field and polarization in superlattices are correlated. Intermixing at interfaces has negligible effect on polarization and transition temperature. Internal electric field, originates from electrostatic coupling, plays a key role in determining the ferroelectric properties of superlattices.

Ortega et al. studied the dielectric permittivity $\text{BaTiO}_3/(\text{Ba}, \text{Sr})\text{TiO}_3$ superlattices (Ortega et al., 2011). They showed that the dielectric permittivity of the superlattices can be tuned by varying the Ba/Sr ratio of the constituent layer without changing the periodicity and the total thickness of the superlattices. This may be another better experimental example of intermixing at the interfaces. In this study, the effect of intermixing at ferroelectric/paraelectric interfaces is noticeable only when the electrostatic coupling is neglected when polarizations in the superlattice align parallel to the interfaces. In this case, superlattices with interdigital electrodes (Harigai et al., 2003) may be another practical example for a quantitative correlation between the properties of a superlattice and the degree of interface effect.

The periodic modulations of internal electric field, dielectric susceptibility and polarization in superlattices are correlated. Formation of intermixed layer at interfaces leads to a periodic modulation of ferroelectric properties in these superlattices. Unlike other uniform polarization model (Roytburd et al., 2005; Pertsev & Tyunina, 2011; Dawber et al., 2007), our model allows the study of inhomogeneous ferroelectric properties in these superlattices. Recent study of local structural distortions in PT/ST superlattices (Torres-Pardo et al., 2011; Zubko et al., 2012) revealed the existence of inhomogeneous ferroelectric properties in superlattices. Their studies showed that theoretical study based on the assumption of uniform polarization throughout the layers in superlattices is most likely not valid (Pertsev & Tyunina, 2011; Chew et al., 2000; Roytburd et al., 2005; Dawber et al., 2007; Neaton & Rabe, 2003), since a highly inhomogeneous polarization extends over 5-6 unit cells was attributed to ferroelectric domains. Therefore, it is worthwhile to extend the current single-domain model to multidomain model of intermixing.

Based on the thermodynamic model of electrostatic coupling and interface intermixing, we also study the polarization reversal in ferroelectric superlattices. Intermixed layers with “switchable” polarization are assumed to form at interfaces of superlattices. Correlation between the dependence of internal electric field and polarization on the applied electric field of the superlattice are examined. Polarization reversal in superlattice at the coercive field is accompanied by a change of sign in the internal electric field. Hysteresis is not only observed in the field dependent of polarization, but also in the dependence of internal electric field on the applied field.

CHAPTER 4

POLARIZATION DISCONTINUITY AND SCREENING CHARGES IN FERROELECTRIC SUPERLATTICES

4.1 Introduction

Ferroelectric superlattices with alternate layered structures provide relatively large area of contact surface at the layer-interfaces that contributes dramatically to the properties which are distinctly different from that of the bulk. It is of particular importance that the presence of defects, such as oxygen vacancies, impurities, localized charges and etc. (Bratkovsky & Levanyuk, 2000) at the interfaces which sensitively affect ferroelectric properties of the superlattices. The intrinsic defects, such as interface intermixing or vacancies, induced during the thin-film growth process are very common and are usually difficult to control experimentally at high temperature by high-energy lasers. The stoichiometry of the deposited films may change in a complicated manner with this deposition condition (Mizoguchi et al., 2011; Ohnishi et al., 2006).

In this chapter, we systematically investigate the polarization discontinuity and screening charge in ferroelectric superlattices based on the Landau-Ginzburg theory (Lim, Chew, Wang, Ong, & Iwata, 2014). Interface mixing leads to polarization continuity or discontinuity in the superlattice. Screening charge with equal but of opposite sign for alternate interface builds up to counteract the depolarization effect in superlattices. The charge density depends on the degree of interface mixing, and it approaches a saturated value when the mismatch of internal field or polarization at interface vanishes. Using $\text{PbTiO}_3/\text{SrTiO}_3$ as a model system, we show how the screening charge accumulates at interface affects the properties of ferroelectric superlattice with polarization discontinuity.

4.2 Literature Review

From the literature, there are not many theoretical reports on work tackling these delicate problems. Lately, Liu and Li studied the effect of space charges on the hysteresis loops of ferroelectric superlattices based on a continuum model, by treating the ferroelectric perovskites as wide band-gap semiconductors (Y. Y. Liu & Li, 2010). Their study shows that the space charges tend to accumulate near the superlattice interface, resulting in large internal field near the interface, and thus enhanced the polarization of the superlattice. Okatan and co-worker developed a thermodynamic model to examine the contribution of localized charges to the polarization and dielectric properties of $\text{PbTiO}_3/\text{SrTiO}_3$ (PT/ST) superlattices (Okatan et al., 2010). Their results show that there exists a critical volume fraction of PT below which the superlattice is in the paraelectric phase.

Recently, Gu et al. studied the interface structures, polarization and electronic properties of PT/ST superlattices from first-principles calculation (Gu, Wang, Xie, & Wu, 2010). A slope-like internal potential is found, indicating the presence of ferroelectricity and effective charge at the interfaces. They show that this kind of electric potential leads to a zigzag local density of states among layers along the vertical direction of the film, which induces the alternative appearance of positive and negative charges at interfaces. In first-principles calculations, Murray and Vanderbilt (Murray & Vanderbilt, 2009) investigated the “polar discontinuity” in superlattices which are formed of alternately stacked groups of II-IV and I-V perovskite layers. Using $\text{SrTiO}_3/\text{KNbO}_3$ superlattices as a model system and assume that the polarizations of the constituents are equal, their studies reveal how the existence of “polar discontinuity” introduces effective compositional charges at the NbO_2/SrO and TiO_2/KO interfaces. They also conclude that the same principles should apply to II-IV/III-III perovskite superlattice. Another example

is the SrTiO₃/LaAlO₃ structures, in which two-dimensional electron gas appears at the interfaces to avoid the “polar catastrophe” (Ohtomo & Hwang, 2004).

We have recently developed a thermodynamic model of ferroelectrics heterostructures (Chew et al., 2003, 2005) and superlattices (Chew et al., 2009; Chew, 2012) with mixing at the interfaces. By including appropriate electrostatic boundary conditions, the effects of electrostatic coupling and interface mixing on the phase transitions of the ferroelectric superlattices are examined (Lim et al., 2012). In this chapter, we present a general model based on the Landau-Ginzburg theory to study the polarization discontinuity and screening charge in ferroelectric superlattices. We consider for the superlattice composed of alternative ferroelectrics and paraelectrics. Interface mixing gives rise to polarization continuity or discontinuity in the superlattices with inhomogeneous polarization near the interfaces (Chew et al., 2003, 2005, 2009; Chew, 2012; Lim et al., 2012). At the interface, screening charge with equal but of opposite sign for alternate interface builds up to counteracts the depolarization field in the superlattice. It is well-known that a depolarization field may be induced by unscreened charges on the surface and interface of a ferroelectric thin film and/or by inhomogeneous polarization distribution in the film (Glinchuk, Eliseev, Stephanovich, & Farhi, 2003). Using PT/ST structures as a model system, we found two possible mechanisms by which the screening charge may build up at the interface, depending on the arrangement of charge at the interfaces, to counteract the depolarization effects in the superlattice. In particular, screening charge may induce an internal field $E_{\sigma,j}$ that acts against the depolarization effect in the constituent layer, and thus reduces the depolarization field $E_{int,PT}$ in the ferroelectric PT layer. Another possibility is that the built-up of these interface charge suppresses the inhomogeneity of polarization at the interface, which forming a superlattice structures with homogeneous polarization across the constituent layer.

4.3 Formalism

We consider for a simple case of a superlattice composed of PT layer as ferroelectric and ST layer as paraelectric with monodomain polarization in the thin films, which is grown on a ST substrate. The model geometry is illustrated in Fig. 4.1(a). In the present study, we take into account the presence of charges of density σ_0 at the internal interfaces in PT/ST superlattices with polarization discontinuity. The charge density σ_0 are equal but of opposite sign for alternate interfaces. We assume that the density of interface charges depends on the degree of mixing at interface. The nominal charge approaches its saturated value σ_0^* when the mismatch of internal electric field or polarization at interface vanishes. There are two types of interface that yield stabilized superlattice structures, depending on the arrangement of charge at interfaces, as depicted in Fig. 4.1(b) and 4.1(c).

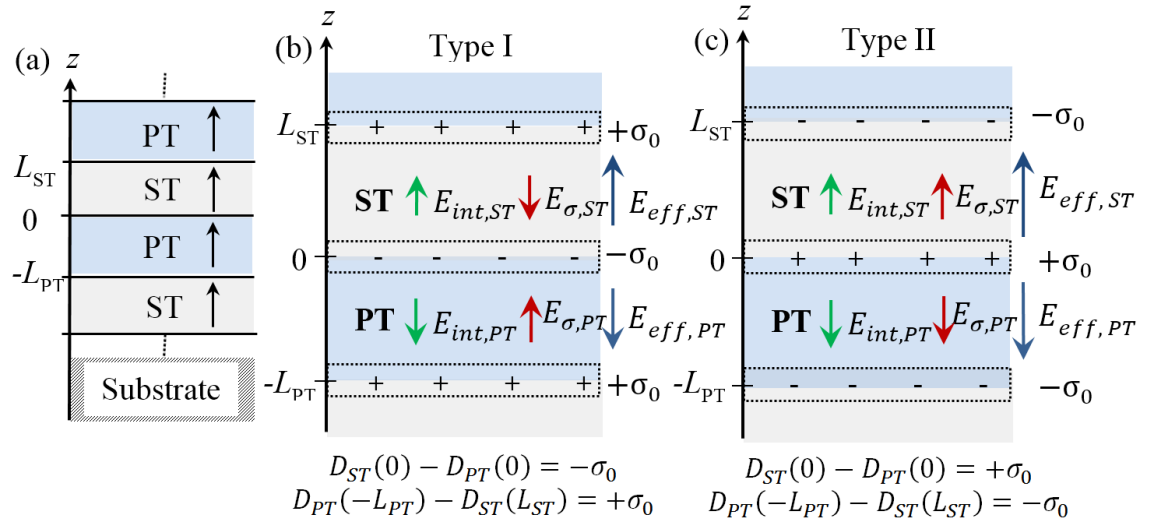


Figure 4.1: (a) Schematic illustrations for a PT/ST superlattice on a ST substrate with thicknesses of PT layer and ST layer are L_{PT} and L_{ST} respectively. Black arrows represent the direction of polarizations in the constituent layer. PT/ST superlattices with alternate interface charge of density σ_0 and their boundary conditions for the (b) type I and (c) type II interfaces. Internal electric field in the PT layer $E_{int,PT}$ (green arrows) is against the direction of PT polarization and acts as a depolarization field, $E_{int,PT} < 0$. The electrostatic coupling between ferroelectric PT layers leads to the appearance of internal electric field $E_{int,ST} > 0$ (green arrows) that tends to induce polarization in the ST layers. As the result of the appearance of alternate interface charge density $\pm\sigma_0$, a charge-induced electric field, $E_{\sigma,j}$ ($j : PT$ or ST) (red arrows) builds up in each layer, leading the existence of effective internal field $E_{eff,j}$ (blue arrows) in the constituent layer j .

At the interfaces, the electric displacement D is discontinuous. The electrostatic boundary conditions describe the two interfaces are

$$\begin{cases} D_{ST}(0) - D_{PT}(0) = \mp \sigma_0, & \text{at } z = 0 \\ D_{PT}(-L_{PT}) - D_{ST}(L_{ST}) = \pm \sigma_0, & \text{at } z = -L_{PT} \text{ or } L_{ST} \end{cases} \quad (4.1)$$

where σ_0 denotes the interface charge density. Hereafter, we denote the interface of type I (see Fig. 4.1(b)) with $D_{ST}(0) - D_{PT}(0) = -\sigma_0$ and $D_{PT}(-L_{PT}) - D_{ST}(L_{ST}) = +\sigma_0$, whereas for the case of superlattice with the electrostatic boundary conditions $D_{ST}(0) - D_{PT}(0) = +\sigma_0$ and $D_{PT}(-L_{PT}) - D_{ST}(L_{ST}) = -\sigma_0$ is represented by the type II interface (see Fig. 4.1(c)).

In superlattices with polarization perpendicularly to the film surfaces, the internal electric field in the ferroelectric layer PT is against the direction of PT polarization and acts as a depolarization field, $E_{int,PT} < 0$, as shown in Fig. 4.1. The electrostatic coupling between ferroelectric PT layers leads to the formation of internal electric field $E_{int,ST} > 0$ that tends to induce polarization in the ST layers (Lim et al., 2012). As a result of the appearance of alternate interface charge density $\pm\sigma_0$, a charge-induced electric field, $E_{\sigma,j}$ ($j : PT$ or ST), builds up in each of the individual layer. The direction of $E_{\sigma,j}$ depends on the arrangement of charge at the interfaces, as shown in Fig. 4.1(b) and 4.1(c). For superlattices with interface of the type I (Fig. 4.1(b)), $E_{\sigma,j}$ is in the opposite direction of $E_{int,j}$ in j layer. Therefore, the charge-induced field $E_{\sigma,j}$ tends to reduce both the depolarization field $E_{int,PT}$ in PT layer, and the internal electric field $E_{int,ST}$ in ST layer. For interface of the type II, the existence of interface charge enhances the depolarization field in PT layer and increases the internal field in ST layer, as shown in Fig. 4.1(c). Therefore, it is clear that a resultant effective internal field $E_{eff,j}$ appears in the constituent layers due to the existence of these internal fields (i.e. $E_{int,j}$ and $E_{\sigma,j}$). In the ST layer,

the electric displacement and the effective internal electric field are respectively given by (in vector notation) $\mathbf{D}_{ST} = \epsilon_0 \mathbf{E}_{eff,ST} + \mathbf{P}_{ST}$ and $\mathbf{E}_{eff,ST} = \mathbf{E}_{int,ST} + \mathbf{E}_{\sigma,ST}$. Similarly, the electric displacement and the effective internal field in PT layer are defined as, $\mathbf{D}_{PT} = \epsilon_0 \mathbf{E}_{eff,PT} + \mathbf{P}_{PT}$ and $\mathbf{E}_{eff,PT} = \mathbf{E}_{int,PT} + \mathbf{E}_{\sigma,PT}$, respectively. It is clear now that the direction of the charge-induced field $\mathbf{E}_{\sigma,j}$ depends upon the type of interfaces, as shown in Fig. 4.1(b) and 4.1(c).

In this study, we will systematically examine how the screening charge builds up at interfaces (i.e. the type I and II interfaces) counteracts the depolarization effects in ferroelectric superlattices. By assuming that the polarization varies spatially and is pointing along the z -direction, the thermodynamic model of current system is followed exactly the formalism of electrostatic coupling and interface intermixing in ferroelectric superlattices as elucidated in Section 3.3. The only different part is the new electrostatic boundary conditions as depicted in Eq. (4.1) compared to the case without the interface charge in Eq. (3.8). This is because of the discontinuity of normal component of electric displacement due to interface charges density $\pm\sigma_0$. Besides that the continuity of tangential component of electric field are also required at interfaces.

In this study, the spatial dependence of internal electric field (or electrostatic potential) and polarization are numerically obtained. The average polarization of each individual layer is defined as $P_{PT} = \left(\int_{-L_{PT}}^0 p_{PT} dz \right) / L_{PT}$ and $P_{ST} = \left(\int_0^{L_{ST}} p_{ST} dz \right) / L_{ST}$, whereas the average polarization of the superlattice is given by $P = \left(\int_{-L_{PT}}^0 p_{PT} dz + \int_0^{L_{ST}} p_{ST} dz \right) / L$ with periodic thickness $L = L_{PT} + L_{ST}$. Similarly, the average effective internal electric field of each individual layer is $E_{eff,PT} = \left(\int_{-L_{PT}}^0 E_{eff,PT}(z) dz \right) / L_{PT}$ and $E_{eff,ST} = \left(\int_0^{L_{ST}} E_{eff,ST}(z) dz \right) / L_{ST}$, and the average effective internal field is expressed as $E_{eff} = \left(\int_{-L_{PT}}^0 E_{eff,PT} dz + \int_0^{L_{ST}} E_{eff,ST} dz \right) / L$.

4.4 Result and Discussion

Figure 4.2 and 4.3 show the spatial dependence of polarization and internal electric field of PT/ST superlattices. We first examine the effect of interface mixing in superlattice without the presence of screening charges at the interface, as shown in Fig. 4.2. $\lambda_0 = 0$ describes no mixing at the interface. Both the internal electric field and polarization remain uniform throughout the PT and ST layers. For $\lambda_0 \neq 0$, an intermixed layer, with properties different from the individual layer, is formed at interface region $z = 0$. The existence of intermixed layer gives rise to inhomogeneous polarization and internal electric field near the interfaces. The continuity or discontinuity of polarization and internal electric field across the interface depends on λ_0 . As the value of λ_0 increases from 0 to ξ_0 , the polarization mismatch $|p_{I,ST}(0) - p_{I,PT}(0)| = \Delta p_I$ and internal field mismatch $E_{I,ST}(0) - E_{I,PT}(0) = \Delta E_I$ at the interfaces reduce. The mismatches completely disappear when $\lambda_0 \sim \xi_0$, followed by a continuous variation of polarization and internal field across the interface.

In Fig. 4.3, we investigate the effect of screening charges on the polarization and internal electric field profiles for a PT/ST superlattice with polar discontinuity at interfaces. In the calculation, the value of λ_0 is set as $0.01\xi_0$. For a charge-free superlattice (black line), a weak inhomogeneity of polarization and internal field can be found near the interface. The polarization mismatch Δp_I and internal electric field mismatch ΔE_I are $\sim 0.0034C/m^2$ and $\sim 3.8325 \times 10^8 V/m$, respectively. Let us now look at the polarization and internal field profiles of the superlattices with σ_0 . In Fig. 4.3, the label σ_0 represents the charge density at the interface $z = 0$ (see Fig. 4.1), whereas the σ_0^{*+} and σ_0^{*-} indicate the positive and negative value of saturated charge density at $z = 0$ respectively. We first examine the polarization and internal field profiles of superlattices with type I interface of $\sigma_0 < 0$ (red line), as shown in Fig. 4.3. As the density of interface charge $|\sigma_0|$ in-

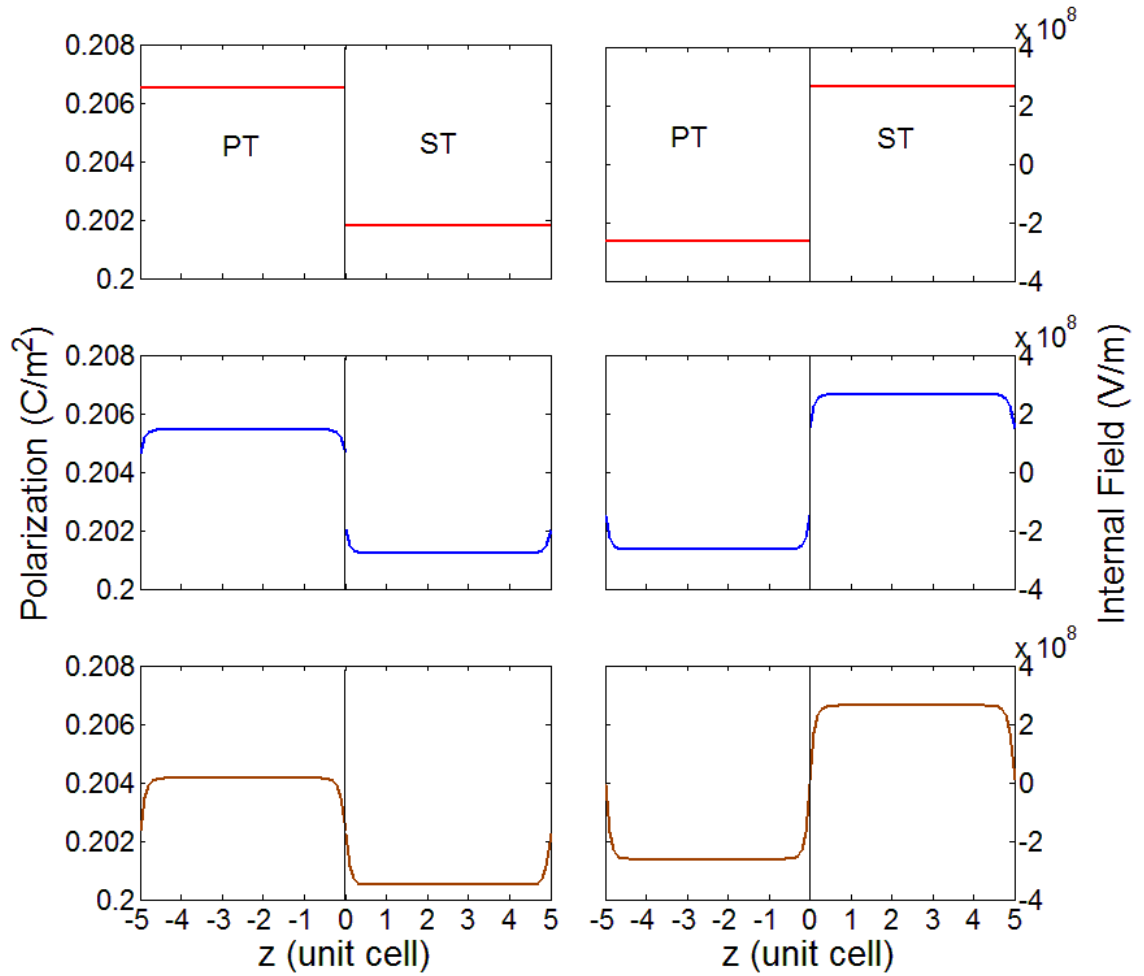


Figure 4.2: Polarization and internal electric field profiles of PT/ST superlattices with no interface charge. The values of λ_0 are: 0 (red line), $0.02\xi_0$ (blue line) and ξ_0 (brown line).

creases, the polarization mismatch Δp_I increases, whereas the mismatch of internal field ΔE_I decreases because the charge-induced field $E_{\sigma,j}$ counteracts the internal field $E_{int,j}$ of the constituent layer. The interface charge density $|\sigma_0|$ approaches a saturated value of $|\sigma_0| \sim 0.014C/m^2 \equiv |\sigma_0^{*-}|$ when $\Delta E_I \sim 0$, at which the polarization mismatch at the interface reaches its maximum value of $\Delta p_I \sim 0.0137C/m^2 \equiv \Delta p_I^*$.

For interfaces with type II $\sigma_0 > 0$ (blue line), however, ΔE_I increases whereas Δp_I decreases with increasing σ_0 . In this case, it is found that σ_0 saturates at $\sigma_0^{*+} \sim 0.0045C/m^2$. At the saturated charge density σ_0^{*+} , the inhomogeneous polarization near the interfaces is completely suppressed by the charge-induced field $E_{\sigma,j}$. The polarization profiles of the constituent layer are homogeneous across the interface, i.e. $P_{PT} = P_{ST}$ (of course $\Delta p_I \sim 0$).

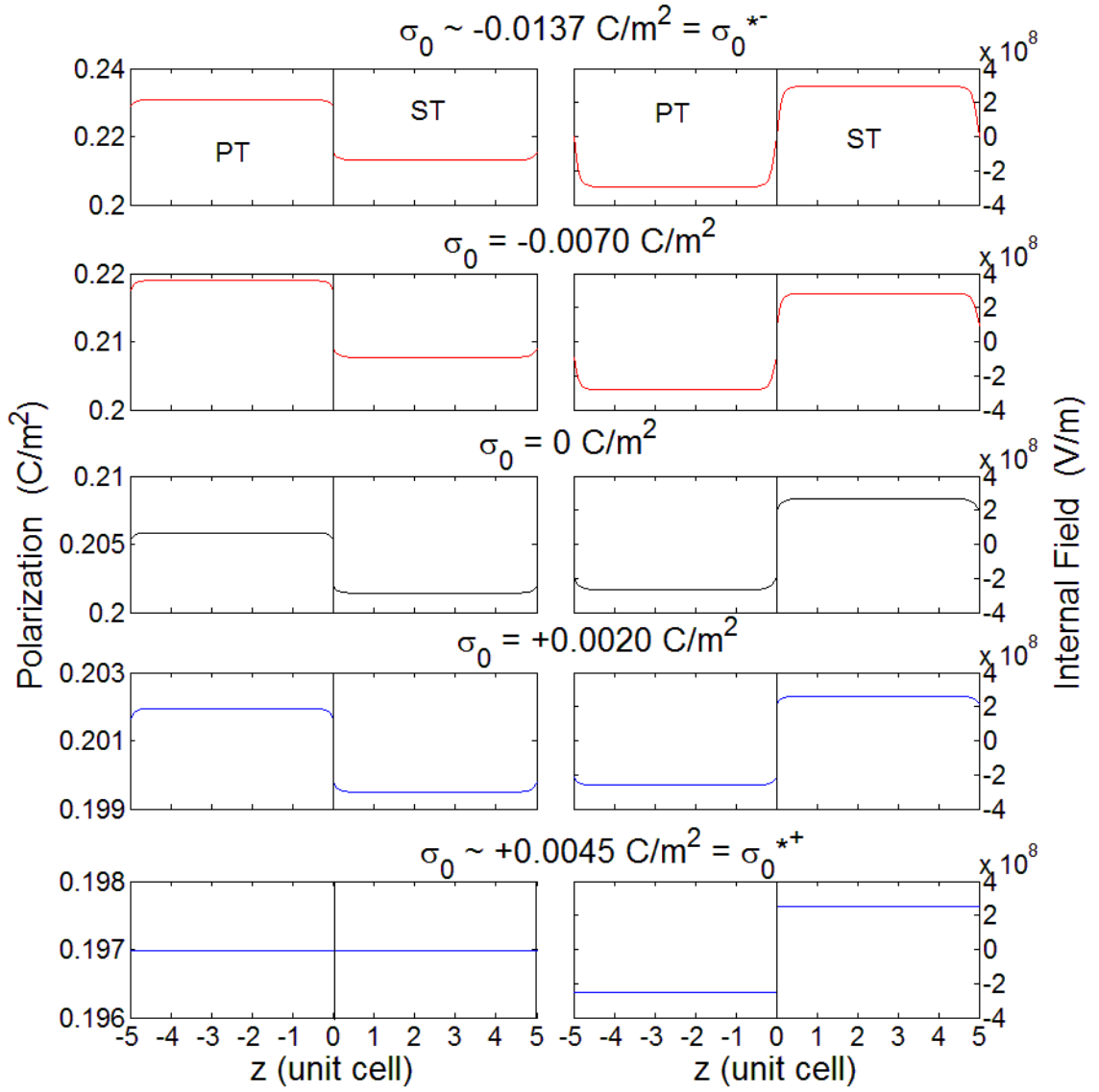


Figure 4.3: Polarization and internal electric field profiles of PT/ST superlattices with interface of type I (red color) and type II (blue color) for different interface charge density σ_0 . In the figure, σ_0 represents the charge density at interface $z = 0$. Black lines are the profiles for charge-free superlattices σ_0 . The values of λ_0 is set as $0.01\xi_0$.

In this case, the superlattice behaves like a “single crystal”. The internal field profile also becomes homogenous throughout the constituent layer. The internal field of the two layers compensates between each other, and thus, $E_{PT} + E_{ST} = 0$. In this case, however, the internal field mismatch ΔE_I reaches its maximum value $\Delta E_I \sim 5.0786 \times 10^8 \text{ V/m} \equiv \Delta E_I^*$. Changes in polarization and internal electric field as a result of a change in interface charge density σ_0 are associated with the appearance of charge-induced internal field, which depending on the type of interface (as shown in Fig. 4.1). Compared to the su-

perlattice with the interface of type I, the overall profile of polarization enhances with increasing σ_0 , whereas the profile of polarization suppresses in the type II interface. In both interfaces, the change in polarization and internal field at interface due to the interface charge density of $\pm\sigma_0$ satisfy the electrostatic boundary conditions (4.1).

In order to gain further insight on the effect of screening charge on internal field mismatch ΔE_I and polarization mismatch Δp_I at polar discontinuity interfaces, we calculate Δp_I and ΔE_I as a function of interface charge density σ_0 for the two interfaces, as shown in Fig. 4.4. In the figure, the horizontal axis represents the interface charge density σ_0 at interface $z = 0$ (see Fig. 4.1). The graph of the type I interface $\sigma_0 < 0$ is represented by the red shaded area, whereas the blue shaded area corresponds to the superlattice with interface of type II $\sigma_0 > 0$. Here, we examine three different thickness ratios, L_{PT}/L_{ST} (unit cell), namely, 6/4, 5/5 and 4/6 for different value of λ_0 . Generally, the gap of polarization Δp_I and internal field ΔE_I of a charge-free superlattice $\sigma_0 = 0$ decreases with increasing λ_0 . For the type I interface (the red shaded area), ΔE_I decreases linearly with increasing $|\sigma_0|$ whereas Δp_I is enhanced. Upon further increasing $|\sigma_0|$, ΔE_I is completely vanished whereas Δp_I reaches a maximum value Δp_I^* . At a certain σ_0 value corresponds to the saturated charge density σ_0^{*-} , ΔE_I completely vanishes, whereas Δp_I reaches a maximum value. It is interesting to see that $|\sigma_0^{*-}|$ shifts to a lower value with increasing λ_0 . This is expected because Δp_I and ΔE_I decreases with increasing λ_0 for a charge-free superlattice, as shown in Fig. 4.2. We now look at the effect of interface charge and intermixing on Δp_I and ΔE_I of superlattices with the type II interface (the blue shaded area). It is seen that the internal field mismatch ΔE_I increases with increasing σ_0 , whereas Δp_I decreases. For three different thickness ratio, 6/4, 5/5 and 4/6, the Δp_I disappears at a saturated density of σ_0^{*+} , namely $\sim 0.0079C/m^2$, $\sim 0.0045C/m^2$ and $\sim 0.0019C/m^2$ respectively, at which ΔE_I reaches its maximum value ΔE_I^* . It is interesting to find that the

saturated charge density σ_0^{*+} is independent of λ_0 , though σ_0^{*+} can be tuned by varying the thickness ratio of L_{PT} to L_{ST} .

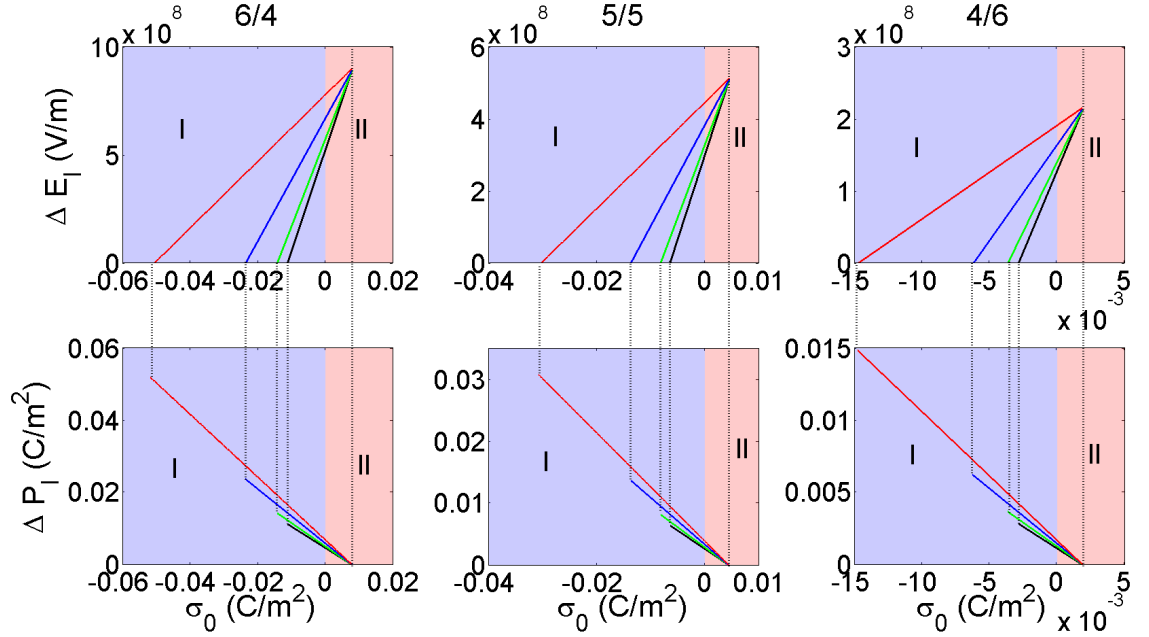


Figure 4.4: Polarization mismatch Δp_I and internal field mismatch ΔE_I as a function of interface charge density σ_0 at $z = 0$ for three different thickness ratios L_{PT}/L_{ST} (unit cell) of 6/4, 5/5 and 4/6. The values of λ_0 are: 0.005 ξ_0 (red line), 0.01 ξ_0 (blue line), 0.016 ξ_0 (green line), and 0.02 ξ_0 (black line). Blue shaded area denotes the type I interface, whereas with the area shaded with red color corresponds to the type II case. In the figure, the charge-free superlattices are described by $\sigma_0 = 0$, which is located at the border between the two shaded areas. Dotted lines in the upper and lower figures indicate the “saturated” charge density σ_0^* and its corresponding Δp_I^* or ΔE_I^* .

Based on the same conditions as in Fig. 4.4, we also plot the average polarization in the whole superlattice (P), the average polarization in PT layer (P_{PT}) and in ST layer (P_{ST}) versus interface charge density σ_0 , as shown in Fig. 4.5(a). Generally, all the value of polarization P , P_{PT} and P_{ST} increase as the thickness ratio L_{PT}/L_{ST} increases. In the case of type I interface (the red shaded area), it is seen that all the polarizations P , P_{PT} and P_{ST} increase with increasing $|\sigma_0|$. On the other hand, for the type II interface (the blue shaded area), all the polarizations P , P_{PT} and P_{ST} decrease with increasing σ_0 . It is clearly seen that the differences of polarization between different value of λ_0 are very small. Therefore, it suggests that the interface intermixing has a negligible effect on polarization even with the existence of interface charge.

More interesting results can be seen in the dependence of internal electric field E_{eff} , $E_{eff,PT}$ and $E_{eff,ST}$ on interface charge density σ_0 at $z = 0$ as shown in Fig. 4.5(b). Overall, all the value of internal electric field $|E_{eff}|$, $|E_{eff,PT}|$, and $|E_{eff,ST}|$ tend to increase when thickness ratio L_{PT}/L_{ST} increases. In the case of type I interface, the magnitude of internal electric field $|E_{eff}|$, $|E_{eff,PT}|$, and $|E_{eff,ST}|$ increase with increasing $|\sigma_0|$. But for the type II interface, the magnitude of internal electric field $|E_{eff}|$, $|E_{eff,PT}|$, and $|E_{eff,ST}|$ decrease with increasing σ_0 . Contrary to the case of polarization, the interface intermixing has a more obvious influence on internal electric field of the superlattices. As the value of λ_0 increases, the magnitude of average internal electric, $|E_{eff}|$ in the whole superlattice increases, whereas the magnitude of average internal electric in each individual layer, $|E_{eff,PT}|$ and $|E_{eff,ST}|$ decrease.

Figure 4.6(a) illustrates P and E_{eff} as a function of thickness ratio L_{PT}/L_{ST} for PT/ST superlattices with the saturated interface charge density σ_0^* at interface $z = 0$. Three different λ_0 values (i.e. $0.001\xi_0$ (*), $0.005\xi_0$ (o) and $0.01\xi_0$ (x)) are calculated for the superlattice with interface of the type I, whereas only $\lambda_0 = 0.01\xi_0$ (Δ) is obtained for the type II interface because σ_0^* is not dependent on λ_0 (as discussed in Fig. 4.4). For comparison, a charge-free superlattice of $\lambda_0 = \xi_0$ with polarization and internal electric field vary continuously across interface is calculated (dash lines with symbol \square). Generally, the polarization P and the depolarization field $E_{eff} < 0$ increase with increasing the thickness ratio L_{PT}/L_{ST} . The saturated charge density σ_0^* corresponds to the disappearance of ΔE_I (type I) or Δp_I (type II) also increases with increasing thickness ratio L_{PT}/L_{ST} . For the type II interface (Δ), it is found that the internal field E_{eff} of superlattice is almost disappeared, indicating that the depolarization field in PT $E_{eff,PT}$ and the internal field in ST layers $E_{eff,ST}$ nearly cancel with each other (as shown in Fig. 4.6(b) and Fig. 4.6(c)). More interestingly, the polarizations P of the type II interface is almost the same as that of the charge-free superlattice (dash lines with symbol \square) though their

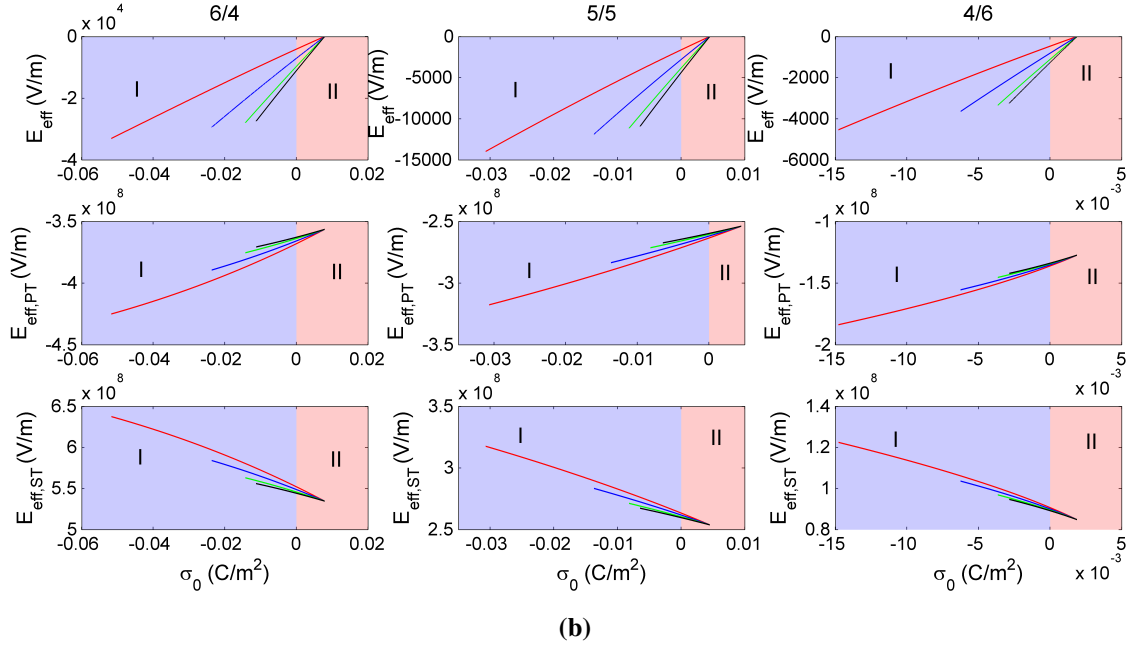
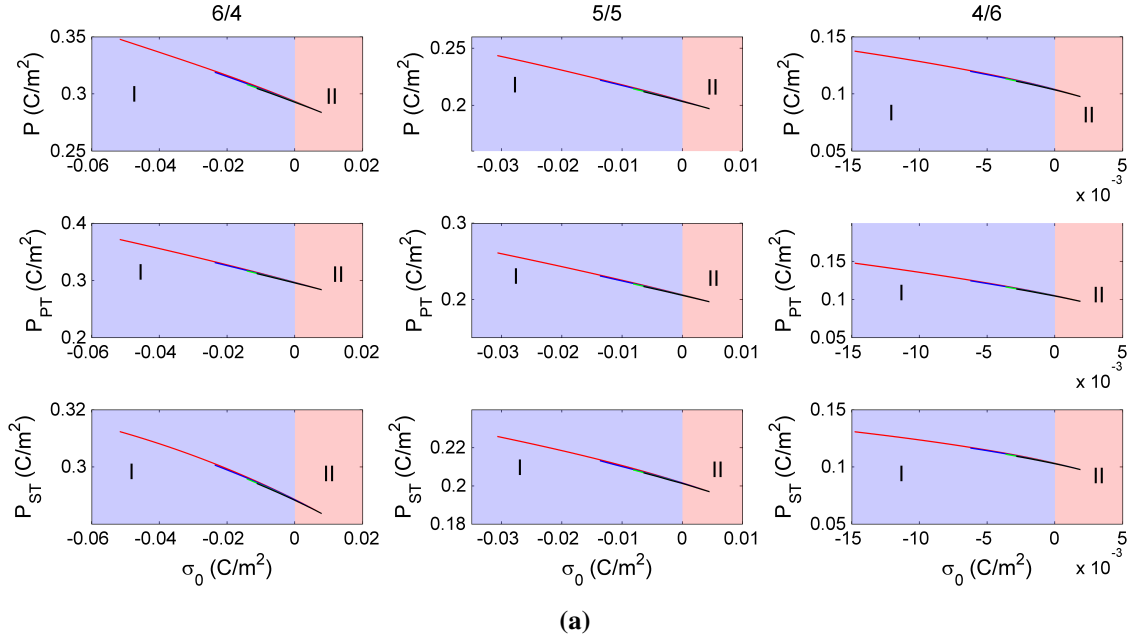


Figure 4.5: (a)Polarization and (b)internal electric field as a function of interface charge density σ_0 at $z = 0$ for three different thickness ratios L_{PT}/L_{ST} (unit cell) of 6/4, 5/5 and 4/6. The values of λ_0 are: $0.005\xi_0$ (red line), $0.01\xi_0$ (blue line), $0.016\xi_0$ (green line), and $0.02\xi_0$ (black line). Blue shaded area denotes the type I interface, whereas with the area shaded with red color corresponds to the type II case.

profiles of polarization and internal field are quite different (see Figs. 4.2 and 4.3). The results also reveal that the degree of interface mixing effect on polarization and internal electric field is more obvious in the type I interface.

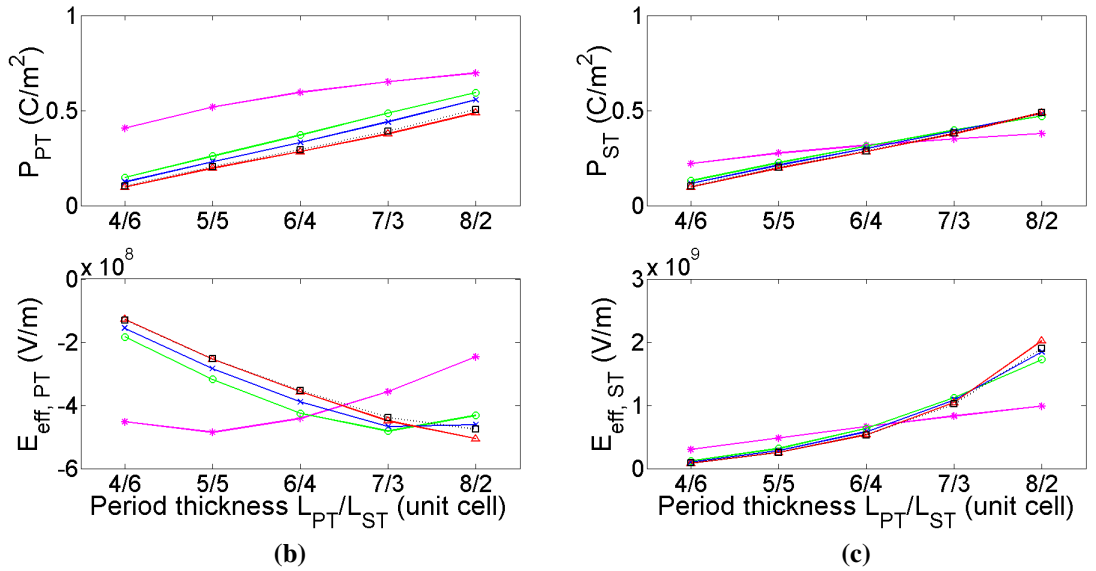
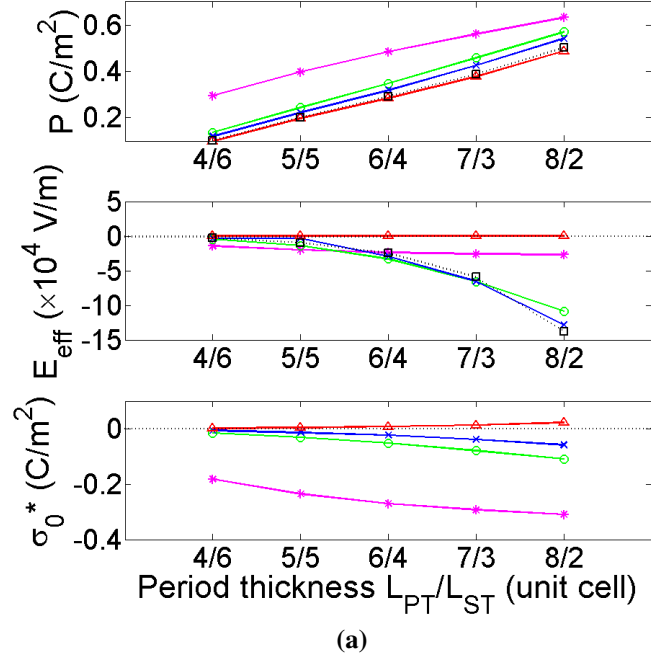


Figure 4.6: (a) Polarization P and internal electric field E_{eff} as a function of period thickness for PT/ST superlattices with saturated interface charge density σ_0^* . The values of λ_0 are: $0.001\xi_0$ (*), $0.005\xi_0$ (○) and $0.01\xi_0$ (×) for the superlattice with the type I interface, whereas $\lambda_0 \neq 0$ (△) represents the type II interface. Dash line with symbol (□) indicates a charge-free superlattice with $\lambda_0 = \xi_0$.

4.5 Conclusion

In summary, we have studied the effect of polarization discontinuity and interface charge in ferroelectric superlattices. Interface mixing leads to polarization continuity or discontinuity in the superlattices with inhomogeneous internal field and polarization near

the interfaces. At interface, screening charge with equal but of opposite sign for alternate interface builds up to counteracts the depolarization field in the superlattice. The charge density is assumed to depend on the degree of mixing at interface, and it approaches its saturated value when the mismatch of internal field or polarization at interface vanishes. The alternating appearance of screening charge at interface $\pm\sigma_0$ induces internal fields $E_{\sigma,j}$ in the constituent layers, and plays an important role in governing the ferroelectric properties. Our study reveals two possible mechanisms by which the screening charge may build up at interface, depending on the arrangement of charge at the interfaces, to counteract the depolarization effects in the superlattice. The screening charge may build up at the interface to induce an internal field $E_{\sigma,j}$ that acts against the depolarization effect in the constituent layer. Another possibility is that the built-up of these charge suppresses the inhomogeneity of polarization at interface, which forming a superlattice with homogeneous polarization across the constituent layer.

CHAPTER 5

EFFECT OF COMPOSITION AND INTERFACE INTERMIXING ON FERROELECTRIC SUPERLATTICES

5.1 Introduction

In this chapter, we have developed a thermodynamic model based on the Landau-Ginzburg theory to study the effect of composition and interface intermixing on ferroelectric properties of $\text{BaTiO}_3/\text{Ba}_x\text{Sr}_{1-x}\text{TiO}_3$ (BT/BST) superlattices (Chew, Lim, Ong, & Iwata, 2014). Dependence of the lattice parameters and the substrate-induced misfit strain of BST layer in BT/BST superlattices on Ba/Sr content are obtained. Effect of composition and interface intermixing on ferroelectricity of superlattices are examined by investigating the modulated profiles of ferroelectric properties (such as polarization and internal electric field) and the mismatch in the properties at the interface. Our study reveals that the polarization behaviors of BT/BST superlattices can be manipulated by varying the Ba/Sr content in BST layer without changing the period thickness of superlattices. The effect of Ba/Sr content on polarization behavior of BT/BST superlattices is stronger than the effect of interface intermixing on polarization of the superlattices.

This chapter will be devoted to study BT/BST superlattices under two different circumstances that depend on the direction of polarization. First, we will discuss the in-plane polarization case for BT/BST superlattices that grown on SmScO_3 . Second, the case of out-of-plane polarization for BT/BST superlattices that grown on SrTiO_3 will be investigated as well. The reasons of the aforementioned chosen substrate will be elucidated in detail in each section.

5.2 Literature Review

Functional properties in a ferroelectric superlattice can be manipulated by varying its thickness ratio (Dawber et al., 2007) as well as by modifying the lattice mismatch at film-substrate interface (Schlom et al., 2007). In the case of $\text{BaTiO}_3/(\text{Ba,Sr})\text{TiO}_3$ superlattices, it is found that the polarization and dielectric properties can be modified by varying Ba/Sr content in $(\text{Ba,Sr})\text{TiO}_3$ layer (Ortega et al., 2011, 2013). They found that the misfit strain of the superlattices can be tuned by changing the composition of BST.

Several thermodynamic models based on the Landau-Ginzburg theory have been proposed recently to study the ferroelectric properties of $\text{BaTiO}_3/\text{SrTiO}_3$ superlattices (Qiu, 2010; Y. Y. Liu & Li, 2010). Qiu studied the effect of volume fraction of ST layer in $\text{BaTiO}_3/\text{SrTiO}_3$ superlattice (Qiu, 2010). Their results show that the dielectric properties are largely dependent on both the volume fraction of the SrTiO_3 layer and the domain wall energy parameter. By treating ferroelectrics as semiconductors instead of insulators, Liu et al. examined the effect of space charge on the hysteresis loop behaviours of $\text{BaTiO}_3/\text{SrTiO}_3$ superlattices (Y. Y. Liu & Li, 2010). They found that the space charges tend to accumulate near the superlattice interface, resulting in large electric field near the interface, and thus enhanced polarization and asymmetric hysteresis loop. Those works, however, do not consider the effect of interface intermixing and/or composition in $\text{BaTiO}_3/(\text{Ba,Sr})\text{TiO}_3$ superlattices.

In superlattice structures, intermixed layers may form at interfaces between two ferroelectrics (Shin et al., 2010; Ishibashi et al., 2000). These interface intermixed layers with properties different from those of the constituent layers may affect the properties of the superlattice structure (Cooper et al., 2007; Pertsev & Tyunina, 2011). A thermodynamic model has been proposed to study the effect interface intermixing on phase transition (Ishibashi & Iwata, 2007), modulated polarization (Chew et al., 2008), dielectric

behaviours (Chew et al., 2009) and polarization reversal (Chew et al., 2011a, 2011c) in ferroelectric superlattices (Chew, 2012). Recently, we further extend the model by taking into account the electrostatic coupling and interface intermixing in epitaxial ferroelectric superlattice (Lim et al., 2012; Chew et al., 2013).

To the best of our knowledge, the study of $\text{BaTiO}_3/\text{Ba}_x\text{Sr}_{1-x}\text{TiO}_3$ superlattices by phenomenological theory has not been reported until now. Therefore in this chapter, we aim to investigate the combine influence of composition and interface intermixing on ferroelectricity of $\text{BaTiO}_3/\text{Ba}_x\text{Sr}_{1-x}\text{TiO}_3$ (BT/BST) superlattices based on Landau-Ginzburg theory. In particular, we investigate the influence of Ba/Sr content in BST layer and interface intermixing on polarization of BT/BST superlattices with fixed period thickness by looking at the modulated profiles of polarization or internal electric field and the mismatch in polarization or internal internal field at interface.

5.3 In-plane Polarization Case

We first consider a ferroelectric superlattice with in-plane polarization consisting of alternate BaTiO_3 (BT) layer and $\text{Ba}_x\text{Sr}_{1-x}\text{TiO}_3$ (BST) layer on a SmScO_3 substrate, as shown in Fig. 5.1. SmScO_3 is orthorhombic and it could induce tensile strain at the substrate interface, hence an induced in-plane polarization (Borodavka et al., 2013). Since the in-plane lattice parameters of the SmScO_3 substrate and BaTiO_3 are almost the same, i.e. almost no strain is applied to the BaTiO_3 layers by the underlying substrate (Soukiassian et al., 2008). Changes in the Ba/Sr content will only affect the internal strain of the BST layer. Therefore, the influence of Ba/Sr content and interface intermixing on the ferroelectricity in BT/BST superlattices can be investigated in isolation from other effects. By assuming the polarization aligns along the surfaces or interfaces, the effect of electrostatic coupling between ferroelectric layers in the superlattice can be neglected (Lim et al.,

2012). In-plane ferroelectric properties of a superlattice can be experimentally measured using interdigital electrodes (Harigai et al., 2003).

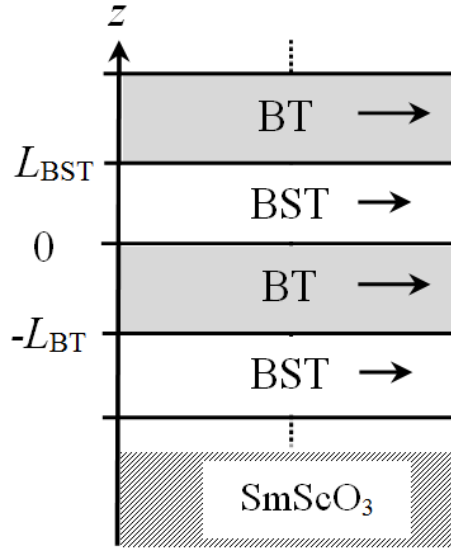


Figure 5.1: Schematic illustrations for a BT/BST superlattice on a SmScO_3 substrate with thicknesses of BT layer and BST layer are L_{BT} and L_{BST} , respectively. Arrows represent the direction of polarization.

5.3.1 Formalism

The Helmholtz free energy per unit area for one period of the BT/BST superlattice can be expressed as the following: (Lim et al., 2012; Pertsev et al., 2000)

$$F = \int_{-L_{BT}}^0 f_{BT} dz + \int_0^{L_{BST}} g_{BST} dz + F_I \quad (5.1)$$

where the first and second terms denote the free energy per unit area of BT layer with thickness L_{BT} and the free energy per unit area of BST layer with thickness L_{BST} , respectively and F_I is the interface energy same as Eq. (3.3) and can be applied for this new system as written in Eq. (5.12)

The free energy density of BT layer with the in-plane polarization p_{BT} is as follows (Lim et al., 2012; Pertsev et al., 2000)

$$f_{BT} = \alpha_{BT}^* p_{BT}^2 + \beta_{BT}^* p_{BT}^4 + \gamma_{BT} p_{BT}^6 + \varphi_{BT} p_{BT}^8 + \frac{\kappa_{BT}}{2} \left(\frac{dp_{BT}}{dz} \right)^2 + \left(\frac{c_{11,BT}^2 + c_{11,BT} c_{12,BT} - 2c_{12,BT}^2}{c_{11,BT}} \right) u_{m,BT}^2 \quad (5.2)$$

where an eighth-order polynomial of Landau free energy expansion is used for BT (Shirokov et al., 2009). For the solid solution BST with composition x , the free energy density g_{BST} can be expressed using the known thermodynamic potentials g_{ST} and g_{BT} for end member of the solid solution $x = 0$ (ST: SrTiO₃) and $x = 1$ (BT: BaTiO₃) as (Shirokov, Torgashev, Bakirov, & Lemanov, 2006; Shirokov et al., 2009)

$$g_{BST} = (1 - x)g_{ST} (p_{BST}, u_{m,BST} - \Delta_{ST}) + xg_{BT} (p_{BST}, u_{m,BST} - \Delta_{BT}) \quad (5.3)$$

where the thermodynamic potential g_j ($j : BT$ or ST)

$$g_j = \alpha_j^* p_{BST}^2 + \beta_j^* p_{BST}^4 + \gamma_j p_{BST}^6 + \varphi_{BT} p_{BST}^8 + \frac{\kappa_j}{2} \left(\frac{dp_{BST}}{dz} \right)^2 + \left(\frac{c_{11,j}^2 + c_{11,j} c_{12,j} - 2c_{12,j}^2}{c_{11,j}} \right) u_{m,j}^2 \quad (5.4)$$

where p_{BST} corresponds to the in-plane polarization of the solid solution BST layer. The normalized expansion coefficients are given by (Pertsev et al., 2000)

$$\alpha_j^* = \alpha_j - \left(g_{11,j} + g_{12,j} - 2 \frac{c_{12,j}}{c_{11,j}} g_{12,j} \right) u_j \quad (5.5)$$

and

$$\beta_j^* = \beta_j - \frac{g_{12,j}^2}{2c_{11,j}} \quad (5.6)$$

where α_j , β_j , φ_j and are the Landau coefficients. $c_{11,j}$ and $c_{12,j}$ are the elastic stiffness coefficients, whereas $g_{11,j}$ and $g_{12,j}$ denote the electrostrictive constants. $u_{m,BT} = (a_S - a_{BT})/a_S$ denotes the in-plane misfit strain of BT layer induced by the substrate due to the lattice mismatch (Y. Y. Liu, Zhu, Li, & Li, 2010). a_{BT} is the unconstrained equivalent cubic-cell lattice constant of BT layer and a_S is the lattice parameter of the substrate.

For the solid solution BST layer with composition x , the in-plane misfit strain induced by the substrate for each end member of the solution are given by (Shirokov et al., 2006, 2009; Y. Y. Liu et al., 2010)

$$u_{m,j} = u_{m,BST} - \Delta_j = (a_S - a_x)/a_S - \Delta_j \quad (5.7)$$

which comprises both the substrate-induced misfit strain in BST layer, $u_{m,BST}$ and the lattice strain of the end members, Δ_j (j : BT or BST). a_x is the equilibrium lattice parameter of the solid solution BST layer. After the complete compensation of internal elastic forces (Shirokov et al., 2006, 2009):

$$(1-x) \left. \frac{\partial g_{ST}(p_{BST}, u_{m,BST} - \Delta_{ST})}{\partial u} \right|_{p_{BST}, u=0} + x \left. \frac{\partial g_{BT}(p_{BST}, u_{m,BST} - \Delta_{BT})}{\partial u} \right|_{p_{BST}, u=0} = 0 \quad (5.8)$$

Eqs. (5.3) and (5.8) yield

$$a_x = \frac{(1-x)\tau a_{ST} + x a_{BT}}{(1-x)\tau + x} \quad (5.9)$$

and the lattice parameters of the solid solution end constituent layers are given by

$$\left. \begin{aligned} a_{BT} &= a_x(1 + \Delta_{BT}) \\ a_{ST} &= a_x(1 + \Delta_{ST}) \end{aligned} \right\}. \quad (5.10)$$

The lattice strain of the end members Δ_{BT} and Δ_{ST} are

$$\left. \begin{aligned} \Delta_{BT} &= \frac{(1-x)\tau\delta}{(1-x)\tau + (1+\delta)x} \\ \Delta_{ST} &= \frac{x\delta}{(1-x)\tau + (1+\delta)x} \end{aligned} \right\}, \quad (5.11)$$

respectively. Here, $\tau = (c_{11,ST} + 2c_{12,ST}) / (c_{11,BT} + 2c_{12,BT})$ and $\delta = (a_{BT} - a_{ST})/a_{ST}$.

If $x = 1$, we have $\Delta_{BT} = 0$ and $a_x = a_{BT}$ and $a_x = a_{BT}$. In this case, $g_{BST} = g_{BT} = f_{BT}$ and $u_{m,BT} = (a_S - a_{BT})/a_S$, which is the free energy of the BT layer on a substrate and the in-plane misfit strain of BT layer induced by the substrate, respectively.

The interface energy is given by (Lim et al., 2012)

$$F_I = \frac{\lambda_0}{2\epsilon_0} \left[(p_{I,BT}(0) - p_{I,BST}(0))^2 + (p_{I,BT}(-L_{BT}) - p_{I,BST}(L_{BST}))^2 \right], \quad (5.12)$$

where $p_{I,j}$ denotes the interface polarization of constituent layer j . ϵ_0 is the dielectric permittivity in vacuum. λ_0 is the temperature-independent interface parameter describes the strength of interface mixing effect in the superlattice. This interface intermixing has already been discussed in both Section 2.5 and Subsection 3.3.1, so this discussion will not be repeated here.

5.3.2 Result and Discussion

In the calculations, we assume the length of 1 unit cell (*u.c.*) $\approx 0.4nm$ (Fong et al., 2004). The characteristic length is defined as $\xi_0 = \sqrt{\kappa / (\alpha_{0Ba} T_{0Ba})} \sim 0.6nm$ where α_{0BT} is the zero temperature of α_j and T_{0BT} is the transition temperature of BT, corresponds to the estimated length of domain wall half-width (Fong et al., 2004; Stephanovich et al., 2005). Unless otherwise specified, the periodic thickness of the BT/BST superlattice is fixed at $L_{BT} = L_{BST} = 5 u.c.$ All the Helmholtz free energy coefficients for layers BT and ST constituent are listed in Table 5.1.

Table 5.1: The Helmholtz free energy coefficients for BT (Shirokov et al., 2009) and ST (Dawber et al., 2007).

	BT	ST	Units
α	$4.124(T - T_{0BT})$	$7.45(T - T_{0ST})$	$\times 10^5 \text{JmC}^{-2}$
β	0.54012	2.02	$\times 10^9 \text{Jm}^5 \text{C}^{-4}$
γ	1.294	-	$\times 10^8 \text{Jm}^9 \text{C}^{-6}$
φ	3.863	-	$\times 10^{10} \text{Jm}^{13} \text{C}^{-8}$
T_0	388	51.64	K
g_{11}	1.163	1.25	$\times 10^{10} \text{JmC}^{-2}$
g_{12}	-2.448	-1.08	$\times 10^6 \text{JmC}^{-2}$
c_{11}	1.7278	3.36	$\times 10^{11} \text{Jm}^{-3}$
c_{12}	8.1958	10.7	$\times 10^{11} \text{Jm}^{-3}$
κ	5.761	5.761	$\times 10^{-11} \text{Jm}^3 \text{C}^{-2}$

We first examine the change in lattice parameters and internal strain of the solid solution BST layer with variable Ba/Sr concentrations, as shown in Fig. 5.2. Note here that the lattice constants in the paraelectric phase or cubic perovskite state for BT and ST are $a_{BT} = 3.99\text{\AA}$ and $a_{ST} = 3.905\text{\AA}$, respectively, whereas the lattice parameter of SmScO₃ substrate is $a_s = 3.991\text{\AA}$. Thus, the lattice parameter of the solid solution BST layer increases with increasing Ba content, as expected (Ortega et al., 2011). The internal strain of BT layer is $u_{m,BT} = (a_s - a_{BT})/a_s = 2.5056 \times 10^{-4}$, whereas the internal strain of BST layer can be modified by varying the Ba/Sr content. In this case, it is seen that the in-plane tensile strain induced by the lattice mismatch between the SmScO₃ substrate and the solid solution BST layer decreases with increasing Ba content.

Let us now investigate the effect of composition and interface intermixing on the profile of polarization and the mismatch in polarization at interface in the BT/BST superlattices with fixed periodic thickness, as illustrated in Fig. 5.3. When $\lambda_0 = 0$, it means that there is no intermixing. In this case, the polarization remains homogeneous throughout the BT and BST layers. If $\lambda_0 \neq 0$, an intermixed layer with properties different from those of the constituent layers is formed at interface. The formation of intermixed layer at interfaces gives rise to an inhomogeneity of polarization near interfaces. The continuity or discontinuity of polarization across the interface depends on the nature of intermixed

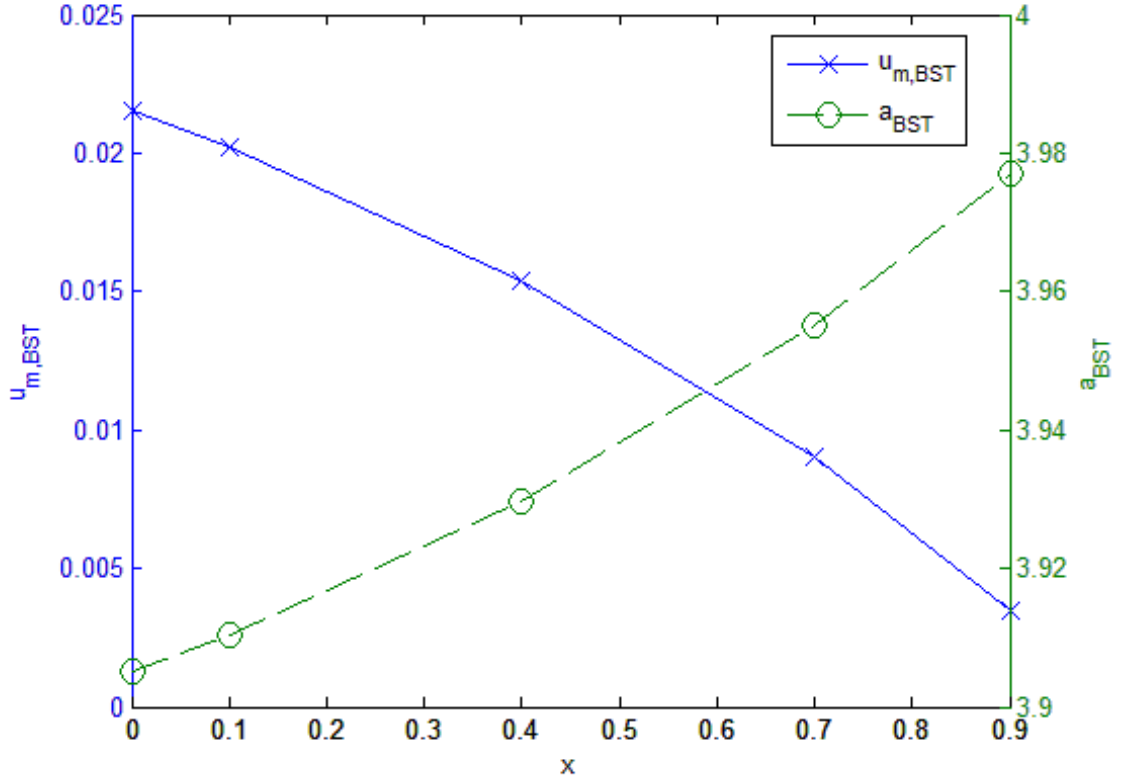


Figure 5.2: Lattice parameter BST a_{BST} (green) and substrate-induced misfit strain (blue) in BST- x layer $u_{m,BST}$ of BT/BST superlattices grown on SmScO_3 at $T = 298\text{K}$ as a function of composition x .

layer. The intermixed layer plays an important role in determining the polarization modulation profiles in the superlattice. In addition, the mismatch in polarization or the gap of polarization at interface decreases with increasing λ_0 value, as shown in Fig. 5.4.

The effects of Ba/Sr content of BST layer on the profile of polarization and the mismatch in polarization at interface in the BT/BST superlattices are more interesting, as shown in Fig. 5.3. If no intermixing at interface $\lambda_0 = 0$, the polarization of the solid solution BST layer in BT/BST superlattices increases with increasing Ba content. Since $\lambda_0 = 0$, the changes of polarization in the BST layer do not affect the ferroelectric properties of the neighboring BT layer in BT/BST superlattices. With increasing Ba content in BST layer, the gap of polarization at interface decreases, as shown in Fig. 5.4. This is reasonable because the internal strain in the solid solution BST layer decreases and the

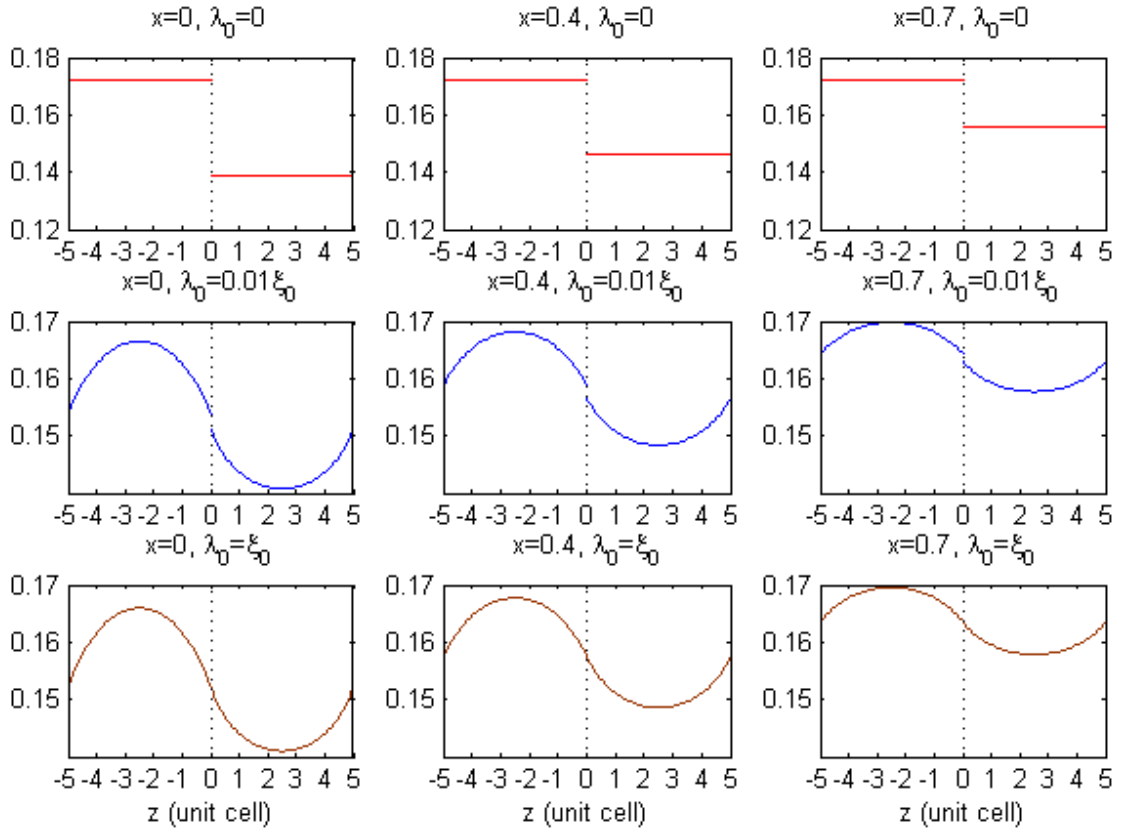


Figure 5.3: Polarization profiles of a BT/BST superlattice with only an in-plane component at $T = 298K$ with composition $x = 0.7, 0.4$ and 0 . The values of λ_0 are: 0 (red line), $0.01\xi_0$ (blue line) and ξ_0 (brown line).

BST layer approaches the BT end constituent layer, as the Ba content increases. For the case of the BT/BST superlattice with $\lambda_0 \neq 0$, the change of Ba/Sr content in the solid solution BST layer not only affect the mismatch of polarization at interface, but it also affects the polarization behavior of the neighboring constituent layer, i.e. the BT layer. Compared with the case of the BT/BST superlattice with $\lambda_0 \neq 0$, the decrease in the gap of polarization at interface due to the Ba/Sr composition for the case of the superlattice with $\lambda_0 \neq 0$ is more significant, as depicted in Fig. 5.4.

In Fig. 5.5, we investigate the effect of Ba/Sr composition and interface intermixing on the polarization behaviors of a BT/BST superlattice. The average polarization of the superlattice P is defined by $P = \left(\int_{-L_{BT}}^0 p_{BT} dz + \int_0^{L_{BST}} p_{BST} dz \right) / L$ with periodic thickness $L = L_{BT} + L_{BST}$. In general, the polarization P of a BT/BST superlattice increases with increasing Ba content, as expected. This is because the solid solution BST layer

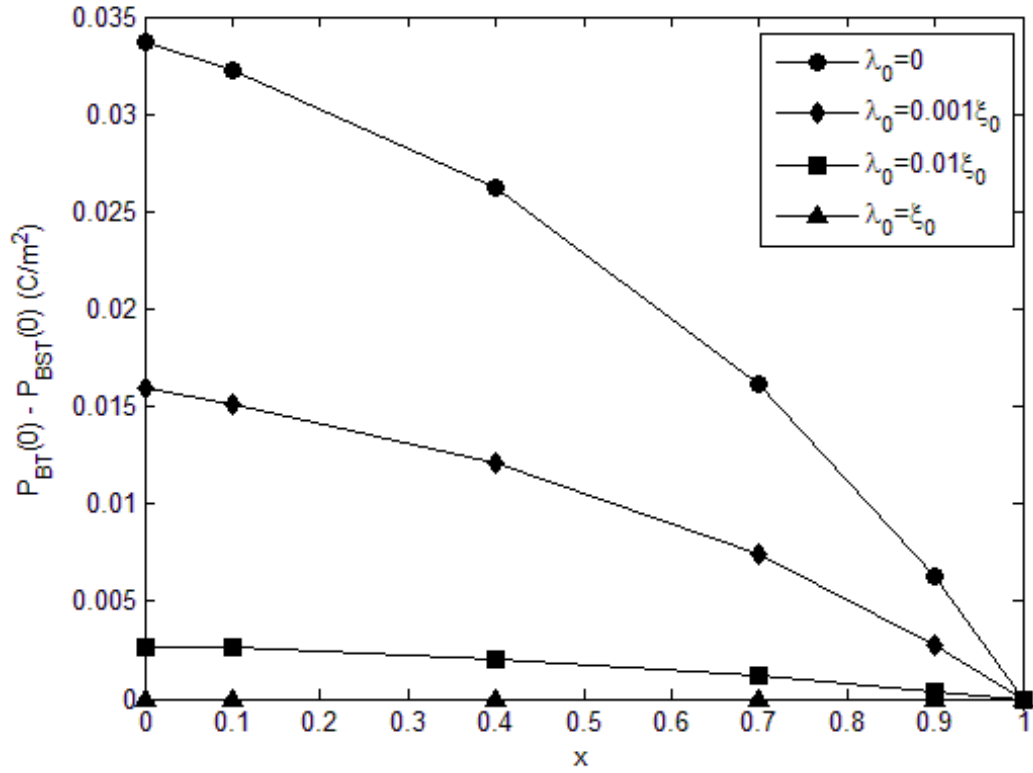


Figure 5.4: Mismatch in polarization at interface $P_{BT}(0) - P_{BST}(0)$ of a BT/BST superlattice at $T = 298K$ as a function of composition x .

approaches the BT end member with increasing Ba content. In addition, the in-plane tensile strain induced by the lattice mismatch between the SmScO_3 substrate and the solid solution BST layer decreases, as the Ba content increases. Compared with the effect of interface intermixing on polarization P of BT/BST superlattice, it is clear to see that the influence of Ba/Sr content on ferroelectric properties of the BT/BST superlattice is more obvious.

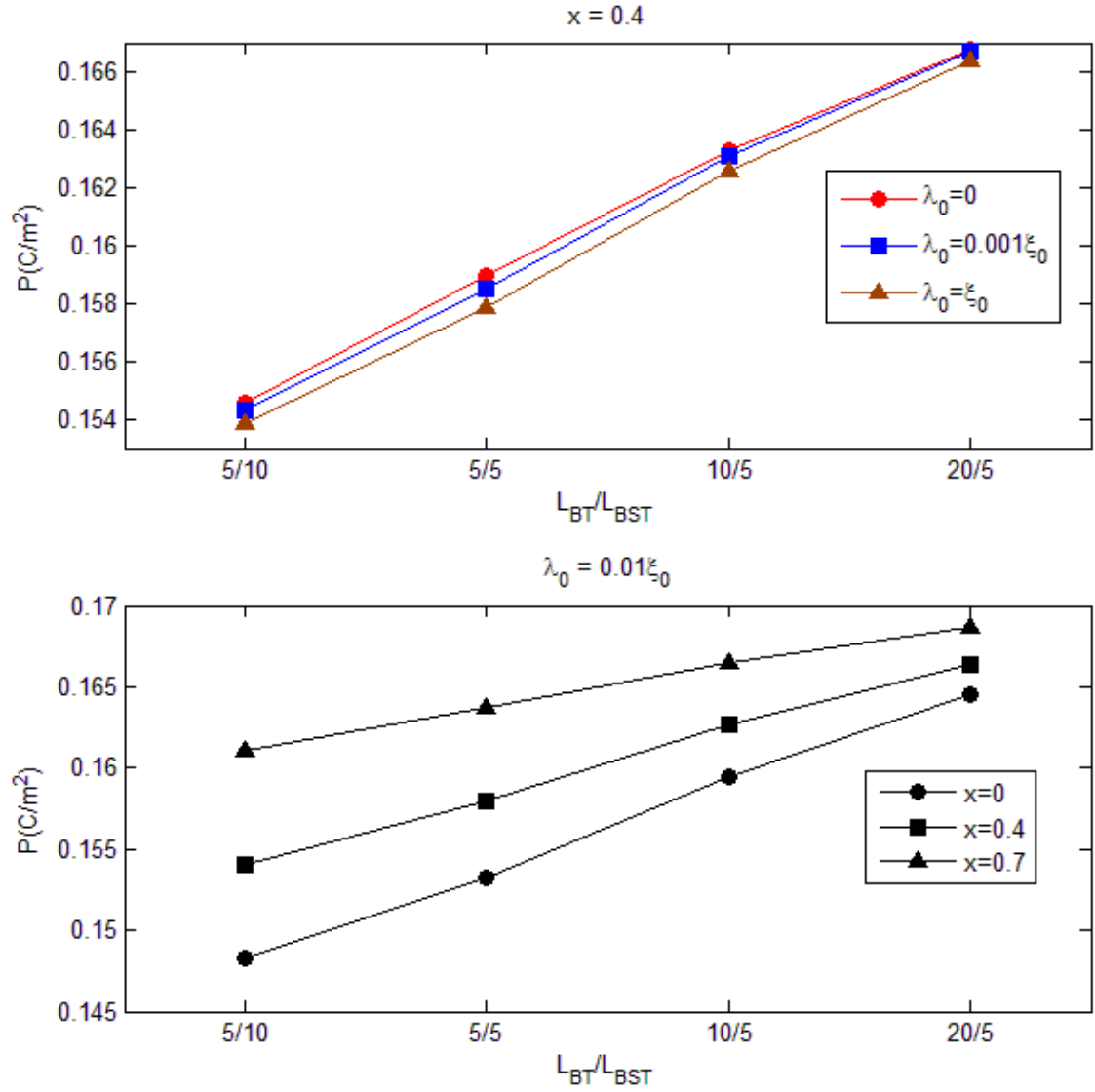


Figure 5.5: Polarization P of a BT/BST superlattice with only an in-plane component at $T = 298\text{K}$ as a function of composition x . The values of λ_0 are: 0 (red line), $0.001\xi_0$ (blue line) and ξ_0 (brown line).

5.4 Out-of-plane Polarization Case

In order to study the case of out-of-plane polarization, we consider the BT/BST superlattice grown on SrTiO₃, as shown in Fig. 5.6. Our intention of selecting SrTiO₃ as a substrate for BT/BST superlattice is to produce a compressive strain on BT and BST layers by increasing the elongation of the lattice vector perpendicular to the surface or interface. Consequently, it leads to a strong preference for out-of-plane polarization in BT/BST superlattice. The SmScO₃ substrate is not a best choice to study the case of out-of-plane polarization, because the lattice parameters of the SmScO₃ substrate is larger than SrTiO₃ and almost same as BaTiO₃. As a result, it tends to induce a tensile strain on BST layer that elongates its lattice vector parallel to the surface or interface and thus suppressed the out-of-plane polarization. On the other hand, the BaTiO₃/SrTiO₃ superlattice which grown on SrTiO₃ substrate has a higher transition temperature compare to SmScO₃ substrate according to the experimental works by Soukiassian et al., 2008.

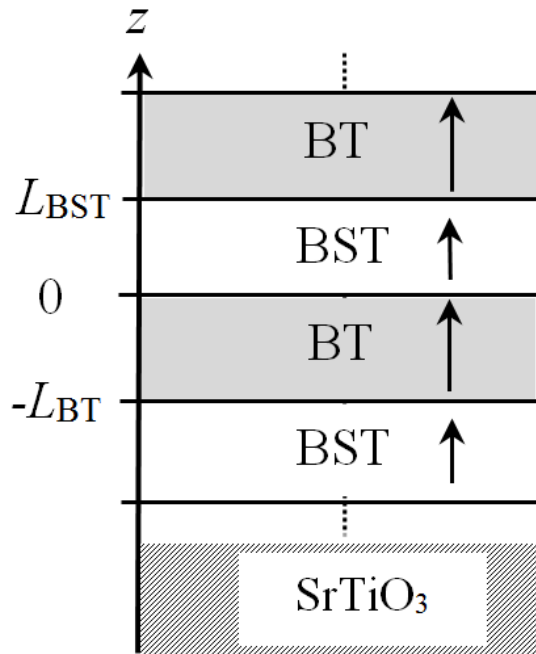


Figure 5.6: Schematic illustrations for a BT/BST superlattice on a SrTiO₃ substrate with thicknesses of BT layer and BST layer are L_{BT} and L_{BST} , respectively. Arrows represent the direction of polarization.

5.4.1 Formalism

For the case of superlattice with out-of-plane polarization, an appropriate electrostatic boundary condition are required. As discussed in Chapter 3, it is expected that the electrostatic coupling between ferroelectric layers will lead to the formation of internal electric field in the dielectric layers. The method of derivation of phenomenological thermodynamic potential of solid solutions for the case of out-of-plane polarization is similar to what have been discussed in Section 5.3, only the renormalized coefficients α_j and β_j are different and the reason for this is the following: the renormalized coefficients α_j and β_j in Eq. (5.2) to (5.4) are responsible for the in-plane tensile strain which induced by SmScO_3 substrate due to lattice mismatch. For the case of out-of-plane polarization using SrTiO_3 substrate, it will induce an in-plane compressive strain on the BT/BST superlattices. Therefore, the renormalized coefficients α_j is replaced by

$$\alpha_j'^* = \alpha_j + 2 \left(\frac{c_{12j}}{c_{11j}} g_{11j} - g_{12j} \right) u_{mj} \quad (5.13)$$

and β_j is replaced by

$$\beta_j'^* = \beta_j - \frac{g_{11j}^2}{2c_{11j}}. \quad (5.14)$$

Similarly, the Helmholtz free energy per unit area for one period of the BT/BST superlattice in Eq. (5.1) can be generalized to include the energy of internal electric field (Lim et al., 2012)

$$F = \int_{-L_{BT}}^0 \left\{ f'_{BT} - \frac{1}{2} E_{d,BT} p_{BT} \right\} dz + \int_0^{L_{BST}} \left\{ g'_{BST} - \frac{1}{2} E_{d,BST} p_{BST} \right\} dz + F_I, \quad (5.15)$$

where $E_{d,j}$ corresponds to the internal electric field of layer j : BT or BST. Basically, the definition of f'_{BT} and g'_{BST} are the same as f_{BT} and g_{BST} as shown in Eq. (5.2) to (5.4), only the new renormalized coefficients α_j' and β_j' are substituted to account for the

induced compressive strain by the ST substrate. The interface energy, F_I is the same as given in Eq. (5.12).

Due to the electrostatic coupling between the layer of superlattices, the physics of ferroelectric superlattice must satisfy the Maxwell's equations in matter, $\nabla \cdot (\mathbf{D}) = 0$ and $\nabla \times \mathbf{E}$, where $\mathbf{D} = \epsilon_0 \mathbf{E} + \mathbf{P}$ and $E_j = E_{d,j} + E_{ext}$. Hence, the electrostatic potentials in layer j : BT or BST are the same as given in Eq. (3.7). Furthermore, the electrostatic boundary conditions at interface require the continuity of the normal component of electric displacement and the continuity of the tangential component of the electric field,

$$D_{BT} = D_{BST}, \quad \varphi_{BT} = \varphi_{BST}. \quad (5.16)$$

where $E_j = -\nabla\varphi$, in term of electrostatic potential.

5.4.2 Result and Discussion

The method of calculations and the Helmholtz free energy coefficients that we used in this study are similar to the case of in-plane polarization as discussed in Subsection 5.3.2.

First of all, the change of lattice parameters and internal strain of the solid solution BST layer with variable Ba/Sr concentrations is shown in Fig. 5.7. Similar to the in-plane polarization case, the lattice constants in the paraelectric phase or cubic perovskite state for BT and ST are $a_{BT} = 3.99\text{\AA}$ and $a_{ST} = 3.905\text{\AA}$, respectively. According to calculations, the internal strain of BT layer is $u_{m,BT} = (a_s - a_{BT})/a_s = -0.0218$, whereas the internal strain of BST layer can be modified by varying the Ba/Sr content. In this out-of-plane polarization case, it is seen that the magnitude of in-plane compressive strain induced by the lattice mismatch between the SrTiO_3 substrate and the solid solution BST layer increases with increasing Ba content.

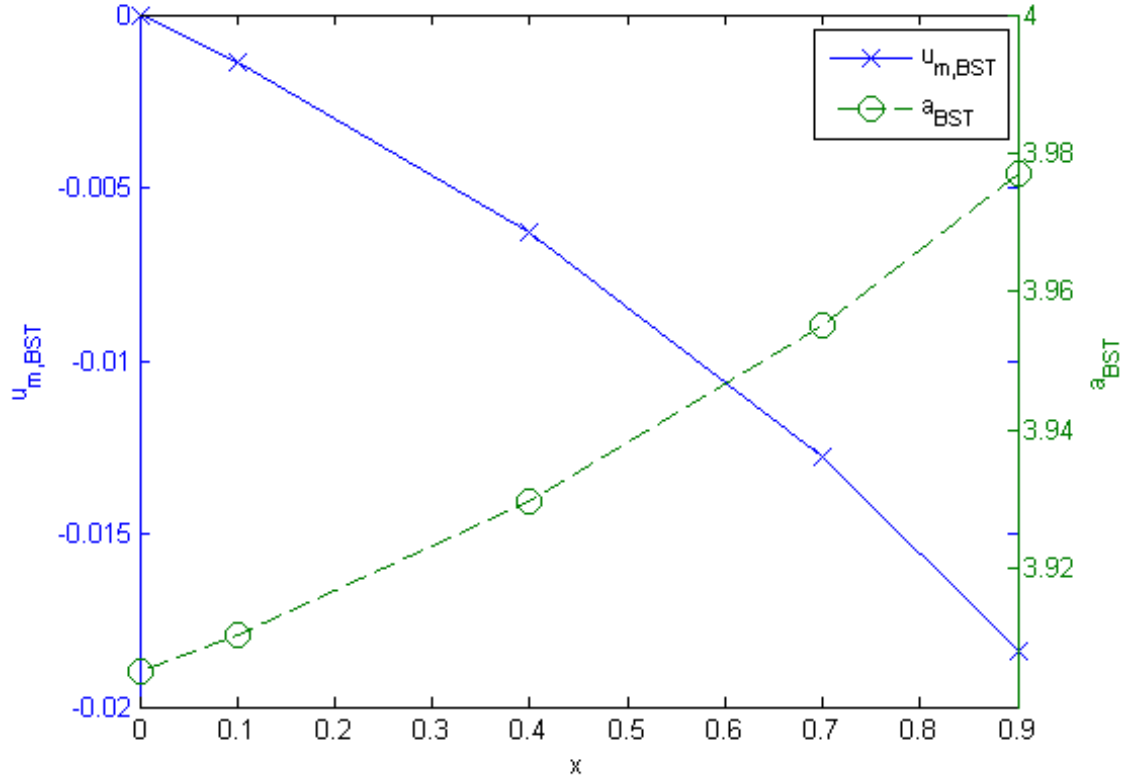


Figure 5.7: Lattice parameter BST a_{BST} (green) and substrate-induced misfit strain (blue) in BST- x layer $u_{m,BST}$ of BT/BST superlattices grown on SrTiO₃ at $T = 298K$ as a function of composition x .

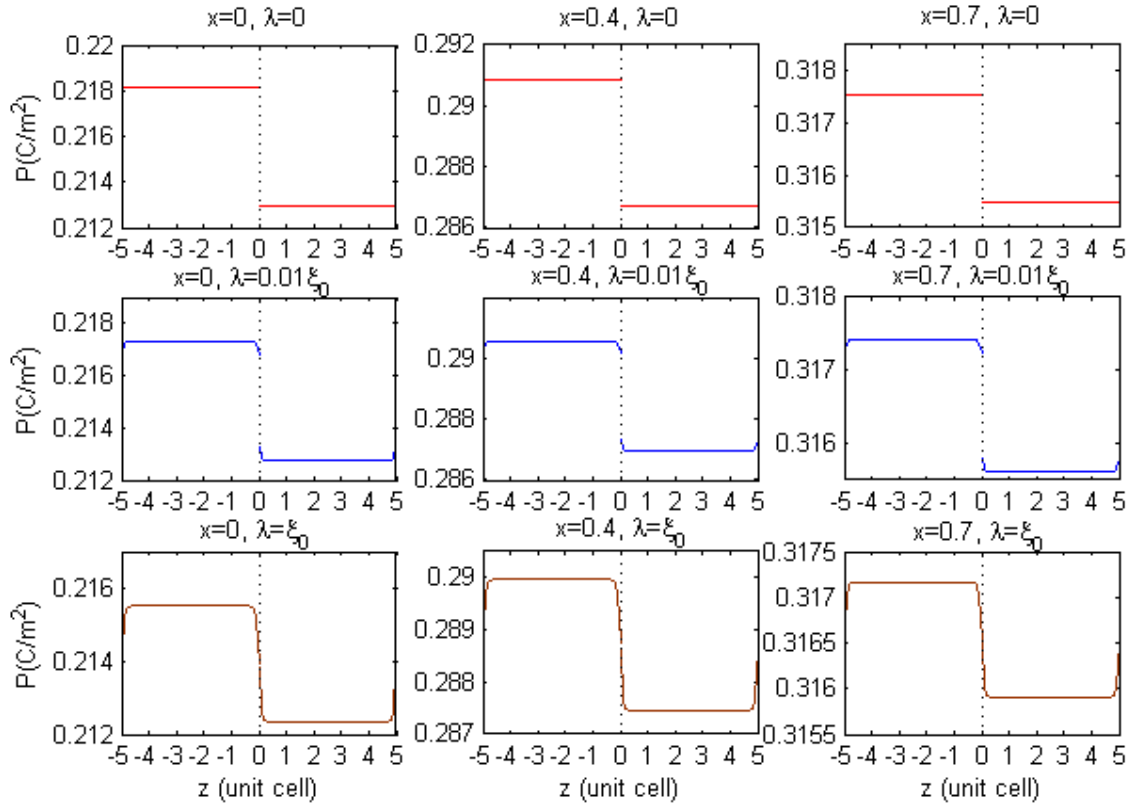
Let us now study the effect interface intermixing on the profile of polarization and internal electric field at interface in the BT/BST superlattices with fixed periodic thickness. Fig. 5.8 shows the profiles of polarization and internal electric field of BT/BST superlattices with $L_{BT} = L_{BST} = 5$ u.c. for different values of λ_0 and Ba content, x in BST layer. First of all, we investigate the change of polarization and internal electric field profiles when the value of λ_0 is varied. When $\lambda_0 = 0$, no intermixing occurs and the both the internal electric field and polarization remain homogeneous throughout the BT and BST layers. When $\lambda_0 \neq 0$, an intermixed layer is formed at interface and eventually leads to an inhomogeneity of polarization and internal electric field near interfaces. Similar to in-plane polarization case, the mismatch or the gap of polarization and internal electric field at interface decrease with increasing λ_0 value, as shown in Fig. 5.9. Apparently the out-

of-plane polarization profile becomes more flatten compare to the in-plane polarization profile due to the internal electric field, as shown in Fig. 5.3.

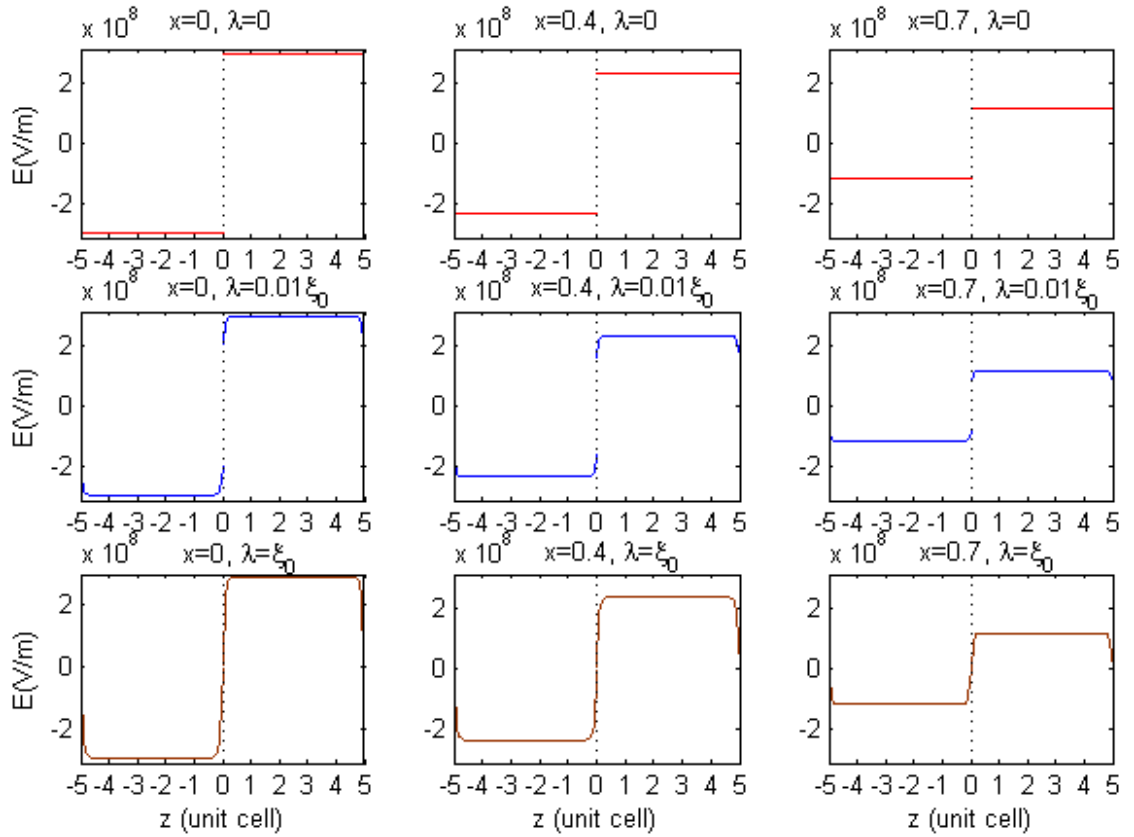
Next we examine the effects of Ba/Sr content of BST layer on the profile of polarization and internal electric field in the BT/BST superlattices. The polarization of the BT layer and solid solution BST layer in BT/BST superlattices increases with increasing Ba content, as shown in Fig. 5.8. On the contrary, the magnitude of internal electric field in BT layer and solid solution BST layer of BT/BST superlattices decreases with the rise of Ba content. Overall, the mismatch in polarization and internal electric field at interface decrease with further increasing Ba content in BST layer, as shown in Fig. 5.9. This is due to the fact that the BST layer approaches the BT end constituent layer and the whole BT/BST superlattice resembles the BT bulk material as the Ba content increases.

In Fig. 5.10, we compare the effect of Ba/Sr composition and interface intermixing on the ferroelectric properties of a BT/BST superlattice. It can be seen that the intermixing at interfaces has a negligible effect on polarization. On the other hand, the internal electric field in BT/BST superlattices shows a very interesting behavior. In the case of $\lambda_0 \neq 0$, there is a change of sign in internal electric field when the thickness ratio, $L_{BT}/L_{BST} \approx 2$. In the region of $L_{BT}/L_{BST} \lesssim 2$, the sign of internal electric field is negative and it acts as a depolarization field in BT/BST superlattices. On the contrary, the internal electric field becomes positive in the region of $L_{BT}/L_{BST} \gtrsim 2$ and it tends to induce polarization in BT/BST superlattices. This peculiar result indicates that the sign of internal electric field in BT/BST superlattices can be manipulated by changing the thickness ratio. Similar to in-plane polarization case, the polarization of BT/BST superlattice increases with increasing Ba content. Note that when $x = 0$, BST layer become purely ST layer and this explains why the internal electric field in the superlattice is negative (acting as a depolarization field) and there is a minimum as reported in Lim et al., 2012 (Please refer to Section 3.5). The value of internal electric field of the superlattice become more positive

when x is increasing, this is because the BST layer approaches the BT end constituent layer and becoming a ferroelectric with its own spontaneous polarization. Evidently, the influence of Ba/Sr content on polarization P of the BT/BST superlattice is more profound compare to the effect of interface intermixing.



(a)



(b)

Figure 5.8: Profiles of polarization $P(C/m^2)$ and internal electric field $E(V/m)$ of BT/BST superlattice with only an out-of-plane component at $T = 298K$ with composition $x = 0.7, 0.4$ and 0 . The values of λ_0 are: 0 (red line), $0.01\xi_0$ (blue line) and ξ_0 (brown line).

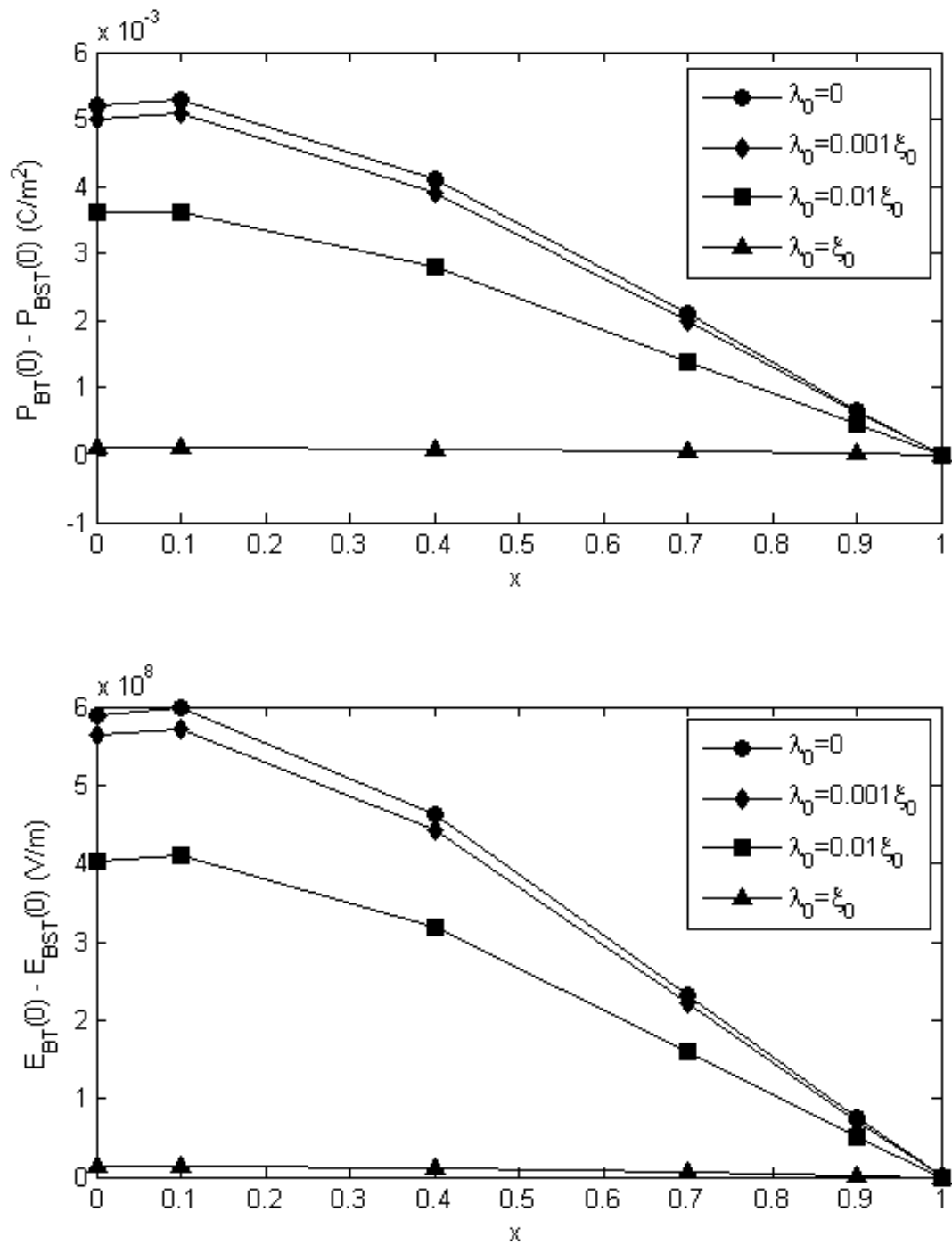


Figure 5.9: Mismatch in polarization and internal electric field at interface of a BT/BST superlattice at $T = 298K$ as a function of composition x .

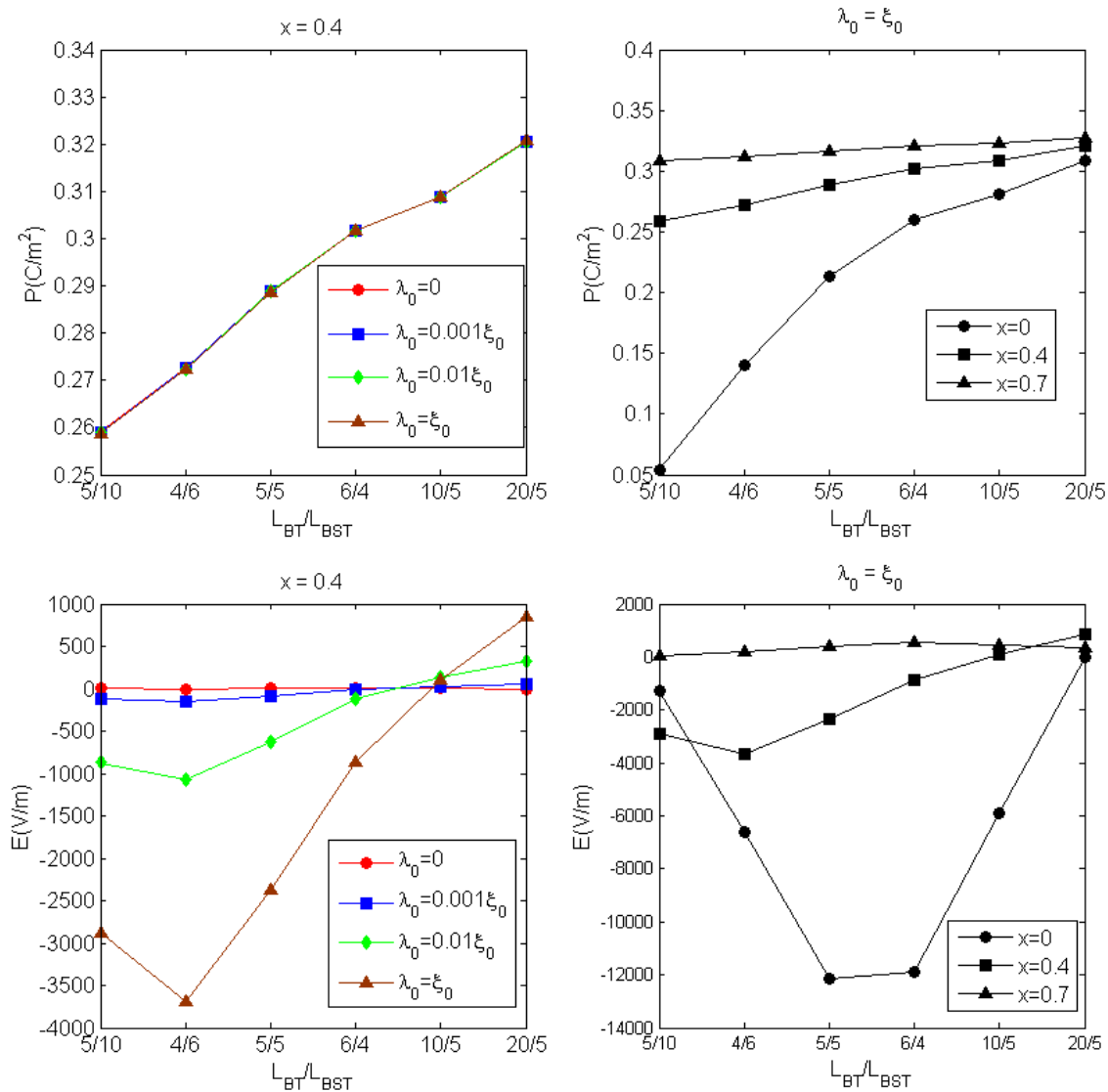


Figure 5.10: Polarization P and internal electric field E of a BT/BST superlattice with only out-of-plane component at $T = 298K$ as a function of composition x . The values of λ_0 are: 0 (red line), $0.001\xi_0$ (blue line), $0.01\xi_0$ (green line) and ξ_0 (brown line).

5.5 Conclusion

In conclusion, we have studied the effect of Ba/Sr content and interface intermixing on ferroelectricity of a superlattice consisting of alternate BT layer and BST layer within the framework of the Landau-Ginzburg theory. For a BT/BST superlattice with polarization aligns along the surfaces or interfaces, the effect of electrostatic coupling in the superlattice can be ignored. Two different cases with respect to the direction of polarization are considered (i) in-plane polarization and (ii) out-of-plane polarization. For the case of superlattice with in-plane polarization, SmScO_3 substrate is chosen. Whereas SrTiO_3 substrate is chosen for out-of-plane polarization. Our studies indicates that the ferroelectricity of BT/BST superlattice can be tailored by varying Ba/Sr content of BST layer without changing the period thickness of BT/BST superlattices. The effect of Ba/Sr content on polarization of BT/BST superlattices is more significant than the effect of interface intermixing on polarization of the superlattice.

CHAPTER 6

CONCLUSIONS AND FUTURE WORKS

6.1 Conclusions

In this thesis, we have studied the phase transition in ferroelectric superlattices on the basis of Landau-Ginzburg theory. By introducing an interface energy term in the free energy, the formation of intermixed layer with properties different from its individual layers at the interface can be described. These intermixed layers are mutually coupled through the local polarization at interfaces. As a result, polarization continuity or continuity at interfaces is determined by the nature of these intermixed layers.

It is seen that the electrostatic coupling between ferroelectric layers plays a dominant role in the polarization enhancement of ferroelectric/paraelectric superlattices. Internal electric field, originates from the electrostatic coupling, strongly induces the polarization of paraelectric layer. The spatial dependence of these ferroelectric properties extends into the bulk over a distance governed by the correlation length ξ_0 of its constituent layer. We reveal that interface intermixing has negligible effect on polarization and transition temperature of superlattices with polarization perpendicular to interface, based on the current single-domain model. Even if no intermixing is considered, the polarization of both the ferroelectric and paraelectric layer are almost the same. Thus, it is expected that intermixing does not have a significant effect on the polarization (and thus, the transition temperature). This effect is noticeable only if the electrostatic coupling is neglected when polarizations align parallel to interfaces. In the present work, it allows the description of inhomogeneous ferroelectric properties in superlattices through the interface intermixing effect.

We extend our work on interface intermixing in ferroelectric superlattices with electrostatic coupling to investigate the polarization reversal. Our results reveal that polarization hysteresis in ferroelectric superlattices is accompanied by hysteresis in internal electric fields. This hysteresis in internal electric field has never been reported in literature before. The underlying physical mechanisms which induce the internal electric field dependence of applied electric field can be discussed by looking at the polarization and internal field profiles.

In our model, we have established the correlation between the internal electric field and ferroelectric properties such as polarization and dielectric susceptibility. Internal electric field (e.g. depolarization field) originates from electrostatic coupling is well-known and understood to have significant impact on the ferroelectric properties. To our knowledge, no previous work has been found on the attempt to correlate the internal electric field with ferroelectric properties. We discuss the intermixing dependence of spatially-modulated internal electric field, dielectric susceptibility and polarization, and established the correlation between these properties. We also illustrate how the “step” structure of buried ferroelectric/paraelectric interfaces depends on intermixing (i.e. polar continuity or discontinuity at interfaces). Therefore, the spatially-modulated profiles of these ferroelectric properties could provide useful information to understand superlattices.

Based on our proposed thermodynamic model, we study the polarization discontinuity and screening charge in ferroelectric superlattices which due to the existence of screening charge at interface with equal but of opposite sign for alternate interface. This screening charge depends on the degree of interface mixing and it approaches a saturated value when the mismatch of internal field or polarization at interface vanishes. According to our results, there are two possible mechanisms of screen charge density at interfaces. The first mechanism as shown in Fig. 4.1(b) (hereafter we denote it as type I interface),

suggested that the screening charge at interface may arrange itself in such a way that it produces a charge-induced electric field, $E_{\sigma,j}$ that acts against the resultant effective internal field, $E_{eff,j}$ in each constituent layer j . On the other hand, as shown in Fig. 4.1(c) (henceforth denoted as type II interface), the second mechanism of screening charge at interface can produce a charge-induced electric field, $E_{\sigma,j}$ that has the same direction as the resultant effective internal field, $E_{eff,j}$. To sum up, in the case of type I interface, the presence of screen charge tends to enhance the polarization and internal electric field in superlattices, whereas the polarization and internal electric field are suppressed in the case of type II interface, hence it forms a homogeneous polarization across the whole superlattice. In conclusion, the properties of ferroelectric superlattice can be influenced by the alternative appearance of accumulated screening charge at interface.

We further extend our thermodynamic model to study the effect of composition and interface intermixing on $\text{BaTiO}_3/\text{Ba}_x\text{Sr}_{1-x}\text{TiO}_3$ (BT/BST) superlattices grown on SmScO_3 . In order to focus on the effect of (Ba, Sr) content and interface intermixing on the BT/BST superlattice system, an in-plane polarization is assumed. This assumption allows us to study the effects (i.e. composition and intermixing) in isolation with the effect of electrostatic coupling (Lim et al., 2012). Our choice of SmScO_3 as substrate is with an intention to induce the tensile stress upon the superlattice which leads to the in-plane polarization. Since the in-plane lattice parameters of the SmScO_3 substrate and BaTiO_3 are almost the same, i.e. almost no strain is applied to the BaTiO_3 layers by the underlying substrate. Therefore, changes in the Ba/Sr content will only affect the internal strain of the BST layer. In summary, we conclude that the changes in the composition (Ba,Sr content) on polarization of BT/BST superlattice are more important than the degree of interface intermixing.

6.2 Future Works

As emphasized in the thesis, the ability of our approach to describe the inhomogeneous properties in superlattices via intermixing will facilitate future work on modeling involving multidomains, as well as will establish the correlation between internal electric field and functional properties of superlattices (such as phase diagram, polarization, dielectric susceptibility, switching, etc). Our approach is general and can be applied to heterostructures, e.g. thin films, superlattices and multilayer system.

Since polarization, internal electric field and dielectric susceptibilities are correlated, the spatial dependence of all these ferroelectric properties are actually governed by the correlation length. In fact, it is a quantity that measures the thickness of domain wall (strictly, “partial-domain walls” in the present study), and it plays an important role in understanding the polarization reversal in ferroelectrics. Hence, we can extend our works in Section 3.7 to study the dynamics of polarization switching in a superlattice with the effects of electrostatic coupling and interface intermixing by using the Landau Khalatnikov equation (Chew et al., 2011c).

The future trend toward acceptance of lead-free materials in electronics has led to many investigations in finding other alternative material to replace PZT (lead zirconate titanate) which has an outstanding piezoelectric property. A recent experiment reported that a lead-free solid solution (BCZT) $\text{Ba}(\text{Ti}_{0.8}\text{Zr}_{0.2})\text{O}_3 - (\text{Ba}_{0.7}\text{Ca}_{0.3})\text{TiO}_3$ shown a high piezoelectric coefficient which is comparable to PZT (W. Liu & Ren, 2009). In light of this recent finding, we can extend our works in Chapter 5 to study the lead-free ferroelectric superlattices which involving solid solution ferroelectrics, such as $(\text{Ba}, \text{Ca})\text{TiO}_3$, $\text{Ba}(\text{Zr}, \text{Ti})\text{O}_3$, $(\text{Bi}, \text{Na})\text{TiO}_3$, $(\text{Bi}, \text{K})\text{TiO}_3$, etc. Therefore, we hope to report some interesting results in near future.

Ultimately, the future study of this research must encompass the combination of experimental measurements and theoretical calculations to quantitatively determine the degree of the interface effects and its influence on the ferroelectric properties of superlattice. It is anticipated that by controlling and manipulating the interface effects, it can lead to other interesting and potentially useful applications (Zubko et al., 2011).

REFERENCES

- Aguado-Puente, P., García-Fernández, P., & Junquera, J. (2011). Interplay of couplings between antiferrodistortive, ferroelectric, and strain degrees of freedom in monodomain $\text{PbTiO}_3/\text{SrTiO}_3$ superlattices. *Physical Review Letters*, *107*, 217601.
- Aguado-Puente, P., & Junquera, J. (2012). Structural and energetic properties of domains in $\text{PbTiO}_3/\text{SrTiO}_3$ superlattices from first principles. *Physical Review B*, *85*(18), 184105.
- Anderson, P. W. (1984). *Basic notions of condensed matter physics*. Menlo Park, Calif: Benjamin/Cummings Pub. Co., Advanced Book Program.
- Anderson, P. W. (2004). Some general thoughts about broken symmetry. In *A career in theoretical physics*. Hackensack N.J.: World Scientific.
- Bao, D. (2008). Multilayered dielectric/ferroelectric thin films and superlattices. *Current Opinion in Solid State and Materials Science*, *12*(3–4), 55–61.
- Baudry, L., & Tournier, J. (2001). Lattice model for ferroelectric thin film materials including surface effects: Investigation on the “depolarizing” field properties. *Journal of Applied Physics*, *90*(3), 1442–1454.
- Blinc, R. (2011). *Advanced ferroelectricity*. Oxford: Oxford University Press.
- Blinc, R., & Žekš, B. (1974). *Soft modes in ferroelectrics and antiferroelectrics*. Amsterdam : North-Holland Pub. Co. ; New York : American Elsevier Pub. Co.
- Blundell, S. (2001). *Magnetism in condensed matter*. Oxford: Oxford University Press.
- Borodavka, F., Gregora, I., Bartasyte, A., Margueron, S., Plausinaitiene, V., Abrutis, A., & Hlinka, J. (2013). Ferroelectric nanodomains in epitaxial PbTiO_3 films grown on SmScO_3 and TbScO_3 substrates. *Journal of Applied Physics*, *113*(18), 187216.
- Bousquet, E., Dawber, M., Stucki, N., Lichtensteiger, C., Hermet, P., Gariglio, S., ... Ghosez, P. (2008). Improper ferroelectricity in perovskite oxide artificial superlattices. *Nature*, *452*(7188), 732–736.
- Bratkovsky, A. M., & Levanyuk, A. P. (2000). Ferroelectric phase transitions in films with depletion charge. *Physical Review B*, *61*(22), 15042.
- Bratkovsky, A. M., & Levanyuk, A. P. (2005). Smearing of phase transition due to a surface effect or a bulk inhomogeneity in ferroelectric nanostructures. *Physical Review Letters*, *94*(10), 107601.
- Bratkovsky, A. M., & Levanyuk, A. P. (2009). Continuous theory of ferroelectric states in ultrathin films with real electrodes. *Journal of Computational and Theoretical Nanoscience*, *6*(3), 465–489.
- Bruchhausen, A., Fainstein, A., Soukiassian, A., Schlom, D. G., Xi, X. X., Bernhagen, M., ... Uecker, R. (2008). Ferroelectricity-induced coupling between light and terahertz-frequency acoustic phonons in $\text{BaTiO}_3/\text{SrTiO}_3$ superlattices. *Physical Review Letters*, *101*, 197402.
- Callori, S. J., Gabel, J., Su, D., Sinsheimer, J., Fernandez-Serra, M. V., & Dawber, M. (2012). Ferroelectric $\text{PbTiO}_3/\text{SrRuO}_3$ superlattices with broken inversion symmetry. *Physical Review Letters*, *109*(6), 067601.
- Chaikin, P. M., & Lubensky, T. C. (1995). *Principles of condensed matter physics*. Cambridge: Cambridge University Press.
- Chandra, P., & Littlewood, P. B. (2007). A Landau primer for ferroelectrics. In K. M. Rabe, C. H. Ahn, & J.-M. Triscone (Eds.), *Physics of ferroelectrics : a modern perspective*. Berlin, New York: Springer.

- Chang, L.-W., Alexe, M., Scott, J. F., & Gregg, J. M. (2009). Settling the “dead layer” debate in nanoscale capacitors. *Advanced Materials*, 21(48), 4911–4914.
- Chapra, S. C., & Canale, R. P. (2006). *Numerical Methods for Engineers*. Singapore: Mc Graw Hill.
- Chen, L.-Q. (2008). Phase-field method of phase transitions/domain structures in ferroelectric thin films: A review. *Journal of the American Ceramic Society*, 91(6), 1835–1844.
- Chenskii, E. V., & Tarasenko, V. V. (1982). Theory of phase transitions into inhomogeneous states in organic ferroelectrics in an external electric field. *Zhurnal Experiment. Teor. Fiziki*, 83, 1089–1099.
- Chew, K.-H. (2012). Recent applications of landau-ginzburg theory to ferroelectric superlattices: A review. *Solid State Phenomena*, 189, 145-167.
- Chew, K.-H., Ishibashi, Y., & G. Shin, F. (2005). Ferroelectric hysteresis loops as the manifestation of interface-aided polarization reversals in heterostructures. *Journal of the Physical Society of Japan*, 74(8), 2338–2346.
- Chew, K.-H., Ishibashi, Y., & G. Shin, F. (2006). A lattice model for ferroelectric superlattices. *Journal of the Physical Society of Japan*, 75(6), 064712.
- Chew, K.-H., Ishibashi, Y., G. Shin, F., & L. W. Chan, H. (2003). Theory of interface structures in double-layer ferroelectrics. *Journal of the Physical Society of Japan*, 72(9), 2364–2368.
- Chew, K.-H., Iwata, M., & Shin, F. G. (2009). Polarization modulation profiles in ferroelectric superlattices. *Ferroelectrics Letters Section*, 36(1-2), 12–19.
- Chew, K.-H., Iwata, M., Shin, F. G., & Ishibashi, Y. (2008). Exact expressions for dielectric susceptibilities in the paraelectric phase of ferroelectric superlattices based on the ginzburg-landau theory. *Integrated Ferroelectrics*, 100(1), 79–87.
- Chew, K.-H., Lim, K.-G., Ong, L.-H., & Iwata, M. (2013). Influence of interface intermixing and periodicity on internal electric field and polarization in ferroelectric superlattices. *Ceramics International*, 39, S301–S305.
- Chew, K.-H., Lim, K.-G., Ong, L.-H., & Iwata, M. (2014). Effect of composition and interface intermixing on polarization behaviors of BaTiO₃/(Ba, Sr)TiO₃ superlattices. *Physica Status Solidi (A)*, 211, 1698–1703. doi: 10.1002/pssa.201330457
- Chew, K.-H., Ong, L.-H., & Iwata, M. (2011a). Influence of dielectric stiffness, interface, and layer thickness on hysteresis loops of ferroelectric superlattices. *Journal of Applied Physics*, 110(5), 054108.
- Chew, K.-H., Ong, L.-H., & Iwata, M. (2011b). Intrinsic interface coupling in ferroelectric heterostructures and superlattices. In M. Lallart (Ed.), *Ferroelectrics - characterization and modeling*. INTECH Open Access Publisher. Retrieved from <http://www.intechopen.com/books/ferroelectrics-characterization-and-modeling/intrinsic-interface-coupling-in-ferroelectric-heterostructures-and-superlattices> doi: 10.5772/16518
- Chew, K.-H., Ong, L.-H., & Iwata, M. (2011c). Switching dynamics in ferroelectric superlattices. *Current Applied Physics*, 11(3), 755–761.
- Chew, K.-H., Ong, L.-H., Osman, J., & Tilley, D. R. (2000). Hysteresis loops of ferroelectric bilayers and superlattices. *Applied Physics Letters*, 77(17), 2755–2757.
- Chiu, S.-J., Liu, Y.-T., Lee, H.-Y., Yu, G.-P., & Huang, J.-H. (2011). Growth of BiFeO₃/SrTiO₃ artificial superlattice structure by {RF} sputtering. *Journal of Crystal Growth*, 334(1), 90 - 95.
- Christen, H., Boatner, L. A., Budai, J. D., Chisholm, M. F., Géa, L. A., Marrero, P. J., & Norton, D. P. (1996). The growth and properties of epitaxial KNbO₃ thin films and KNbO₃/KTaO₃ superlattices. *Applied Physics Letters*, 68(11), 1488-1490.

- Christen, H.-M., Specht, E. D., Norton, D. P., Chisholm, M. F., & Boatner, L. A. (1998). Long-range ferroelectric interactions in $\text{KTaO}_3/\text{KNbO}_3$ superlattice structures. *Applied Physics Letters*, 72(20), 2535-2537.
- Cooper, V. R., Johnston, K., & Rabe, K. M. (2007). Polarization enhancement in short period superlattices via interfacial intermixing. *Physical Review B*, 76, 020103.
- Cui, L., Lü, T., Xu, X., & Zhou, J. (2009). Theoretical study on the mechanism of abnormal dielectric susceptibility behaviors of ferroelectric bilayer films. *Journal of Applied Physics*, 105(10), 104104.
- Dalal, N., & Bussmann-Holder, A. (Eds.). (2007). *Ferro- and antiferroelectricity: Order/disorder versus displacive*. New York: Springer-Verlag Berlin Heidelberg.
- Dalal, N., Klymachyov, A., & Bussmann-Holder, A. (1998). Coexistence of order-disorder and displacive features at the phase transitions in hydrogen-bonded solids: Squaric acid and its analogs. *Physical Review Letters*, 81, 5924–5927.
- Damjanovic, D. (1998). Ferroelectric, dielectric and piezoelectric properties of ferroelectric thin films and ceramics. *Reports on Progress in Physics*, 61(9), 1267.
- Das, H., Spaldin, N. A., Waghmare, U. V., & Saha-Dasgupta, T. (2010). Chemical control of polar behavior in bicomponent short-period superlattices. *Physical Review B*, 81(23), 235112.
- Dawber, M., & Bousquet, E. (2013). New developments in artificially layered ferroelectric oxide superlattices. *MRS Bulletin*, 38(12), 1048–1055.
- Dawber, M., Lichtensteiger, C., Cantoni, M., Veithen, M., Ghosez, P., Johnston, K., ... Triscone, J.-M. (2005). Unusual behavior of the ferroelectric polarization in $\text{PbTiO}_3/\text{SrTiO}_3$ superlattices. *Physical Review Letters*, 95, 177601.
- Dawber, M., Rabe, K. M., & Scott, J. F. (2005). Physics of thin-film ferroelectric oxides. *Reviews of Modern Physics*, 77, 1083-1130.
- Dawber, M., Stucki, N., Lichtensteiger, C., Gariglio, S., Ghosez, P., & Triscone, J.-M. (2007). Tailoring the properties of artificially layered ferroelectric superlattices. *Advanced Materials*, 19(23), 4153-4159.
- Defaÿ, E. (2011). The thermodynamic approach. In E. Defaÿ (Ed.), *Ferroelectric dielectrics integrated on silicon*. London : ISTE ; Hoboken, NJ : Wiley.
- Devonshire, A. (1949). Theory of barium titanate. *Philosophical Magazine*, 40(309), 1040-1063.
- Dove, M. T. (2003). *Structure and dynamics: An atomic view of materials*. Oxford: Oxford University Press.
- Fatuzzo, E., & Merz, W. J. (1967). *Ferroelectricity*. Amsterdam: North-Holland Pub. Co.
- Feng, D., & Jin, G. (2005). *Introduction to condensed matter physics* (Vol. 1). Hackensack, NJ: World Scientific.
- Fong, D. D., Cionca, C., Yacoby, Y., Stephenson, G. B., Eastman, J. A., Fuoss, P. H., ... Stern, E. A. (2005). Direct structural determination in ultrathin ferroelectric films by analysis of synchrotron x-ray scattering measurements. *Physical Review B*, 71, 144112.
- Fong, D. D., Stephenson, G. B., Streiffer, S. K., Eastman, J. A., Auciello, O., Fuoss, P. H., & Thompson, C. (2004). Ferroelectricity in ultrathin perovskite films. *Science*, 304(5677), 1650–1653.
- Ghosez, P., & Junquera, J. (2006). First-principles modeling of ferroelectric oxides nanostructures. In M. Rieth & W. Schommers (Eds.), *Handbook of theoretical and computational nanotechnology*. Stevenson Ranch, Calif.: American Scientific Publishers.
- Ginzburg, V. L. (1945). Dielectric properties of ferroelectrics and barium titanate. *Zh. Eksp. Teor. Fiz.*, 15,

- Ginzburg, V. L. (2005). Some remarks on ferroelectricity, soft modes, and related problems. In *About science, myself, and others*. Bristol: Institute of Physics Pub.
- Ginzburg, V. L., Sobyenin, A. A., & Levanyuk, A. P. (1983). General theory of light scattering near phase transitions in ideal crystals. In H. Z. Cummins & A. P. Levanyuk (Eds.), *Light scattering near phase transitions*. Oxford: Elsevier Science.
- Glinchuk, M. D., Eliseev, E. A., Stephanovich, V. A., & Farhi, R. (2003). Ferroelectric thin film properties—depolarization field and renormalization of a “bulk” free energy coefficients. *Journal of applied physics*, 93(2), 1150–1159.
- Grindlay, J. (1970). *An introduction to the phenomenological theory of ferroelectricity*. Oxford: Pergamon Press.
- Gu, M., Wang, J., Xie, Q. Y., & Wu, X. S. (2010). Structural and electronic properties of PbTiO₃/SrTiO₃ superlattices from first principles. *Physical Review B*, 82(13), 134102.
- Harigai, T., Tanaka, D., Kakemoto, H., Wada, S., & Tsurumi, T. (2003). Dielectric properties of BaTiO₃/SrTiO₃ superlattices measured with interdigital electrodes and electromagnetic field analysis. *Journal of Applied Physics*, 94(12), 7923-7925.
- Haun, M. J., Furman, E., Jang, S. J., McKinstry, H. A., & Cross, L. E. (1987). Thermodynamic theory of PbTiO₃. *Journal of Applied Physics*, 62(8), 3331-3338.
- Heaviside, O. (1892). On the forces, stresses, and fluxes of energy in the electromagnetic field. *Philosophical Transactions of the Royal Society of London. (A.)*, 183, 423-480.
- Hoffmann-Eifert, S., Richter, D., & Kinstry, S. T.-M. (2012). Dielectric, ferroelectric, and optical properties. In R. Waser (Ed.), *Nanoelectronics and information technology: Advanced electronic materials and novel devices*. Weinheim: Wiley-VCH.
- Hosokura, T., Iwaji, N., Nakagawa, T., Ando, A., Takagi, H., Sakabe, Y., & Hirao, K. (2011). (100)-oriented SrTiO₃/BaTiO₃ artificial superlattices fabricated by chemical solution deposition. *Crystal Growth & Design*, 11(10), 4253-4256.
- Ho Tsang, C., Chew, K.-H., Ishibashi, Y., & G. Shin, F. (2004). Structure of interfaces in layered ferroelectrics of first and/or second order transition. *Journal of the Physical Society of Japan*, 73(11), 3158–3165.
- Hung, C.-L., Chueh, Y.-L., Wu, T.-B., & Chou, L.-J. (2005). Characteristics of constrained ferroelectricity in PbZrO₃/BaZrO₃ superlattice films. *Journal of Applied Physics*, 97(3), 034105.
- Ishibashi, Y. (1990). A model of polarization reversal in ferroelectrics. *Journal of the Physical Society of Japan*, 59(11), 4148-4154.
- Ishibashi, Y. (1992). On polarization reversals in ferroelectrics. *Integrated Ferroelectrics*, 2(1-4), 41-49.
- Ishibashi, Y., & Iwata, M. (2007). Landau-ginzburg theory of phase transition of ferroelectric superlattices. *Ferroelectrics*, 354(1), 8–12.
- Ishibashi, Y., Ohashi, N., & Tsurumi, T. (2000). Structural refinement of X-ray diffraction profile for artificial superlattices. *Japanese Journal of Applied Physics*, 39(Part 1, No. 1), 186-191.
- Iwata, M., Orihara, H., & Ishibashi, Y. (2001). Theory of morphotropic phase boundary in solid solution systems of perovskite-type oxide ferroelectrics: Engineered domain configurations II. *Japanese Journal of Applied Physics*, 40(Part 1, No. 2A), 703-707.
- Jiang, A. Q., Scott, J. F., Lu, H., & Chen, Z. (2003). Phase transitions and polarizations in epitaxial BaTiO₃/SrTiO₃ superlattices studied by second-harmonic generation. *Journal of Applied Physics*,

93(2), 1180-1185.

- Jiang, J. C., Pan, X. Q., Tian, W., Theis, C. D., & Schlom, D. G. (1999). Abrupt $\text{PbTiO}_3/\text{SrTiO}_3$ superlattices grown by reactive molecular beam epitaxy. *Applied Physics Letters*, 74(19), 2851-2853.
- Jo, J. Y., Chen, P., Sichel, R. J., Callori, S. J., Sinsheimer, J., Dufresne, E. M., ... Evans, P. G. (2011). Nanosecond dynamics of ferroelectric/dielectric superlattices. *Physical Review Letters*, 107, 055501.
- Joas, C., & Katzir, S. (2011). Analogy, extension, and novelty: Young schrödinger on electric phenomena in solids. *Studies in History and Philosophy of Science Part B: Studies in History and Philosophy of Modern Physics*, 42(1), 43 - 53.
- Johnston, K., Huang, X., Neaton, J. B., & Rabe, K. M. (2005). First-principles study of symmetry lowering and polarization in $\text{BaTiO}_3/\text{SrTiO}_3$ superlattices with in-plane expansion. *Physical Review B*, 71, 100103.
- Kesim, M. T., Cole, M. W., Zhang, J., Misirlioglu, I. B., & Alpay, S. P. (2014). Tailoring dielectric properties of ferroelectric-dielectric multilayers. *Applied Physics Letters*, 104(2), 022901.
- Kim, J., Kim, Y., Kim, Y. S., Lee, J., Kim, L., & Jung, D. (2002). Large nonlinear dielectric properties of artificial $\text{BaTiO}_3/\text{SrTiO}_3$ superlattices. *Applied Physics Letters*, 80(19), 3581-3583.
- Kretschmer, R., & Binder, K. (1979). Surface effects on phase transitions in ferroelectrics and dipolar magnets. *Physical Review B*, 20, 1065-1076.
- Landau, L. D., & Lifshitz, E. M. (1980). *Statistical physics, part 1*. Oxford: Butterworth Heinemann.
- Landau, L. D., Pitaevskii, L. P., & Lifshits, E. M. (1998). *Electrodynamics of continuous media*. Oxford: Butterworth Heinemann.
- Lee, D., Behera, R. K., Wu, P., Xu, H., Li, Y. L., Sinnott, S. B., ... Gopalan, V. (2009). Mixed Bloch-Néel-Ising character of 180° ferroelectric domain walls. *Physical Review B*, 80, 060102.
- Lee, H. N., Christen, H. M., Chisholm, M. F., Rouleau, C. M., & Lowndes, D. H. (2005). Strong polarization enhancement in asymmetric three-component ferroelectric superlattices. *Nature*, 433(7024), 395-399.
- Le Marrec, F., Farhi, R., El Marssi, M., Dellis, J. L., Karkut, M. G., & Ariosa, D. (2000). Ferroelectric $\text{PbTiO}_3/\text{BaTiO}_3$ superlattices: Growth anomalies and confined modes. *Physical Review B*, 61(10), R6447.
- Levanyuk, A. P., & Misirlioglu, I. B. (2011). Phase transitions in ferroelectric-paraelectric superlattices. *Journal of Applied Physics*, 110(11), 114109.
- Li, S., Eastman, J. A., Vetrone, J. M., Newnham, R. E., & Cross, L. E. (1997). Dielectric response in ferroelectric superlattices. *Philosophical Magazine B*, 76(1), 47-57.
- Li, Y. L., Hu, S. Y., Tenne, D., Soukiassian, A., Schlom, D. G., Chen, L. Q., ... Jia, Q. X. (2007). Interfacial coherency and ferroelectricity of $\text{BaTiO}_3/\text{SrTiO}_3$ superlattice films. *Applied Physics Letters*, 91(25), 252904.
- Lichtensteiger, C., Zubko, P., Stengel, M., Aguado-Puente, P., Triscone, J.-M., Ghosez, P., & Junquera, J. (2012). Ferroelectricity in ultrathin-film capacitors. In G. Pacchioni & S. Valeri (Eds.), *Oxide ultrathin films : science and technology*. Weinheim, Germany: Wiley-VCH.
- Lim, K.-G., & Chew, K.-H. (2014). Interface-induced modifications of polarization in nanoscale ferroelectric superlattices. *Advanced Materials Research*, 895, 477-480.
- Lim, K.-G., Chew, K.-H., & Ong, L.-H. (2013). Hysteretic internal electric fields and polarization reversal in ferroelectric superlattices. *Ferroelectrics*, 451(1), 41-47.

- Lim, K.-G., Chew, K.-H., Ong, L.-H., & Iwata, M. (2012). Electrostatic coupling and interface intermixing in ferroelectric superlattices. *EPL (Europhysics Letters)*, *99*(4), 46004.
- Lim, K.-G., Chew, K.-H., Ong, L.-H., & Iwata, M. (2013). Modulated internal electric field, dielectric susceptibility and polarization in ferroelectric superlattices. *Ceramics International*, *39*, S307–S310.
- Lim, K.-G., Chew, K.-H., Wang, D. Y., Ong, L.-H., & Iwata, M. (2014). Charge compensation phenomena for polarization discontinuities in ferroelectric superlattices. *EPL (Europhysics Letters)*, *108*, 67011. doi: 10.1209/0295-5075/108/67011
- Lines, M. E., & Glass, A. M. (1977). *Principles and applications of ferroelectrics and related materials*. Oxford [Eng.]: Clarendon Press.
- Liu, W., & Ren, X. (2009). Large piezoelectric effect in pb-free ceramics. *Physical Review Letters*, *103*(25), 257602.
- Liu, Y. Y., & Li, J. Y. (2010). Space charges and size effects in semiconducting ferroelectric BaTiO₃/SrTiO₃ superlattices. *Applied Physics Letters*, *97*(4), 042905.
- Liu, Y. Y., Zhu, Z. X., Li, J.-F., & Li, J. Y. (2010). Misfit strain modulated phase structures of epitaxial Pb(Zr_{1-x}Ti_x)O₃ thin films: The effect of substrate and film thickness. *Mechanics of Materials*, *42*(8), 816–826.
- Lü, T., & Cao, W. (2002). Generalized continuum theory for ferroelectric thin films. *Physical Review B*, *66*(2), 024102.
- Ma, Y.-q., Shen, J., & Xu, X.-h. (2000). Coupling effects in ferroelectric superlattice. *Solid State Communications*, *114*(9), 461–464.
- Misirlioglu, I. B., Akcay, G., Zhong, S., & Alpay, S. P. (2007). Interface effects in ferroelectric bilayers and heterostructures. *Journal of Applied Physics*, *101*(3), 036107–036107.
- Misirlioglu, I. B., Alexe, M., Pintilie, L., & Hesse, D. (2007). Space charge contribution to the apparent enhancement of polarization in ferroelectric bilayers and multilayers. *Applied physics letters*, *91*(2), 022911.
- Misirlioglu, I. B., Kesim, M. T., & Alpay, S. P. (2014). Strong dependence of dielectric properties on electrical boundary conditions and interfaces in ferroelectric superlattices. *Applied Physics Letters*, *104*(2), 022906.
- Mizoguchi, T., Ohta, H., Lee, H.-S., Takahashi, N., & Ikuhara, Y. (2011). Controlling interface intermixing and properties of SrTiO₃-based superlattices. *Advanced Functional Materials*, *21*(12), 2258–2263.
- Muralt, P. (2000). Ferroelectric thin films for micro-sensors and actuators: a review. *Journal of Micromechanics and Microengineering*, *10*(2), 136.
- Murray, É. D., & Vanderbilt, D. (2009). Theoretical investigation of polarization-compensated II – IV/IV perovskite superlattices. *Physical Review B*, *79*(10), 100102.
- Neaton, J. B., & Rabe, K. M. (2003). Theory of polarization enhancement in epitaxial BaTiO₃/SrTiO₃ superlattices. *Applied Physics Letters*, *82*(10), 1586–1588.
- Nye, J. F. (1972). *Physical properties of crystals their representation by tensors and matrices*. Oxford: Clarendon Press.
- Ohnishi, T., Koinuma, H., & Lippmaa, M. (2006). Pulsed laser deposition of oxide thin films. *Applied surface science*, *252*(7), 2466–2471.
- Ohtomo, A., & Hwang, H. Y. (2004). A high-mobility electron gas at the LaAlO₃/SrTiO₃ heterointerface. *Nature*, *427*(6973), 423–426.

- Okatan, M. B., Misirlioglu, I. B., & Alpay, S. P. (2010). Contribution of space charges to the polarization of ferroelectric superlattices and its effect on dielectric properties. *Physical Review B*, 82(9), 094115.
- Omura, M., Adachi, H., & Ishibashi, Y. (1991). Simulations of ferroelectric characteristics using a one-dimensional lattice model. *Japanese Journal of Applied Physics*, 30(Part 1, No. 9B), 2384-2387.
- Omura, M., Adachi, H., & Ishibashi, Y. (1992). Simulations of polarization reversals by a two-dimensional lattice model. *Japanese Journal of Applied Physics*, 31(Part 1, No. 9B), 3238-3240.
- Omura, M., Mihara, T., & Ishibashi, Y. (1993). Simulations of switching characteristics in ferroelectrics. *Japanese Journal of Applied Physics*, 32(Part 1, No. 9B), 4388-4392.
- Ong, L.-H., Lee, T.-Y., & Chew, K.-H. (2012). Calculations on switching characteristics of ferroelectric–paraelectric superlattices. *Ceramics International*, 38, S3–S7.
- Ortega, N., Kumar, A., Maslova, O. A., Yuzyuk, Y. I., Scott, J. F., & Katiyar, R. S. (2011). Effect of periodicity and composition in artificial BaTiO₃/(Ba,Sr)TiO₃ superlattices. *Physical Review B*, 83(14), 144108.
- Ortega, N., Kumar, A., Resto, O., Maslova, O. A., Yuzyuk, Y. I., Scott, J. F., & Katiyar, R. S. (2013). Compositional engineering of BaTiO₃/(Ba,Sr)TiO₃ ferroelectric superlattices. *Journal of Applied Physics*, 114(10), 104102.
- Pertsev, N. A., Janolin, P.-E., Kiat, J.-M., & Uesu, Y. (2010). Enhancing permittivity of ferroelectric superlattices via composition tuning. *Physical Review B*, 81(14), 144118.
- Pertsev, N. A., Tagantsev, A. K., & Setter, N. (2000). Phase transitions and strain-induced ferroelectricity in SrTiO₃ epitaxial thin films. *Physical Review B*, 61, R825-R829.
- Pertsev, N. A., & Tyunina, M. (2011). Interfacial nanolayers and permittivity of ferroelectric superlattices. *Journal of Applied Physics*, 109(12), 126101.
- Pertsev, N. A., Zembilgotov, A. G., & Tagantsev, A. K. (1998). Effect of mechanical boundary conditions on phase diagrams of epitaxial ferroelectric thin films. *Physical Review Letters*, 80, 1988-1991.
- Posadas, A.-B., Lippmaa, M., Walker, F. J., Dawber, M., Ahn, C. H., & Triscone, J.-M. (2007). Growth and novel applications of epitaxial oxide thin films. In K. M. Rabe, C. H. Ahn, & J.-M. Triscone (Eds.), *Physics of ferroelectrics : a modern perspective*. Berlin, New York: Springer.
- Qiu, J. H. (2010). Effect of domain wall on the dielectric properties of the BaTiO₃/SrTiO₃ superlattices. *Solid State Communications*, 150(23), 1052–1055.
- Qu, B., Zhong, W., & Zhang, P. (1995). Polarization and dielectric susceptibility of ferroelectric superlattice. *Japanese journal of applied physics*, 34(8R), 4114.
- Qu, B. D., Evstigneev, M., Johnson, D. J., & Prince, R. H. (1998). Dielectric properties of BaTiO₃/SrTiO₃ multilayered thin films prepared by pulsed laser deposition. *Applied Physics Letters*, 72(11), 1394-1396.
- Qu, B. D., Zhong, W. L., & Prince, R. H. (1997). Interfacial coupling in ferroelectric superlattices. *Physical Review B*, 55, 11218–11224.
- Qu, B. D., Zhong, W. L., & Zhang, P. L. (1994). Curie temperature of a ferroelectric superlattice described by the transverse ising model. *Physics Letters A*, 189(5), 419–422.
- Rabe, K. M. (2005). Theoretical investigations of epitaxial strain effects in ferroelectric oxide thin films and superlattices. *Current Opinion in Solid State and Materials Science*, 9(3), 122 - 127.
- Rabe, K. M., & Ghosez, P. (2007). First-principles studies of ferroelectric oxides. In K. M. Rabe, C. H. Ahn, & J.-M. Triscone (Eds.), *Physics of ferroelectrics : a modern perspective*. Berlin, New York: Springer.

- Ranjith, R., Kundys, B., & Prellier, W. (2007). Periodicity dependence of the ferroelectric properties in bifeo₃/srtio₃ multiferroic superlattices. *Applied Physics Letters*, 91(22), 222904.
- Ranjith, R., Nikhil, R., & Krupanidhi, S. B. (2006). Interfacial coupling and its size dependence in PbTiO₃ and PbMg_{1/3}Nb_{2/3}O₃ multilayers. *Physical Review B*, 74(18), 184104.
- Ricinschi, D., Ishibashi, Y., Iwata, M., & Okuyama, M. (2001). Analysis of switching in perovskite ferroelectrics on the tetragonal side of the morphotropic phase boundary using a landau-theory-based lattice model with polarization vector rotations. *Japanese Journal of Applied Physics*, 40(Part 1, No. 8), 4990-4997.
- Ricinschi, D., Lerescu, A. I., & Okuyama, M. (2000). Investigation of fatigue mechanisms in Pb(Zr, Ti)O₃ films from a correlated analysis of hysteresis parameters in a lattice model with distributed polarization clamping. *Japanese Journal of Applied Physics*, 39(Part 2, No. 10A), L990-L992.
- Rijnders, G., & Blank, D. H. A. (2005). Materials science: Build your own superlattice. *Nature*, 433(7024), 369-370.
- Ríos, S., Ruediger, A., Jiang, A. Q., Scott, J. F., Lu, H., & Chen, Z. (2003). Orthorhombic strontium titanate in BaTiO₃ – SrTiO₃ superlattices. *Journal of Physics: Condensed Matter*, 15(21), L305-L309.
- Roytburd, A. L., Zhong, S., & Alpay, S. P. (2005). Dielectric anomaly due to electrostatic coupling in ferroelectric-paraelectric bilayers and multilayers. *Applied Physics Letters*, 87(9), 092902.
- Sawyer, C. B., & Tower, C. H. (1930). Rochelle salt as a dielectric. *Physical Review*, 35, 269-273.
- Schlom, D. G., Chen, L.-Q., Eom, C.-B., Rabe, K. M., Streiffer, S. K., & Triscone, J.-M. (2007). Strain tuning of ferroelectric thin films. *Annual Review of Materials Research*, 37, 589-626.
- Schrödinger, E. (1912, November). Aus sen sitzungsberichten der kaiserl. akademie der wissenschaften in wien., studien uer kinetik der dielektrika, dam schmelzpunkt, pyround und piezoelektrizität. *Mathem.-Naturw. Klasse, Bd. CXXI, Abt. Iia*.
- Schwenk, D., Fishman, F., & Schwabl, F. (1990). Soft modes in ferroelectric superlattices. *Ferroelectrics*, 104(1), 349-354.
- Scott, J. F. (2000). *Ferroelectric memories*. Berlin: Springer.
- Scott, J. F. (2007). Applications of modern ferroelectrics. *Science*, 315(5814), 954-959.
- Scott, J. F. (2013). Prospects for ferroelectrics: 2012-2022. *ISRN Materials Science, 2013, Article ID 187313, doi:10.1155/2013/187313*.
- Sepliarsky, M., Asthagiri, A., Phillpot, S., Stachiotti, M., & Migoni, R. (2005). Atomic-level simulation of ferroelectricity in oxide materials. *Current Opinion in Solid State and Materials Science*, 9(3), 107 - 113.
- Sepliarsky, M., Phillpot, S. R., Wolf, D., Stachiotti, M. G., & Migoni, R. L. (2001). Long-ranged ferroelectric interactions in perovskite superlattices. *Physical Review B*, 64(6), 060101.
- Sethna, J. P. (2006). *Statistical mechanics: Entropy, order parameters, and complexity*. Oxford: Oxford University Press.
- Shen, J., & Ma, Y.-q. (2000). Long-range coupling interactions in ferroelectric superlattices. *Physical Review B*, 61, 14279-14282.
- Shen, J., & Ma, Y.-q. (2001). Long-range coupling interactions in ferroelectric sandwich structures. *Journal of Applied Physics*, 89(9), 5031-5035.
- Shimuta, T., Nakagawara, O., Makino, T., Arai, S., Tabata, H., & Kawai, T. (2002). Enhancement of remanent polarization in epitaxial BaTiO₃/SrTiO₃ superlattices with “asymmetric” structure. *Journal*

of *Applied Physics*, 91(4), 2290-2294.

- Shin, J., Borisevich, A. Y., Meunier, V., Zhou, J., Plummer, E. W., Kalinin, S. V., & Baddorf, A. P. (2010). Oxygen-induced surface reconstruction of SrRuO₃ and its effect on the BaTiO₃ interface. *ACS nano*, 4(7), 4190–4196.
- Shirokov, V. B., Torgashev, V. I., Bakirov, A. A., & Lemanov, V. V. (2006). Concentration phase diagram of Ba_xSr_{1-x}TiO₃ solid solutions. *Physical Review B*, 73(10), 104116.
- Shirokov, V. B., Yuzyuk, Y. I., Dkhil, B., & Lemanov, V. V. (2009). Phenomenological theory of phase transitions in epitaxial Ba_xSr_{1-x}TiO₃ thin films. *Physical Review B*, 79(14), 144118.
- Sigman, J., Norton, D. P., Christen, H. M., Fleming, P. H., & Boatner, L. A. (2002). Antiferroelectric behavior in symmetric KNbO₃/KTaO₃. *Physical Review Letters*, 88, 097601.
- Soukiassian, A., Tian, W., Vaithyanathan, V., Haeni, J. H., Chen, L. Q., Xi, X., ... Uecker, R. (2008). Growth of nanoscale BaTiO₃/SrTiO₃ superlattices by molecular-beam epitaxy. *Journal of Materials Research*, 23(05), 1417–1432.
- Specht, E. D., Christen, H.-M., Norton, D. P., & Boatner, L. A. (1998). X-ray diffraction measurement of the effect of layer thickness on the ferroelectric transition in epitaxial KTaO₃/KNbO₃ multilayers. *Physical Review Letters*, 80, 4317–4320.
- Stengel, M., & Spaldin, N. A. (2006). Origin of the dielectric dead layer in nanoscale capacitors. *Nature*, 443(7112), 679–682.
- Stengel, M., Vanderbilt, D., & Spaldin, N. A. (2009). Enhancement of ferroelectricity at metal–oxide interfaces. *Nature Materials*, 8(5), 392–397.
- Stephanovich, V. A., Luk'yanchuk, I. A., & Karkut, M. G. (2005). Domain-enhanced interlayer coupling in ferroelectric/paraelectric superlattices. *Physical Review Letters*, 94, 047601.
- Strukov, B. A., & Levanyuk, A. P. (1998). *Ferroelectric phenomena in crystals: Physical foundations*. Berlin: Springer.
- Tabata, H., Tanaka, H., & Kawai, T. (1994). Formation of artificial BaTiO₃/SrTiO₃ superlattices using pulsed laser deposition and their dielectric properties. *Applied Physics Letters*, 65(15), 1970-1972.
- Tagantsev, A. K., Cross, L. E., & Fousek, J. (2010). Domain walls at rest. In *Domains in ferroic crystals and thin films* (chap. 6). New York: Springer.
- Tenne, D. A., Bruchhausen, A., Lanzillotti-Kimura, N. D., Fainstein, A., Katiyar, R. S., Cantarero, A., ... Xi, X. X. (2006). Probing nanoscale ferroelectricity by ultraviolet raman spectroscopy. *Science*, 313(5793), 1614-1616.
- The MathWorks. (2014). *Optimization Toolbox User's Guide*. United States of America: The MathWorks, Inc.
- Tian, W., Jiang, J. C., Pan, X. Q., Haeni, J. H., Li, Y. L., Chen, L. Q., ... Jia, Q. X. (2006). Structural evidence for enhanced polarization in a commensurate short-period BaTiO₃/SrTiO₃ superlattice. *Applied Physics Letters*, 89(9), 092905.
- Tilley, D., & Žekš, B. (1984). Landau theory of phase transitions in thick films. *Solid State Communications*, 49(8), 823 - 828.
- Tilley, D. R. (1988). Landau theory for coupled ferromagnetic and ferroelectric films and superlattices. *Solid state communications*, 65(7), 657–660.
- Torres-Pardo, A., Gloter, A., Zubko, P., Jecklin, N., Lichtensteiger, C., Colliex, C., ... Stéphan, O. (2011). Spectroscopic mapping of local structural distortions in ferroelectric PbTiO₃/SrTiO₃ superlattices at the unit-cell scale. *Physical Review B*, 84, 220102.

- Tsai, H.-N., Liang, Y.-C., & Lee, H.-Y. (2005). Characteristics of sputter-deposited BaTiO₃/SrTiO₃ artificial superlattice films on an LaNiO₃-coated SrTiO₃ substrate. *Journal of Crystal Growth*, 284(1–2), 65 - 72.
- Tsurumi, T., Ichikawa, T., Harigai, T., Kakemoto, H., & Wada, S. (2002a). Dielectric and optical properties of BaTiO₃/SrTiO₃ and BaTiO₃/BaZrO₃ superlattices. *Journal of Applied Physics*, 91(4), 2284–2289.
- Tsurumi, T., Ichikawa, T., Harigai, T., Kakemoto, H., & Wada, S. (2002b). Dielectric and optical properties of BaTiO₃/SrTiO₃ and BaTiO₃/BaZrO₃ superlattices. *Journal of Applied Physics*, 91(4), 2284–2289.
- Valasek, J. (1920). Piezoelectric and allied phenomena in rochelle salt. *Am. Phys. Soc.*, 15, 537.
- Valasek, J. (1921). Piezo-electric and allied phenomena in rochelle salt. *Physical review*, 17, 475–481.
- Wang, N., Lu, H. B., Chen, W. Z., Zhao, T., Chen, F., Peng, H. Y., ... Yang, G. Z. (1999). Morphology and microstructure of BaTiO₃/SrTiO₃ superlattices grown on SrTiO₃ by laser molecular-beam epitaxy. *Applied Physics Letters*, 75(22), 3464–3466.
- Wang, Q., & Shen, M. (2005). Enhancement of remnant polarization in multilayered Bi₄Ti₃O₁₂/(Bi_{3.25}La_{0.75})Ti₃O₁₂ films obtained by chemical solution deposition. *Thin Solid Films*, 473(1), 74 - 79.
- Wang, Z., & Oda, S. (2000). Electrical properties of SrTiO₃/BaTiO₃ strained superlattice films prepared by atomic layer metallorganic chemical vapor deposition. *Journal of The Electrochemical Society*, 147(12), 4615.
- Warusawithana, M. P., Colla, E. V., Eckstein, J. N., & Weissman, M. B. (2003). Artificial dielectric superlattices with broken inversion symmetry. *Physical Review Letters*, 90, 036802.
- Xin, Y., Wang, C. L., Zhong, W. L., & Zhang, P. L. (1999). Pyroelectric properties of ferroelectric superlattice on transverse ising model. *Solid state communications*, 110(5), 265–269.
- Zhao, T., Chen, Z.-H., Chen, F., Shi, W.-S., Lu, H.-B., & Yang, G.-Z. (1999). Enhancement of second-harmonic generation in BaTiO₃/SrTiO₃ superlattices. *Physical Review B*, 60, 1697–1700.
- Zhong, S., Alpay, S. P., & Mantese, J. V. (2006). High dielectric tunability in ferroelectric-paraelectric bilayers and multilayer superlattices. *Applied Physics Letters*, 88(13), 132904.
- Zhong, S., Alpay, S. P., Roytburd, A. L., & Mantese, J. V. (2006). Interlayer coupling in ferroelectric bilayer and superlattice heterostructures. *Ultrasonics, Ferroelectrics and Frequency Control, IEEE Transactions on*, 53(12), 2349–2356.
- Zhong, W., Vanderbilt, D., & Rabe, K. M. (1994). Phase transitions in BaTiO₃ from first principles. *Physical Review Letters*, 73, 1861–1864.
- Zhong, W., Vanderbilt, D., & Rabe, K. M. (1995). First-principles theory of ferroelectric phase transitions for perovskites: The case of BaTiO₃. *Physical Review B*, 52, 6301–6312.
- Zubko, P., Gariglio, S., Gabay, M., Ghosez, P., & Triscone, J.-M. (2011). Interface physics in complex oxide heterostructures. *Annual Review of Condensed Matter Physics*, 2(1), 141–165.
- Zubko, P., Jecklin, N., Torres-Pardo, A., Aguado-Puente, P., Gloter, A., Lichtensteiger, C., ... Triscone, J.-M. (2012). Electrostatic coupling and local structural distortions at interfaces in ferroelectric/paraelectric superlattices. *Nano Letters*, 12(6), 2846–2851.
- Zubko, P., Stucki, N., Lichtensteiger, C., & Triscone, J.-M. (2010). X-ray diffraction studies of 180° ferroelectric domains in PbTiO₃/SrTiO₃ superlattices under an applied electric field. *Physical Review Letters*, 104, 187601.

Appendices

APPENDIX A

VOIGT NOTATION

Voigt notation is very useful to simplify a symmetric tensor by reducing its order. The pairs of indices 11, 22, 33 are replaced by single indices 1, 2, and 3 respectively, and the pairs of indices 23, 13, and 12 are replaced by the single indices 4, 5, and 6 respectively (Dove, 2003). Therefore, we can write the stress tensor as follows:

$$\boldsymbol{\sigma} = \begin{pmatrix} \sigma_{11} & \sigma_{12} & \sigma_{13} \\ \sigma_{21} & \sigma_{22} & \sigma_{23} \\ \sigma_{31} & \sigma_{32} & \sigma_{33} \end{pmatrix} = \begin{pmatrix} \sigma_1 & \sigma_6 & \sigma_5 \\ \sigma_6 & \sigma_2 & \sigma_4 \\ \sigma_5 & \sigma_4 & \sigma_3 \end{pmatrix} \equiv \begin{pmatrix} \sigma_1 \\ \sigma_2 \\ \sigma_3 \\ \sigma_4 \\ \sigma_5 \\ \sigma_6 \end{pmatrix} \quad (\text{A.1})$$

In Voigt notation the stress tensor is simplified to a 6 dimensional vector. The similar method can be applied to strain tensor. The Voigt notation for strains and stresses can be summarized in Table.A1 (Defay, 2011).

Table A1: The Voigt notation with axis 3 perpendicular to the interface.

strain		stress	
$u_1 = u_{11}$	$u_4 = u_{23} + u_{32}$	$\sigma_1 = \sigma_{11}$	$\sigma_4 = (\sigma_{23} + \sigma_{32})/2$
$u_2 = u_{22}$	$u_5 = u_{31} + u_{13}$	$\sigma_2 = \sigma_{22}$	$\sigma_5 = (\sigma_{31} + \sigma_{13})/2$
$u_3 = u_{33}$	$u_6 = u_{12} + u_{21}$	$\sigma_3 = \sigma_{33}$	$\sigma_6 = (\sigma_{12} + \sigma_{21})/2$

APPENDIX B

DIMENSIONLESS SCALING

For numerical studies, it is convenient to rescale the variables in Eqs. (3.1) to Eq. (3.3) into their dimensionless forms. The dimensionless form of Helmholtz free energy per unit area, Eq. (3.1) is $\tilde{f} = \tilde{f}_{FE} + \tilde{f}_{PE} + \tilde{f}_I$, and the detailed forms are given as:

$$\tilde{f}_{FE} = \int_{-\tilde{d}_{FE}}^0 \left[\frac{\alpha_{FE}^*}{\alpha_{0,FE} T_{0,FE}} \tilde{p}_{FE}^2 + \frac{\beta_{FE}^*}{\beta_{FE}} \tilde{p}_{FE}^4 + t_r \tilde{p}_{FE}^6 + \frac{1}{2} \left(\frac{d\tilde{p}_{FE}}{d\zeta} \right)^2 - \frac{1}{2} e_{d,FE} \tilde{p}_{FE} - e_{ext} \tilde{p}_{FE} + \left(\frac{c_{11,FE}^2 + c_{11,FE} c_{12,FE} - 2c_{12,FE}^2}{c_{11,FE}} \right) u_{m,FE}^2 \frac{\beta_{FE}}{\alpha_{0,FE}^2 T_{0,FE}^2} \right] d\zeta, \quad (\text{B.1})$$

$$\tilde{f}_{PE} = \int_0^{\tilde{d}_{PE}} \left[\frac{\alpha_{PE}^*}{\alpha_{0,FE} T_{0,FE}} \tilde{p}_{PE}^2 + \frac{\beta_{PE}^*}{\beta_{FE}} \tilde{p}_{PE}^4 + t_r \gamma_r \tilde{p}_{PE}^6 + \frac{1}{2} \kappa_r \left(\frac{d\tilde{p}_{PE}}{d\zeta} \right)^2 - \frac{1}{2} e_{d,PE} \tilde{p}_{PE} - e_{ext} \tilde{p}_{PE} + \left(\frac{c_{11,PE}^2 + c_{11,PE} c_{12,PE} - 2c_{12,PE}^2}{c_{11,PE}} \right) u_{m,PE}^2 \frac{\beta_{FE}}{\alpha_{0,PE}^2 T_{0,PE}^2} \right] d\zeta \quad (\text{B.2})$$

and

$$\tilde{f}_I = \frac{\lambda_0}{2\epsilon_0 \kappa_{FE}} \xi_0 \left[(\tilde{p}_{FE}(0) - \tilde{p}_{PE}(0))^2 + (\tilde{p}_{FE}(-l_{FE}) - \tilde{p}_{PE}(l_{PE})) \right], \quad (\text{B.3})$$

where the following scaling are used:

$$\begin{aligned} \tilde{f}_j &= f_j/f_0; \quad f_0 = \frac{\alpha_{0,FE}^2 T_{0,FE}^2 \xi_0}{\beta_{FE}}; \quad \tilde{p}_j = p_j/p_0; \quad p_0 = \left(\frac{\alpha_{0,FE} T_{0,FE}}{\beta_{FE}} \right)^{1/2}; \quad \xi_0 = \left(\frac{\kappa_{FE}}{\alpha_{0,FE} T_{0,FE}} \right)^{1/2}; \\ t_r &= \frac{\gamma_{FE} \alpha_{0,FE} T_{0,FE}}{\beta_{FE}^2}; \quad \gamma_r = \gamma_{PE}/\gamma_{FE}; \quad \kappa_r = \kappa_{PE}/\kappa_{FE}; \quad \zeta = z/\xi_0; \quad \tilde{d}_j = d_j/\xi_0; \quad e_{d,j} = E_{d,j}/E_0; \\ e_{ext} &= E_{ext}/E_0; \quad E_0 = \frac{(\alpha_{0,FE} T_{0,FE})^{3/2}}{\beta_{FE}^{1/2}}. \end{aligned}$$

The corresponding Euler-Lagrange equations follow from Eq. (B.1) and Eq. (B.2) are given as:

$$\frac{d^2 \tilde{p}_{FE}}{d\zeta^2} = \frac{2\alpha_{FE}^*}{\alpha_{0,FE} T_{0,FE}} \tilde{p}_{FE} + \frac{4\beta_{FE}^*}{\beta_{FE}} \tilde{p}_{FE}^3 + 6t_r \tilde{p}_{FE}^5 + \frac{1}{2} \frac{d\tilde{\varphi}_{FE}}{d\zeta} - e_{ext} \quad (\text{B.4})$$

and

$$\kappa_r \frac{d^2 \tilde{p}_{PE}}{d\zeta^2} = \frac{2\alpha_{PE}^*}{\alpha_{0,FE} T_{0,FE}} \tilde{p}_{PE} + \frac{4\beta_{PE}^*}{\beta_{FE}} \tilde{p}_{PE}^3 + 6t_r \gamma_r \tilde{p}_{PE}^5 + \frac{1}{2} \frac{d\tilde{\phi}_{PE}}{d\zeta} - e_{ext} \quad (\text{B.5})$$

Whereas, the boundary condition at interfaces in dimensionless form are given as:

$$\left\{ \begin{array}{l} -\frac{d\tilde{p}_{FE}}{d\zeta} \Big|_{\zeta=-\tilde{d}_{FE}} + \frac{\lambda_0}{\kappa_{FE} \epsilon_0} \xi_0 [\tilde{p}_{FE}(-\tilde{d}_{FE}) - \tilde{p}_{PE}(\tilde{d}_{PE})] = 0 \\ \kappa_r \frac{d\tilde{p}_{PE}}{d\zeta} \Big|_{\zeta=0} + \frac{\lambda_0}{\kappa_{FE} \epsilon_0} \xi_0 [\tilde{p}_{FE}(0) - \tilde{p}_{PE}(0)] = 0 \\ \frac{d\tilde{p}_{FE}}{d\zeta} \Big|_{\zeta=0} + \frac{\lambda_0}{\kappa_{FE} \epsilon_0} \xi_0 [\tilde{p}_{FE}(0) - \tilde{p}_{PE}(0)] = 0 \\ -\kappa_r \frac{d\tilde{p}_{PE}}{d\zeta} \Big|_{\zeta=\tilde{d}_{PE}} + \frac{\lambda_0}{\kappa_{FE} \epsilon_0} \xi_0 [\tilde{p}_{FE}(-\tilde{d}_{FE}) - \tilde{p}_{PE}(\tilde{d}_{PE})] = 0. \end{array} \right. \quad (\text{B.6})$$

Similarly, the dimensionless form of electrostatic potential $\tilde{\phi}_j$ according to Maxwell's equations, Eqs. (3.7) are

$$-\epsilon_0 \alpha_{0,FE} T_{0,FE} \frac{d^2 \tilde{\phi}_j}{d\zeta^2} + \frac{d\tilde{p}_j}{d\zeta} = 0, \quad (\text{B.7})$$

where $j = FE$ or PE . Finally, the dimensionless form of electrostatic boundary conditions, Eqs. (3.8) are

$$\left\{ \begin{array}{l} \epsilon_0 \alpha_{0,FE} T_{0,FE} \left[-\frac{d\tilde{\phi}_{FE}}{d\zeta} \Big|_{\zeta=0} + \frac{d\tilde{\phi}_{PE}}{d\zeta} \Big|_{\zeta=0} \right] = -(\tilde{p}_{FE}(0) - \tilde{p}_{PE}(0)), \\ \epsilon_0 \alpha_{0,FE} T_{0,FE} \left[-\frac{d\tilde{\phi}_{FE}}{d\zeta} \Big|_{-\tilde{d}_{FE}} + \frac{d\tilde{\phi}_{PE}}{d\zeta} \Big|_{\tilde{d}_{PE}} \right] = -(\tilde{p}_{FE}(-\tilde{d}_{FE}) - \tilde{p}_{PE}(\tilde{d}_{PE})). \end{array} \right. \quad (\text{B.8})$$

and Eqs. (3.9) are

$$\left\{ \begin{array}{l} \tilde{\phi}_{FE}(0) = \tilde{\phi}_{PE}(0), \\ \tilde{\phi}_{FE}(-\tilde{d}_{FE}) = \tilde{\phi}_{PE}(\tilde{d}_{PE}). \end{array} \right. \quad (\text{B.9})$$

In order to find the dielectric susceptibility, we rewrite the Eqs. (3.15) into dimensionless form:

$$\begin{aligned} \frac{d^2 \chi_{FE}}{d\zeta^2} = & \left(\frac{2\alpha_{FE}^*}{\alpha_{0,FE} T_{0,FE}} + \frac{12\beta_{FE}^*}{\beta_{FE}} \tilde{p}_{FE}^2 + 30t_r \tilde{p}_{FE}^4 \right) \chi_{FE} \\ & - \frac{1}{\alpha_{0,FE} T_{0,FE}} \left(\frac{1}{2\epsilon_0} (\tilde{\chi} - \chi_{FE}) + \frac{1}{\epsilon_0} \right) \end{aligned} \quad (\text{B.10})$$

and

$$\begin{aligned} \kappa_r \frac{d^2 \chi_{PE}}{d\zeta^2} = & \left(\frac{2\alpha_{PE}^*}{\alpha_{0,FE} T_{0,FE}} + \frac{12\beta_{PE}^*}{\beta_{FE}} \tilde{p}_{PE}^2 + 30t_r \gamma_r \tilde{p}_{PE}^4 \right) \chi_{PE} \\ & - \frac{1}{\alpha_{0,FE} T_{0,FE}} \left(\frac{1}{2\epsilon_0} (\tilde{\chi} - \chi_{PE}) + \frac{1}{\epsilon_0} \right). \end{aligned} \quad (\text{B.11})$$

The corresponding boundary conditions, Eqs. (3.16) for the dielectric susceptibility at interface in dimensionless form are:

$$\left\{ \begin{array}{l} - \frac{d\chi_{FE}}{d\zeta} \Big|_{\zeta=-\tilde{d}_{FE}} + \frac{\lambda_0}{\kappa_{FE} \epsilon_0} \xi_0 [\chi_{FE}(-\tilde{d}_{FE}) - \chi_{PE}(\tilde{d}_{PE})] = 0 \\ \kappa_r \frac{d\chi_{PE}}{d\zeta} \Big|_{\zeta=0} + \frac{\lambda_0}{\kappa_{FE} \epsilon_0} \xi_0 [\chi_{FE}(0) - \chi_{PE}(0)] = 0 \\ \frac{d\chi_{FE}}{d\zeta} \Big|_{\zeta=0} + \frac{\lambda_0}{\kappa_{FE} \epsilon_0} \xi_0 [\chi_{FE}(0) - \chi_{PE}(0)] = 0 \\ - \kappa_r \frac{d\chi_{PE}}{d\zeta} \Big|_{\zeta=\tilde{d}_{PE}} + \frac{\lambda_0}{\kappa_{FE} \epsilon_0} \xi_0 [\chi_{FE}(-\tilde{d}_{FE}) - \chi_{PE}(\tilde{d}_{PE})] = 0. \end{array} \right. \quad (\text{B.12})$$

APPENDIX C

NUMERICAL METHODS

For the convenient of numerical calculations, all the equations are rescaled into their dimensionless forms as depicted in Appendix B. Subsequently, the dimensionless form of Euler-Lagrange equations Eq. (B.4) & Eq. (B.5) together with the electrostatic equations (B.7) are transformed into a system of nonlinear equations using the finite difference method (Chapra & Canale, 2006). The central difference approach is used to approximate the first and second derivatives in the Eq. (B.4), Eq. (B.5) and Eqs. (B.7), whereas the first derivatives in the Eqs. (B.6) and Eqs. (B.8) are approximated based on forward difference approach. Finally, the system of nonlinear equations Eq. (B.4), Eq. (B.5) and Eqs. (B.7) are solved numerically with the boundary conditions, i.e. Eqs. (B.6), Eqs. (B.8) and Eqs. (B.9). The numerical calculations are implemented using the Matlab mathematical packages. The nonlinear equations solver “fsolve” based on the “trust-region-dogleg” algorithm from the optimization toolbox of Matlab is employed in the numerical computation. A detailed description of this algorithm and Matlab command will not be given here but it can be found in the Matlab’s help or the Optimization Toolbox User’s Guide (The MathWorks, 2014).

LIST OF PUBLICATIONS

1. Lim, K.-G., Chew, K.-H., Ong, L.-H., & Iwata, M. (2012). Electrostatic coupling and interface intermixing in ferroelectric superlattices. *EPL (Europhysics Letters)*, *99*(4), 46004.
2. Chew, K.-H., Lim, K.-G., Ong, L.-H., & Iwata, M. (2013). Influence of interface intermixing and periodicity on internal electric field and polarization in ferroelectric superlattices. *Ceramics International*, *39*, S301–S305.
3. Lim, K.-G., Chew, K.-H., Ong, L.-H., & Iwata, M. (2013). Modulated internal electric field, dielectric susceptibility and polarization in ferroelectric superlattices. *Ceramics International*, *39*, S307–S310.
4. Lim, K.-G., Chew, K.-H., & Ong, L.-H. (2013). Hysteretic internal electric fields and polarization reversal in ferroelectric superlattices. *Ferroelectrics*, *451*(1), 41–47.
5. Lim, K.-G., & Chew, K.-H. (2014). Interface-induced modifications of polarization in nanoscale ferroelectric superlattices. *Advanced Materials Research*, *895*, 477–480.
6. Chew, K.-H., Lim, K.-G., Ong, L.-H., & Iwata, M. (2014). Effect of composition and interface intermixing on polarization behaviors of BaTiO₃/(Ba, Sr)TiO₃ superlattices. *Physica Status Solidi (A)*, *211*, 1698-1703, doi: 10.1002/pssa.201330457.
7. Lim, K.-G., Chew, K.-H., Wang, D.Y., Ong, L.-H., & Iwata, M. (2014). Charge compensation phenomena for polarization discontinuities in ferroelectric superlattices, *EPL (Europhysics Letters)*, *108*, 67011, doi: 10.1209/0295-5075/108/67011.
8. Chew, K.-H., Lim, K.-G. & Ong, L.-H. (2015). Polarization discontinuity and interface charges in ferroelectric superlattices, *Ferroelectrics* (accepted).

AWARDS

1. “Excellent Poster Award”, at the 8th Asian Meeting on Electroceramics on 1-5 July 2012, Penang, Malaysia.
2. “Best Student Poster Award”, at the 8th Asian Meeting on Ferroelectrics, 9-14 December 2012, Pattaya, Thailand.